PRODUCTION AND STRUCTURE / PROPERTIES OF NYLON-6 CORE / ISOTACTIC POLYPROPYLENE SHEATH BICOMPONENT FIBERS SUITABLE FOR USE IN CARPETING APPLICATIONS.

by

David Godshall

Thesis submitted to the faculty of the Virginia Polytechnic Institute and State University in partial fulfillment of the requirements for the degree of

MASTERS OF SCIENCE

in

Chemical Engineering

APPROVED:

_____

G.L. Wilkes, Chairman

_____ _____

D.G. Baird R.M. Davis

February 1,1999
Blacksburg, VA

PRODUCTION AND STRUCTURE / PROPERTIES OF NYLON-6 CORE / ISOTACTIC POLYPROPYLENE SHEATH BICOMPONENT FIBERS SUITABLE FOR USE IN CARPETING APPLICATIONS.

by

David Godshall

G. L. Wilkes, Chairman

Abstract

Bicomponent fibers consisting of nylon-6 and isotactic polypropylene were produced. In-situ, reactive compatibilization was achieved using a maleic anhydride functionalized polypropylene between the materials at the interface. The overall goal of the research was to produce a bicomponent fiber of these materials that would be suitable for use in commercial carpet applications. Carpet samples produced using nylon-6 core / polypropylene sheath bicomponent fibers displayed stain resistance comparable to a wholly polypropylene carpet. The wear characteristics of these fibers were found to be strongly dependent upon the maleic anhydride content and the molecular weight of the maleic anhydride functionalized polypropylene. Adhesion between the nylon-6 and polypropylene phases, and the mechanical properties of the polypropylene phase were affected by the addition of the functionalized polypropylene. Additional information regarding the processing conditions necessary to produce fibers of the desired cross-section from these materials was obtained using capillary rheometry. A number of analytical techniques including DSC, TGA, and SEM were used to better understand the structure of the maleated materials.

ACKNOWLEDGEMENTS

First and foremost, I am most indebted to Charlie White for his assistance, ideas, long hours, infinite patience, humor, and free lunches. Without Charlie's help at Camac I would still be lost to this day. Thankfully Charlie digs deeper than the surface to see what is there, so first impressions are not everything. When I attempted to burn my hand off with molten polymer during the first few minutes of my first day on sight, he didn't write me off. In reality this thesis should include his name as a co-author as the work herein is every bit as much his as it is mine. I hope I have the opportunity to work with Charlie in the future, both on a professional and a personal level. I know that there is still a lot that he can teach me.

Secondly I would like to thank my advisor, Dr. Wilkes. He too is blessed with infinite patience. For every chance I was given to stumble and fail as I tried to find my way, I was given two chances to find the answers and succeed. It goes without saying that his technical advice was always flawless and timed perfectly. I feel that the time that I have spent in his lab has been among the most educating of my life, thanks to the people that he has brought in, and those "extra" requirements that seem like a hassle, but in reality are the experiences looking back at which I feel I have learned the most during. Thank you Dr. Wilkes for giving me the time and the environment to develop as a young scientific professional. (ok, especially thanks for the generous amount of time…)

And, speaking of the lab environment, I am sure that I owe most of the knowledge that I have acquired over the past two years to my labmates. But, because I feel that I have something more than just a professional relationship with my coworkers, it is also necessary that I thank them for their friendship. Without them I would have surely gone insane. Because of them there is always a reason to come into lab even if I don't feel like working at the time. I hope they forgive me for being such a distraction to them during these times. So, let not the names of Chris, Kurt, Cheng Hong, Varun, Brian, Matt O., and Matt J. not go unmentioned, as they have kept me constantly entertained and amused these years in the big city of Blacksburg.

There were some people behind the scenes outside of Blacksburg that are also responsible for the completion of this work. In Bristol, at Camac, Brendan McSheehy made this project possible, kept us on track, and gave us a direction when we began to wonder what good these fibers could be for. Matthew Studholme provided hours of insightful discussions, and helpful industrial contacts. His scientific and technical knowledge continually impressed me. I sincerely hope that Camac finds a way to fully utilize all of his talents. Lastly down in Bristol, Diane Wright did a wonderful job helping us with wear and stain testing. And, I would be remiss if did not acknowledge the help and entertainment provided by Connie Dixon and the rest of the girls in the testing lab. They always had time for me, and a few things to say if I was willing to listen.

Finally, I would like to give a brief acknowledgement to Dr. Scranton, and Dr. Rangarajan at Michigan State for encouraging, and making me believe that I could be accepted to graduate school and succeed.

TABLE OF CONTENTS

LIST OF TABLES

LIST OF FIGURES

1. Introduction

The combination of two materials into a bicomponent fiber has the potential to express the unique properties of each material in a single fiber. For example, the focus of this research was the production of a nylon-6 core / isotactic polypropylene sheath bicomponent fiber. A bicomponent fiber of this configuration should combine the stain resistance properties of a polypropylene fiber with the durability of a nylon-6 fiber.

The processing window of a bicomponent fiber system is set by the viscosity ratio of the two components as they exit the spinneret. As both materials must pass through the same spin pack assembly, it is required that the final stage of the extrusion step be performed at the same temperature for both materials. Thus, the location of each component's thermal transitions and process stability are also key considerations. Proper matching of the viscosities can produce a fiber of the desired cross-section.

In a bicomponent application where it is desired that the two components remain as a single fiber, additional care must be taken to assure that sufficient adhesion is obtained between the fibers. For the nylon-6, polypropylene system this requires the use of a compatabilizer to improve the adhesion between the chemically dissimilar materials. In this research an in-situ formed compatabilizer was used. Commercially available maleic anhydride functionalized polypropylene was used to form a polypropylene - nylon-6 copolymer at the interface. The process used to produce the maleic anhydride grafted polypropylene has a significant impact on the properties of the starting polypropylene. When a functionalized polypropylene is used in substantial quantities in a fiber, it can adversely affect the mechanical properties of the fiber. Thus to produce a bicomponent fiber from chemically dissimilar materials requires an understanding of the processing window of each material individually and together during spinning, and an appreciation of the role that the structure of the compatabilizer plays in determining the quality of adhesion obtained between the phases.

2. Project Background

2-1. Industrial Carpet Production

The overall quality of a carpet is determined by its performance in several areas, and its ability to retain these characteristics over the its service life. Carpeting not only provides a visually pleasing surface, but also contributes to walking comfort, helps to dampen out noises, and provides a measure of insulation. Qualitatively a carpet's ability to serve these functions over the expected life of the carpet can be described by its performance in relation to the following properties listed in table 2-1.

Table 2-1. Key properties in carpet performance.

Property	**Description**
Wear Resistance	Does the carpet lose face material (fiber mass) due to wear
Appearance Retention	Does the carpet maintain its original texture and height
Color Retention	Does the carpet fade or change color over time
Stain Resistance	How prone to staining from anionic compounds (dye, foodstuffs, etc.)
Soil Resistance	How prone to staining from oil based compounds (dirt, grease, etc.)

Obviously the material from which the carpet fibers are made will greatly impact the performance. There is no one material today used in carpet applications which is capable of providing the best performance in all categories. Before making a comparison of the materials commonly used today, a very brief mention of a few of the commonly used carpet constructions should be made.

Carpet construction refers to the manner in which the face fibers are presented on the backing. Figure 2-1 shows some of the commonly used constructions in the industry today. It is readily apparent from the figure that a single pile loop carpet may have very different wear characteristics than a velour carpet or a shag carpet even if the same materials are used to make the face fiber. The loop pile should resist wear better than the velour carpet all other variables being equal. A velour carpet presents fiber ends to the viewer. Any matting action will tend to expose the sides of the fiber, offering different optical characteristics to the eye, and making wear patterns more noticeable (ref.1).

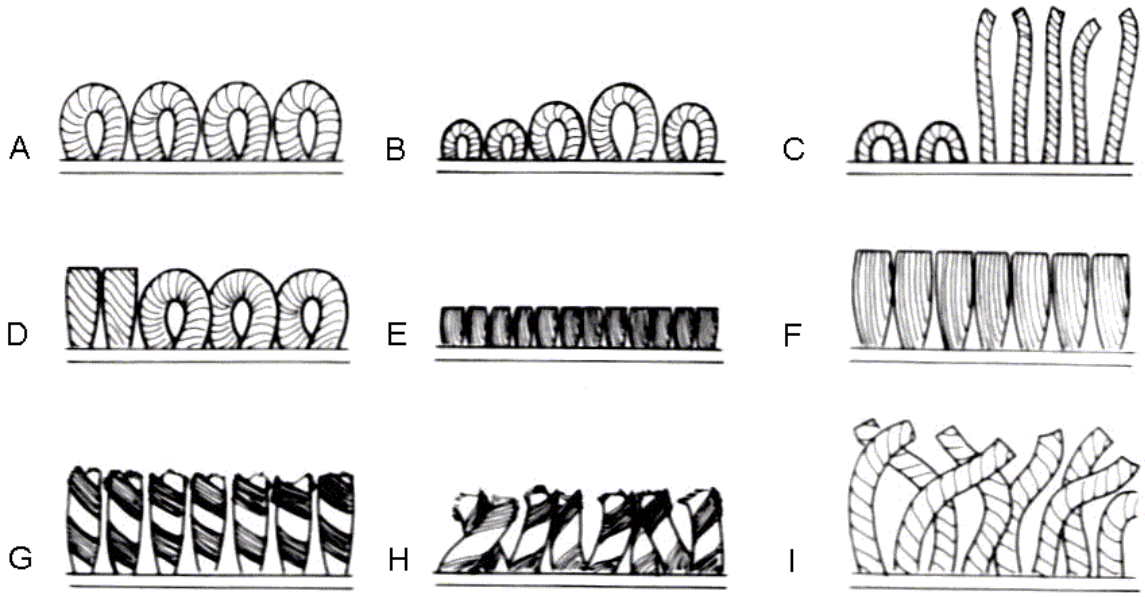

Figure 2-1. Typical carpet constructions:
A - single level pile loop; B - multilevel loop pile; C - multilevel cut and loop; D - tip sheared; E velour; F - plush; G - saxony; H - frieze; I - shag (ref.1).

The single level loop pile construction method is the most common construction style used in applications where large amounts of foot traffic are expected. Finally, the method of attachment of the face fiber to the backing and the packing density (amount of material used per unit area) of the face fiber will also affect how the carpet performs.

Rough comparisons can be made between the materials which are most commonly used in the carpet industry today. Figure 2-2 shows the relative amounts of material that are being used as face fibers in carpet applications in the United States, which represents 55 - 60% of the 2 billion kg/yr. world demand (ref.1).

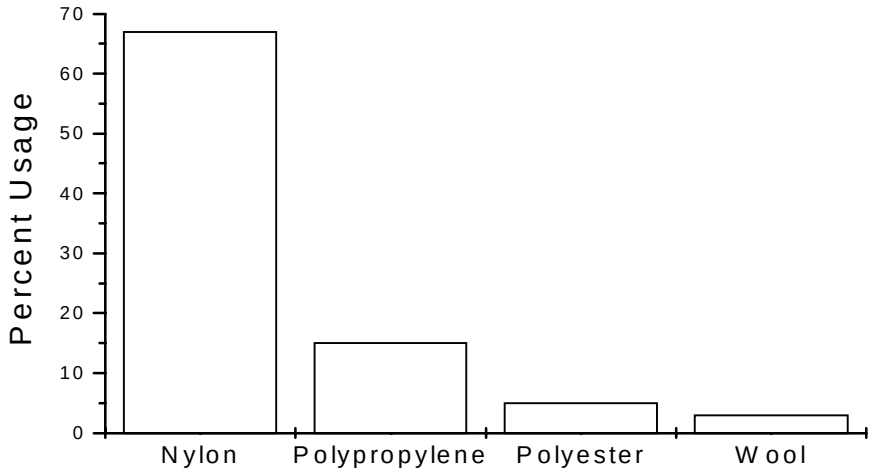

Figure 2-2. 1994 U.S. relative use of common face fibers for carpeting (ref.1).

In general it can be said that both nylon and polypropylene fibers possess excellent wear resistance and can have adequate color stability if the proper stabilizing package is used. However, sulfonated nylon fibers typically have better appearance retention characteristics and soil resistance. Propylene's unique strengths come from its excellent stain resistance, low cost, and lower density, allowing less material to be used to cover the same area. Clearly, a fiber which is characterized by the best properties of nylon and polypropylene would be in high demand by the carpet industry. While no single material exists which displays these properties, it may be possible through a bicomponent fiber structure to obtain the best of both materials. This is the focus of this research project.

2-2. Bicomponent Fiber Spinning

2-2-1. Bicomponent fiber configurations

Bicomponent fiber spinning is the process of spinning fibers which are composed of two or more distinct regions in the fiber's cross-section, which can be subdivided into three main categories: side by side, core/sheath, and "islands in the sea". These different configurations may be placed into any number of possible cross-sectional shapes that are commonly used in monocomponet fibers.

Thus, a wide variety of fibers may be produced, a few examples of which are given in Figure 2-3.

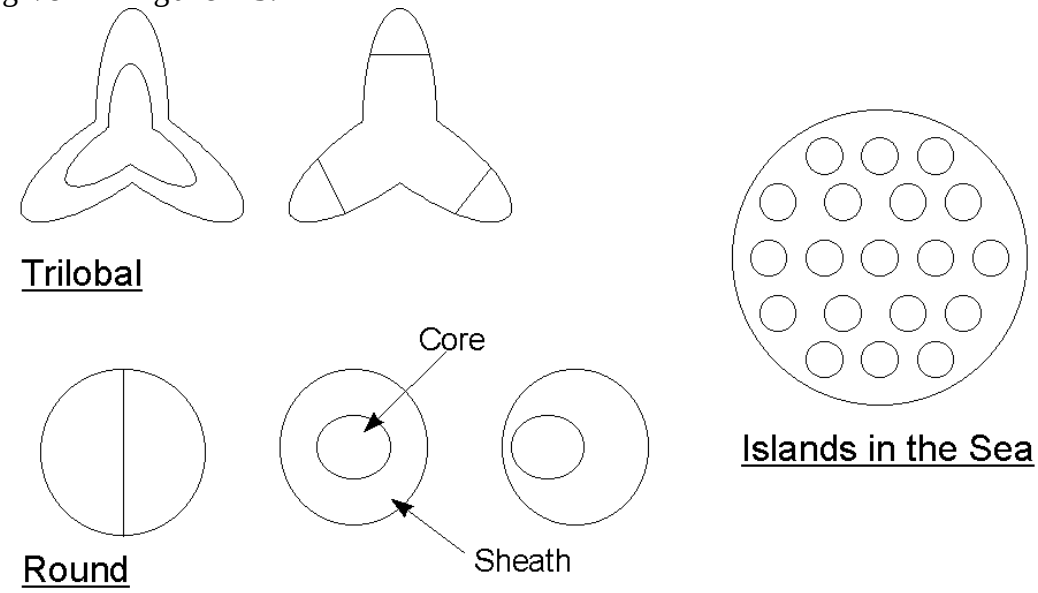

Figure 2-3. Examples of bicomponent fiber cross sections and configurations

Side by side fibers and eccentric core / sheath fibers show the often desired property of self crimping. Differences in contractility upon drawing or heating of the two sides cause the fiber to wrap itself into a helical configuration, the intensity of which will be a function of the materials used and their arrangement. This self crimping behavior produces extra bulk in the yarn, allowing the same mass of fiber to occupy a larger volume. The addition of texture to a fiber is usually accomplished through an additional crimping step in monocomponent fibers. It is not necessary that each "domain" contain different materials. Many bicomponent fibers have been produced in which each section is composed of the same material processed under slightly differently conditions.

The core / sheath configuration presents the possibility of producing a fiber which displays certain individual properties of each component. For example, placing a polypropylene sheath around a nylon core may potentially produce a fiber with the wear resistance of a nylon fiber, while displaying the stain resistance of a polypropylene fiber. A strong bond must be made between the two materials to prevent fiber splitting. A fiber made of chemically different species will require a specialized scheme to enhance the strength of the interface.

Finally, the "islands in the sea" configuration consists of two components which ideally show no adhesion. By making a matrix component consisting of a soluble material, it is possible to remove it at a later time, allowing numerous micro denier fibers to be produced without the process difficulties involved in handling very fine fibers. Recently a general review of the types of

configurations possible, current producers of bicomponents, and producers of bicomponent spin equipment was published (ref.2).

2-2-2. Unique bicomponent spinning problems - equipment.

As one can imagine, the spinning of bicomponent fibers adds complexity and creates unique problems not normally associated with monocomponent fiber spinning. To produce a multiplicity of fibers from one spinneret, the two polymer streams must be split numerous times and then brought together in the proper configuration prior to exiting the spinneret. An example of a bicomponent spin pack is shown in Figure 2-4.

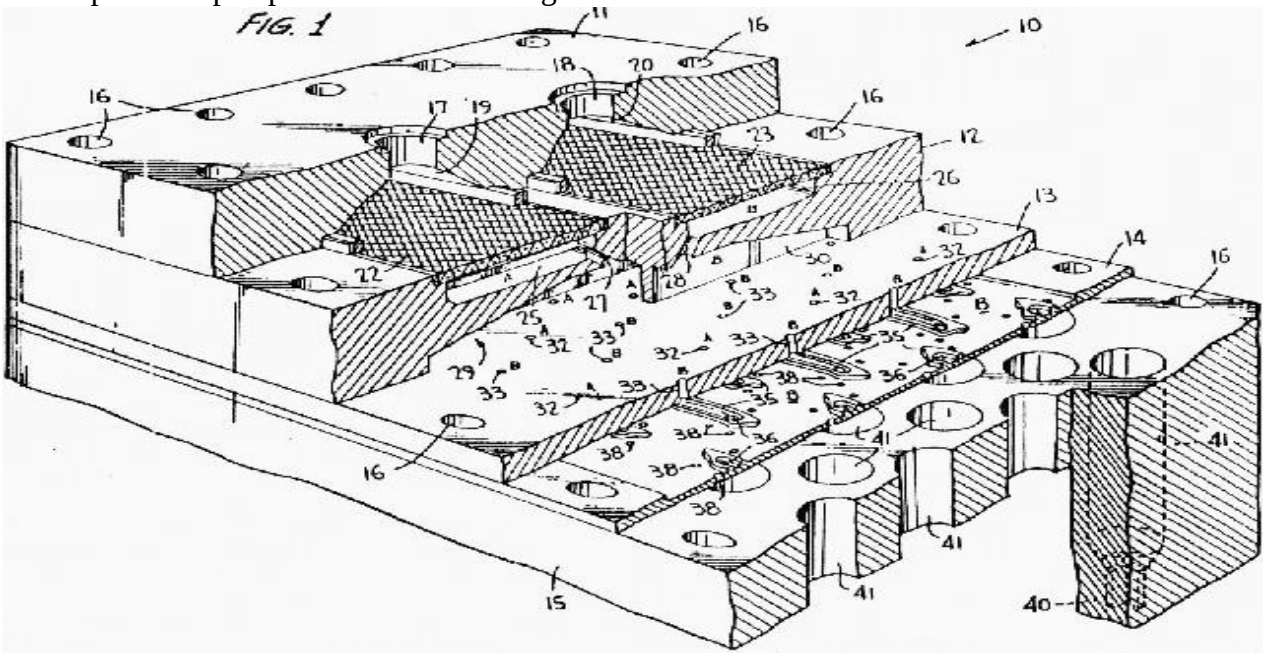

Figure 2-4. Representative bicomponent spin pack. Separate melt streams enter pack from extrusion at points 17 and 18. Filtering and initial distribution occur at points 22 and 23. The two thin plates split the streams multiple times and arrange the streams with the proper configuration prior to contacting in the capillaries, point 41, and exit through the spinneret face, point 40 (ref. 3).

The two polymer streams enter the top of the pack separately. The screens serve to filter and to help evenly distribute the streams across the width of the pack. From here the streams are split and routed to match the number of spinneret orifices. Finally the two polymers are brought together just prior to exiting the spinneret. Many spin packs are quite versatile, allowing a wide range of fibers to be made. The pack shown in Figure 2-4 has interchangeable plates which allow various core / sheath and side by side configurations to be spun. Alternate spinneret faces can also be used to produce any desired overall fiber cross section (round, trilobal, etc.).

2-2-3. Unique bicomponent fiber spinning problems - mechanics.

The concept of taking very different polymers and combining them into a single fiber displaying the best properties of each material is enticing. However there are some limitations on the combinations of materials that may be used together in a bicomponent system. Large differences in viscosity between the materials can complicate the production of the desired cross section, and in extreme cases make the system unspinnable. If a splitable fiber is not the end goal, the two polymers must also be sufficiently compatible at the interface so as to have adequate interfacial adhesion.

In the spin pack just prior to exiting the spinneret the materials come together and then flow in the desired configuration through a capillary. Over this finite length rearrangement of the polymer streams can occur. The degree to which this phenomena occurs, referred to as interface movement, is a strong function of the viscosity difference between the two polymers, and a function of the length to diameter ratio of the capillary for a given set of spinning conditions. Figure 2-5 shows the phenomena observed experimentally. The photographs show cross sections of the extrudate whose melt streams were contacted with the initial configuration shown in the schematic. The figure represents a gradually increasing L/D ratio from 4 to 11 to 18 for a polystyrene (black core), which is more viscous than the polyethylene (white sheath).

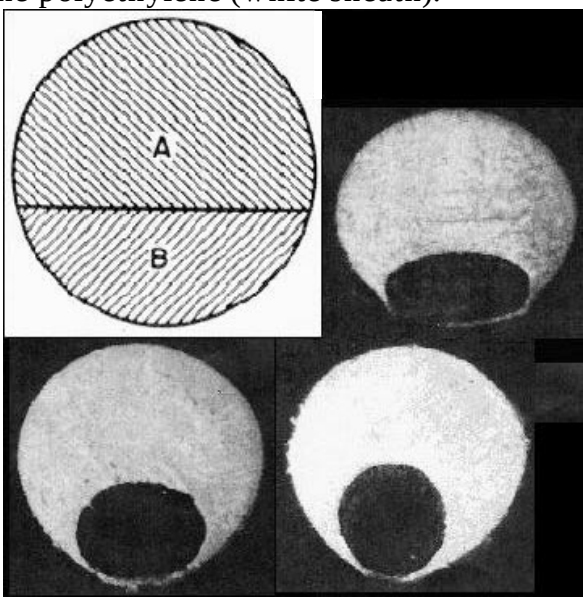

Figure 2-5. Encapsulation of high viscosity component (black) by lower viscosity component (white) for increasing L/D ratio. Schematic shows configuration at entrance of capillary (ref. 4). L/D = 4 at top right. L/D = 18 at bottom right.

Han, as well as several other researchers (refs. 4-7), have shown experimentally that differences in the elastic nature of the two materials have very little if any

effect on the shape or position of the interface formed relative to the effects produced by viscosity differences. The phenomena of interface movement leading to the encapsulation of the more viscous component has been explained by the concept of minimum viscous dissipation by several authors (refs. 8-11). Through numerical simulations of Newtonian, power law, and various viscoelastic models, these authors have obtained the same results which are seen experimentally. As the two polymers traverse the capillary, they will spontaneously rearrange themselves until the configuration which produces the least amount of resistance to flow is obtained. Thus, the material of lower viscosity will move to the regions of greater shear, near the walls, leading to the encapsulation effect.

Large viscosity differences between the two materials can also affect the spinability of the fiber as it exits the spinneret. Differences in viscosity and position in the capillary lead to differing velocities for the two materials. A constant volumetric flow rate for each component can be achieved for various combinations of cross sectional area and velocity. Thus, regardless of the volumetric flow rate ratio, it is likely that one material will be traveling faster than the other within the capillary. Upon exiting the spinneret, the conditions of a shearing flow are removed. The shear free boundary at the surface of the fiber after exiting leads to a flat velocity profile across the fiber. In order to obtain this profile, material anterior to the fiber must accelerate while material interior to the fiber must decelerate. The rearrangement of the velocity profiles within the fiber can lead to an imbalance of forces. This effect is shown schematically in Figure 2-6 for an initially parallel plate flow configuration.

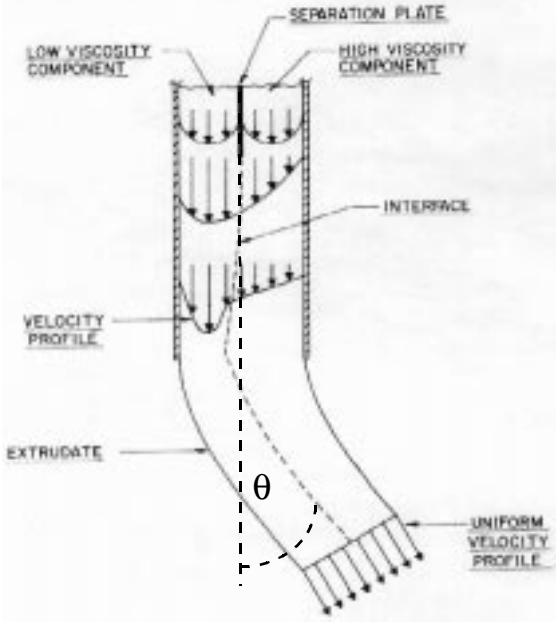

Figure 2-6. Conditions leading to variation in extrudate exit angle, θ, as material exits a parallel plate geometry (adapted form ref. 5).

Intuitively if the fiber is spun as a perfectly symmetric core / sheath fiber this effect will not occur. However, in the production of side by side fibers or any asymmetric fiber, if the viscosity differences are too great, this effect on the extrudate exit angle will be noted. Everage (ref. 5) has studied and confirmed this phenomena and found that as the capillary L/D ratio increased, the magnitude of the exit angle decreased for a side by side bicomponent fiber consisting of two nylon 6's of differing viscosity. This logically occurs as a consequence of the increased wrap around effect for larger L/D ratios which will lead to a more symmetric configuration as the material exits the capillary. In extreme cases, the exit angle may be so great that the extrudate may contact the face of the spinneret and stick as it exits leading to a situation in which it is impossible to spin fibers.

This phenomenon should not be confused with the processes which lead to die swell or non-zero exit angles in mono-component fiber spinning. In single component fiber spinning these effects will be due to the elastic nature of the material "remembering" chain conformations present prior to entering the capillary, and attempting to return to these conformations after exiting the capillary. These elastic effects can occur in a bicomponent system. The exact nature of the effects will be a function of the individual components elasticities and their arrangement in the fiber.

2-3. Polymer Rheology

The viscoelastic nature of a material may well constitute its most important properties in the fiber spinning process. The viscosity of the material will affect the processing characteristics of the material through extrusion, its separation into separate fiber streams in the spin pack, its ability to form a fibrous material after it exits the spinneret, and the final structure of the material at the end of the fiber drawing and take-up process. Rheology is the study of the deformation and flow of materials. Thus, measurements of viscosity and other rheological parameters will be very important in the understanding of the fiber spinning process. There are three basic types of deformation that a material may undergo: shear, elongational, and hydrostatic bulk deformations. In fiber spinning the conditions under which the material is subjected may be divided into two major categories. The first occurs within the extruder and inside the spin pack. Here the polymer will experience essentially shear deformations. After exiting the spinneret the polymer primarily undergoes elongational deformations as it is drawn down the stack. What follows is an introduction to polymer rheology under shear conditions followed by a brief discussion of the elongational flow properties of the materials relevant to this work.

2-3-1. Terminology and representative behavior of polymer melts.

The most common mode of deformation used when discussing the viscosity of a material is that of shear. Figure 2-7 gives a schematic of simple shearing conditions for a single fluid element. The upper surface is subjected to a force while the lower surface is held stationary, resulting in a deformation of the element.

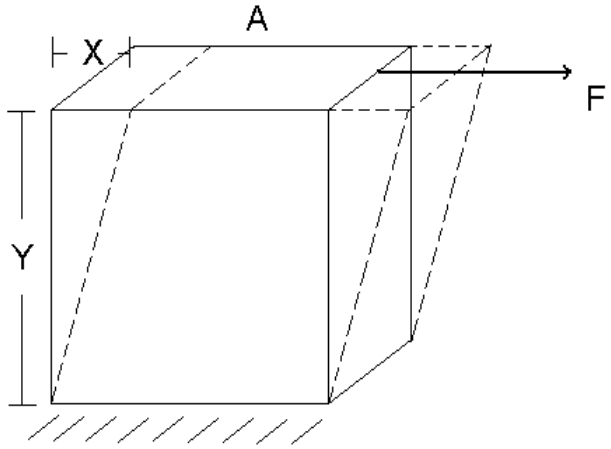

Figure 2-7. Simple Shear

It is now possible to define some terms with respect to Figure 2-7.

$$\tau_{yx} = \frac{F}{A} \tag{1}$$

The shear stress, τ_{yx}, gives a measure of the amount of force which leads to the deformation of the element with respect to a surface on the element, applied in a specific direction.

$$\gamma = \frac{X}{Y} \tag{2}$$

The shear strain, γ, gives an indication of the amount of deformation taking place. It is useful in defining a very commonly used quantity, the shear rate.

$$\dot{\gamma} = \frac{d}{dt}\left(\frac{dX}{dY}\right) = \frac{d\gamma}{dt} \tag{3}$$

The shear rate has units of reciprocal time (sec^{-1}) and gives a measure of the speed at which the shearing strain is changing. The shear stress and the shear rate are linked through the quantity known as viscosity, η. When a shearing stress is applied, the material will provide a degree of resistance to the shearing action. This resistance is characterized by the viscosity. The exact mathematical form of the viscosity function must be determined from experimental measurements.

The simplest model of viscous behavior is termed Newtonian.

$$\underline{\underline{\tau}} = \mu \underline{\underline{\dot{\gamma}}} \tag{4}$$

For a Newtonian fluid shear stress and shear rate tensors are linearly related through the Newtonian viscosity, μ. Figure 2-8 shows some various possible shear stress, shear rate relations.

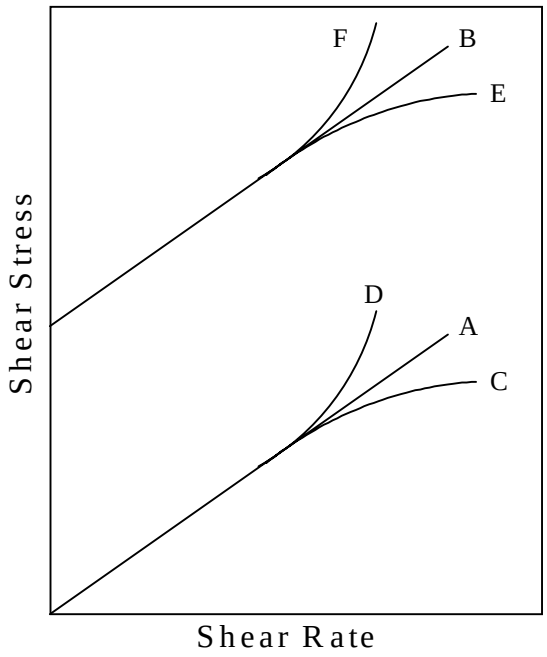

Figure 2-8. Various shear stress / shear rate behaviors (ref.14)

The behaviors above can be classified as follows: (A) Newtonian fluid, a linear relationship, in general common to fluids of low molecular weight species, (C) shear thinning or psuedoplastic, $\dot{\gamma}$ deviates negatively from Newtonian behavior, commonly observed in polymeric systems, (D) shear thickening or dilatant, $\dot{\gamma}$ deviates positively from Newtonian behavior. Curves (B), (E), and (F) represent the equivalent behaviors of (A), (C), and (D) with the addition of Bingham character. A Bingham fluid is one in which a critical stress, termed the yield stress, must be surpassed before any flow will begin.

2-3-2. Functional forms of viscosity.

To mathematically describe the observed stress strain behavior of shear thinning and thickening materials, a number of viscosity functions, commonly referred to as constitutive equations, have been proposed. The simplest model which can describe a non-linear relationship between τ and $\dot{\gamma}$ is the power law model which for the deformation shown in fig. 2-7 could be written as:

$$\tau_{yx} = \eta\dot{\gamma}_{yx}\left|\dot{\gamma}_{yx}^{\,B-1}\right| \tag{5}$$

The value of the constant B, describes the amount of shear thinning (B<1) or shear thickening (B>1) behavior a material shows. The power law model has been used extensively for polymers because it describes their pronounced shear thinning behavior well. Figure 2-9 shows a typical viscosity versus shear rate plot for a shear thinning material at varying temperatures. At low shear rates many polymers have viscosities which are independent of $\dot{\gamma}$, this region is referred to as the Newtonian plateau. The viscosity in this region is often termed the zero shear viscosity, η_o. At higher shear rates the viscosity begins to drop. Eventually a second Newtonian plateau is theoretically possible, though it is possible that degradation due to mechanical chain scission may occur before this point is reached.

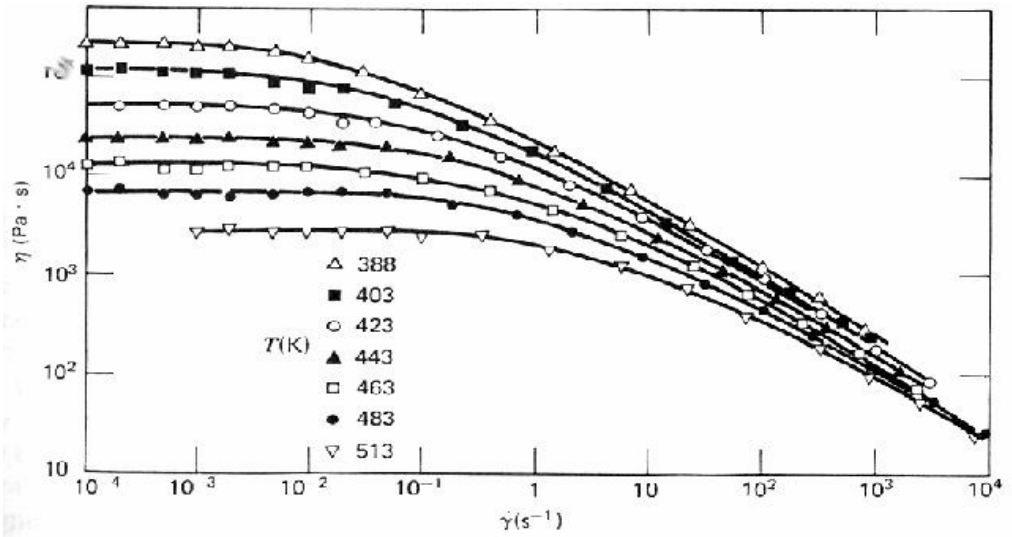

Figure 2-9. Typical shear rate and temperature dependence of a low density polyethylene melt (ref.16)

The viscosity of a polymer is not only a strong function of shear rate, it is also highly dependent upon temperature. Two relations have been set forth which are commonly used to describe the temperature dependence of viscosity. The first relation is the Williams-Landell-Ferry (WLF) equation.

$$\log_{10}\frac{\eta_o(T)}{\eta_o(T^*)} = \frac{-C_1(T-T^*)}{C_2+(T-T^*)} \tag{6}$$

where $\eta_o(T)$ refers to the zero shear viscosity at temperature, T

$\eta_o(T^*)$ refers to the zero shear viscosity at some reference temperature, usually T_g

C_1 and C_2 are constants specific to the polymer though universal values have been found that estimate the behavior for most polymers

The WLF equation has been found to describe viscosity best for temperatures which range from approximately T_g to T_g+100. At higher temperatures the temperature dependence of viscosity is best described by an empirical Arrhenius expression.

$$\eta_o(T) = Ae^{E_a/RT} \tag{7}$$

where $\eta_o(T)$ refers to the zero shear viscosity at temperature, T
A is the pre-exponential factor
E_a is the "Newtonian" activation energy for flow
R is the universal gas constant

It should be noted that while the pre-exponential factor shows molecular weight dependence, the flow activation energy does not.

The activation energy for flow is a function of local chain chemistry and structure. Changes in the structure which increase the stiffness of the backbone (i.e. presence of double bonds, aromatic rings, or bulky side groups) will tend to raise the flow activation energy. The addition of branches to the chain will have a similar effect as the branches will also restrict backbone movement.

The pre-exponential factor accounts for the increase in viscosity which result from the increase in entanglements associated with rising molecular weight, observed in macromolecular systems. Figure 2-10 shows the general effect of the weight average molecular weight on viscosity.

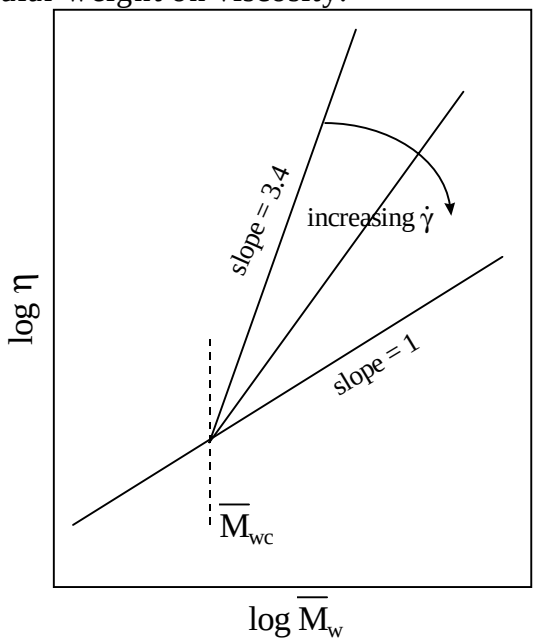

Figure 2-10. Effect of weight average molecular weight, $\overline{M_w}$, on viscosity for many polymer systems (ref. 15).

From the figure it can be seen that once a critical molecular weight, M_{wc}, is achieved the dependence becomes much greater. Below M_{wc} the log - log plot yields a slope of unity. This behavior is characteristic of low molecular weight species. Above M_{wc} the polymer chains have become long enough to entangle. This greatly increases the viscosity resulting in a viscosity dependence on molecular weight to the 3.4 power for most polymers. For polypropylene this critical molecular weight occurs at 7,000 g / mol, while the onset is at 5,000 g / mol for nylon-6 (ref. 75). These values correspond to 167 and 44 repeat units respectively. Table 2-2 provides viscosity data for various materials for comparison to polymer melts.

Table 2-2. Viscosity values of various materials (ref. 13).

Material	η (Pa-sec)
Air	10^{-5}
Water	10^{-3}
Glycerin	10^{0}
Syrup	10^{2}
Polymer melts	10^{2}-10^{6}
Pitch	10^{9}
Glass	10^{21}

2-3-3. Capillary rheometry - theory.

Several instruments have been developed to measure rheological properties in shear. Each instrument has its own individual strengths and weaknesses. The capillary rheometer is capable of measuring rheological properties at shear rates which are comparable to many polymer processes. Figure 2-11 is a schematic view of a capillary rheometer.

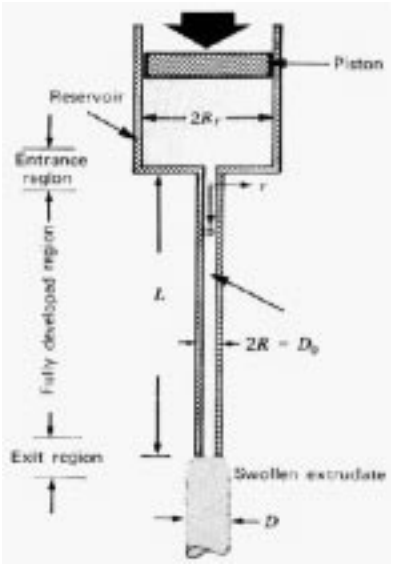

Figure 2-11. Schematic view of a capillary rheometer (ref.79).

Solid polymer is loaded into the reservoir at the top of the rheometer where it is melted at the desired temperature. After this melt time, the plunger is driven down forcing molten polymer through the capillary region. Measurements of the flow rate of material and the force required to move the plunger, corrected for frictional effects, allows the calculation of the material's viscosity. Making a balance of forces (neglecting gravity) on a fluid element within the capillary yields eq. 8.

$$\tau_{rz}(r) = -\left(\frac{r}{2}\right)\left(\frac{dP}{dz}\right) \tag{8}$$

where $\tau_{rz}(r)$ is the shear stress along a surface of constant r in the z direction

$\frac{dP}{dz}$ is the pressure gradient driving flow

Thus, for a capillary of radius R, the shear stress at the wall (r = R) of the capillary, τ_w, can be defined and related to the shear stress as follows.

$$\tau_{rz}(r) = \frac{r}{R}\tau_w \tag{9}$$

From eq. 9 it can be seen that the shear stress in the capillary is a linearly varying function of position, regardless of the material being tested. That is, to this point no constitutive equations have been used. Assuming that fluid only flows in the z direction and that the "no slip" boundary condition applies (u_z=0 @ r=R), and considering that the shear rate is simply the first derivative of the fluid velocity with respect to radial position, the following relations may be derived.

$$u_Z(r) = \int_R^r \dot{\gamma}[\tau(r)]dr = \int_R^r \frac{\tau(r)}{\eta[\tau(r)]}dr \tag{10}$$

Equation 10 provides a relationship between $\dot{\gamma}$, τ, and η. Thus if two of the quantities can be measured, the third can be calculated.

2-3-4. Capillary rheometry - sources of error.

In a capillary rheometer τ and $\dot{\gamma}$ are obtained at the wall of the capillary through measurements of force on the plunger and flow rate respectively. Equation 10 can be used to obtain the Rabinowitsch equation.

$$-\dot{\gamma}_w = \Gamma\left(\frac{3}{4} + \frac{1}{4}\frac{d\ln\Gamma}{d\ln\tau_w}\right) \tag{11}$$

where a new term is introduced, the apparent shear rate, Γ, which can be defined as follows.

$$\Gamma = \frac{4Q}{\pi R^3} \tag{12}$$

The term in parentheses in eq. 11 is commonly referred to as the Rabinowitsch correction. For Newtonian fluids $\dot{\gamma}_w$ and Γ are equivalent because there is no dependence of viscosity on shear rate. However, for non-Newtonian fluids, $\dot{\gamma}_w$ and Γ are not equivalent. A shear thinning material will have a steeper velocity gradient near the wall, where viscosities are determined in capillary rheometry, as compared to a Newtonian fluid. Thus, errors may result if the Rabinowitsch correction is not applied. For a power law fluid, the Rabinowitsch correction factor becomes,

$$\left(\frac{3B+1}{4B}\right) \tag{13}$$

where B is the power law exponent from eq. 5.

Additional corrections can be made to capillary rheometry data to further improve accuracy. Figure 2-12 shows an additional affect which may cause error in measurements.

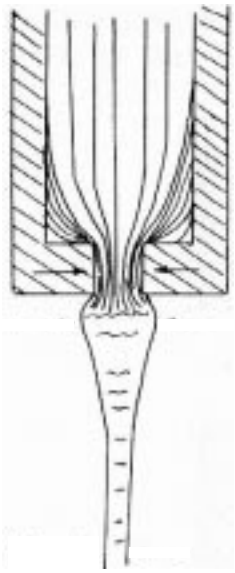

Figure 2-12. Sources of error in capillary rheometry data (adapted from ref. 20).

At the entrance of the capillary in the reservoir, flowing fluid is rapidly forced from a large cross section into a much smaller cross section. This entrance effect leads to an additional pressure drop which can be corrected for by using the method of Bagley (ref.12). The method requires that measurements be taken using two (ideally three or more) capillaries of varying L/D ratio. Additional errors in measurement may arise from the following: the finite amount of kinetic energy added to the system to accelerate the fluid in the reservoir, an additional pressure drop from friction between the plunger and reservoir walls, and from the small pressure dependence of viscosity. Finally, due to the elastic nature of polymer melts, some energy can be stored in the material as it exits the capillary, resulting in a pressure greater than atmospheric in the material at the outlet. This effect manifests itself visibly as die swell, and is due to normal stresses within the material. Normal stress data can be obtained from a capillary

rheometer by measuring the amount of die swell. One author, Cogswell, has shown that elongational viscosity data can be obtained with an analysis of entrance effects. The entrance effects can be related to extensional viscosity because the entrance flow to the capillary will have an elongational component, as shown in Fig. 2-12(ref. 13).

2-3-5. Extensional viscosity.

The viscous response of a material is a function of the deformation type. Earlier it was noted that in the fiber spinning process after the spinneret region material will undergo primarily extensional deformations. Thus, the processability and the development of structure within the fiber in the spin line will be highly dependent upon $\bar{\eta}$, the elongational viscosity of the material. Trouton's rule states that the elongational viscosity in the Newtonian region is three times the shear viscosity.

$$\bar{\eta}_0 = 3\eta_0 \tag{14}$$

Trouton's rule has been verified for many polymers experimentally and it can be shown that in the limit of zero extension rates the relationship holds. It should be emphasized, however, that the rule only applies to the Newtonian region. Based on the above rational it can be seen that the elongational viscosity will likely play a larger role in determining a material's behavior in the spin line than the shear viscosity. Most materials show a similar temperature dependence in elongation as in shear. The response of $\bar{\eta}$ to changing extension rates is more varied. Generally, the dependence is not as strong as the dependence of shear viscosity on shear rate. Figure 2-13 compares the shear and elongational viscosity behavior of a polypropylene at varying deformation rates. From the figure it can be seen that the dependence of $\bar{\eta}$ on extension rate is slightly less than the shear dependence of η. Of relevance to previous discussions, the data in figure 2-12 at low extension rates was obtained from uniaxial extension experiments (solid symbols) while the data at higher extension rates was obtained using entrance loss data from a capillary rheometer (cross hatched data points) using Cogswell's method.

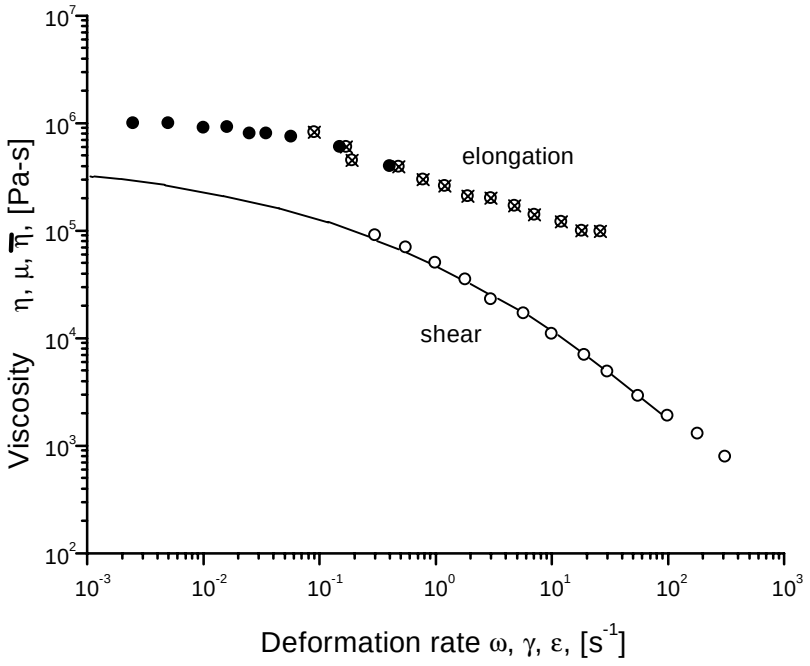

Figure 2-13. Comparison of extensional viscosity and shear viscosity dependence on deformation rate ● uniaxial extension data, ⊗ capillary entrance pressure loss data, O capillary shear data. (replotted from ref.17).

Independently Ishibashi et. al (ref.18) have shown that $\overline{\eta}$ for nylon-6 is relatively insensitive to changes in extension rate. Both ordinary polypropylene and nylon-6 have been shown to obey Trouton's rule at small extension rates. Little data exists for extensional properties relative to shear properties due to the difficulty in obtaining steady state elongational flows experimentally.

2-4. Drawing and Orientation

2-4-1. Processing steps leading to orientation.

As spun, fibers do not posses the mechanical properties necessary for most applications, including carpeting. Only a small amount of chain orientation is achieved during the spinning process. It is standard practice to include a drawing step either in line with spinning or as a separate step in the production of fibers. The drawing step changes the final structure of the fibers, and hence their properties, by increasing the orientation of the chains along the fiber axis. The changes which take place during drawing are largely a function of three parameters: the amount of draw (the draw ratio), the conditions of drawing (temperature, velocity, etc.), and the initial structure of the fiber. Figure 2-14

presents a schematic demonstrating the relative amounts of orientation which are introduced at each step of fiber production.

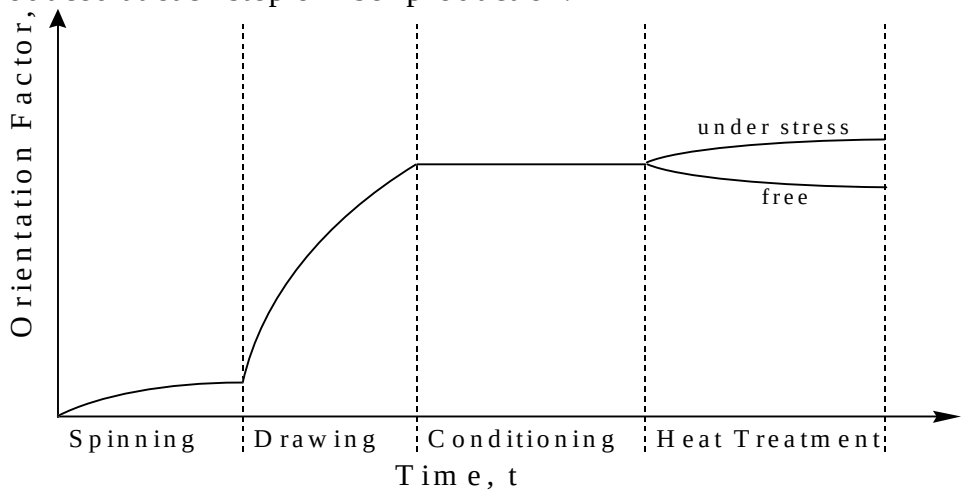

Figure 2-14. Buildup of orientation during processing. (ref.19).

2-4-2. Effect of orientation on crystallization behavior.

Because of the presence of some orientation during spinning and because conditions are changing with time (position) as a fluid element moves down the spin line, the crystallization process results in structures which are different from those obtained from quiescent crystallization. Spherulite formation occurs only in very thick filaments, commonly referred to as bristles, with very little orientation. This is not to say that crystallization must occur in the spin line for the effects of orientation to be felt. PET fibers are a classic example of a material which is often spun into the glassy state with subsequent drawing and heat treatment leading to oriented crystallization.

Nylon-6 does crystallize somewhat during the spinning process, though this crystallinity level will be substantially lower than that of the final commercial fiber. To prevent hydrolysis, nylons must be processed with very little water content. Rapid moisture pickup will occur once the material comes in contact with the environment. Water's effect on a nylon-6 as a plasticizer is so effective that it can decrease T_g from 70°C to as low as -10°C. Thus, additional crystallization will occur on the winder or during storage, increasing the crystal content. Analysis of nylon-6 crystallinity is complicated by the fact that nylon-6 is polymorphic. It is generally believed that two forms exist, the α and γ. The α form appears to be the most stable and is formed under standard spinning conditions and during storage as a result of moisture regain. The γ form is increasingly observed under high speed spinning conditions.

Polypropylene too is polymorphic, the most predominant and stable crystal form being the α form, having a monoclinic structure. The β form, which has hexagonal packing, may in some instances be formed. Additional structures, γ

and δ, have been noted in the literature, but are very rare (ref. 77). All forms are based on the 3_1 helix, with variations in packing and handedness. The relative amounts of each of these forms will largely depend on the melt temperature and the cooling rate. The more stable α form is favored at higher temperatures and slower cooling rates. Polypropylene crystallizes much more rapidly, in general, than nylon-6, thus its crystallinity will change very little after spinning without additional drawing or heating, at conventional cooling rates.

2-4-3. Structural models of fiber.

Several different models have been put forth in an attempt to describe the morphological texture of fibers. No one model has been determined to be satisfactory. One basic model that has been developed is the three phase model. The model is depicted in Figure 2-15.

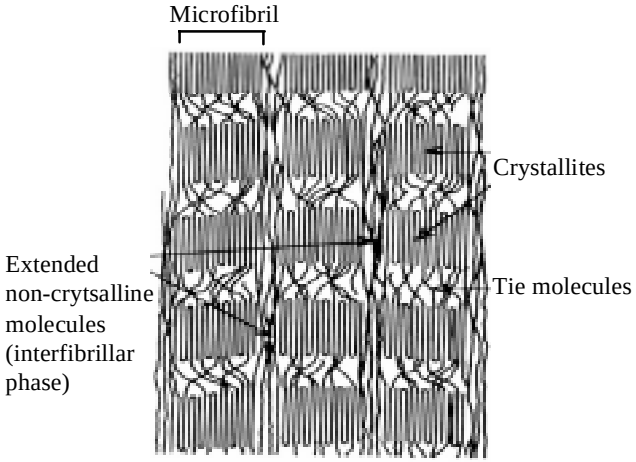

Figure 2-15. Three phase model of fiber structure (ref. 1).

As the name implies, the fiber consists of three distinct phases: oriented crystalline regions, amorphous regions also with preferential orientation along the fiber axis which contain tie molecules connecting crystallites, and highly extended non-crystalline molecules, called the interfibrillar phase. In the three phase model the interfibrillar phase will play a key role in the tensile properties of the fiber. More basic models do not include the interfibrillar phase, thus making the tie molecules the most important factor in determining the observed mechanical properties of the material. It is probable that no one model can describe the texture of all materials produced under all conditions. However, it can be definitively stated that the fiber formation process results in a morphology consisting of oriented crystalline and amorphous regions arranged in structures very different from those obtained under quiescent conditions, for the same semi-crystalline material.

2-5. Thermodynamics of Polymer Blends

2-5-1. Mathematical view of miscibility.

In some instances it is possible to mix different polymers and form a wholly miscible blend. This behavior often occurs when the two materials have favorable specific interactions. Miscibility can be analyzed thermodynamically by considering the Gibb's free energy of mixing for the system, which can be written as a combination of enthalpic and entropic mixing terms.

$$\Delta G_m = \Delta H_m - T\Delta S_m \tag{15}$$

For spontaneous mixing to occur, ΔG_m must be negative. The entropy of mixing term, ΔS_m, will always be positive as mixing increases the disorder of the system, thus making the second half of eq. 15 negative and favorable to mixing. But, in polymer systems because of the long chain nature of the molecules, ΔS_m is often smaller in magnitude than the enthalpy of mixing, ΔH_m. It is this fact that cause polymer miscibility to rely on specific interactions between the species, leading to a negative ΔH_m, to achieve miscibility. The second thermodynamic requirement for miscibility is expressed using the second partial derivative of the Gibb's free energy of mixing with respect to composition as shown in eq. 16.

$$\left(\frac{\partial^2 \Delta G_m}{\partial \Phi_2^2}\right)_{T,P} > 0 \tag{16}$$

The change in Gibb's free energy of mixing for two polymers can be calculated using Flory-Huggins theory. The theory gives a theoretical foundation for mathematically modeling polymer-polymer miscibility. The following equation may be derived from the theory (ref. 72).

$$\Delta G_m = RT\left[N\Phi_1\Phi_2\chi_{12} - \left(x_1 \ln\Phi_1 + x_2 \ln\Phi_2\right)\right] \tag{17}$$

where R is the universal gas constant
T is the absolute temperature
N is the total number of lattice sites in the system
Φ_i is the volume fraction of species i
χ_{12} is the Flory-Huggins interaction parameter between the species
x_i is the mole fraction of species i

Because the terms contained in the parentheses in eq. 17 involve taking the natural log of fractional numbers, these terms will always be negative. The interaction parameter, χ_{12}, is closely associated with the enthalpic interactions of the blend species. The value of χ_{12} may be negative, positive, or zero (athermal

mixing). Solubility parameters may be used to model values of χ_{12} in systems without specific interactions, as in eq. 18.

$$\chi_{12} = \frac{\upsilon\left(\delta_1 - \delta_2\right)^2}{RT} \tag{18}$$

where ν is the molar segmental volume of the species
δ_i is the solubility parameter of species i

In this model, χ_{12} cannot have negative values. Therefore, to achieve miscibility, χ_{12} should be made as small as possible. For materials of interest to this particular project, polypropylene and nylon 6-6, the values of the solubility parameter are 9.4 and 13.6 $(cal/cm^3)^{1/2}$ for polypropylene and nylon 6-6 respectively (ref. 72). A general rule of thumb for solubility states that the absolute value of the difference between the solubility parameters of the species should be less than 1 $(cal/cm^3)^{1/2}$ for solubility. Obviously from these values polypropylene and nylon-6 (owing to the chemical similarity between nylon-6 and nylon6-6) will not form a miscible blend. This is not surprising since polypropylene is olefinic while nylon-6 is somewhat polar. On a molecular scale this means that there will be little if any diffusion leading to entanglement of nylon-6 and polypropylene chains during bicomponent spinning. Therefore to spin a bicomponent fiber consisting of these two materials some scheme must be developed to provide adequate adhesion between the components.

2-5-2. Compatibilization using block and graft copolymers.

In the blending of polymers, to achieve systems with adequate mechanical properties, complete miscibility is not necessary. However, the characteristics of the material will tend to improve as the two materials become increasingly compatible. As compatibility increases, the average domain size of the dispersed phase will decrease and the ability to transfer stresses from one domain to another without separation will increase. This trend can be thought of one in which the interfacial adhesion of the two materials is being increased. Figure 2-16 gives a schematic of each of these types and a conceptual picture of how they increase compatibility.

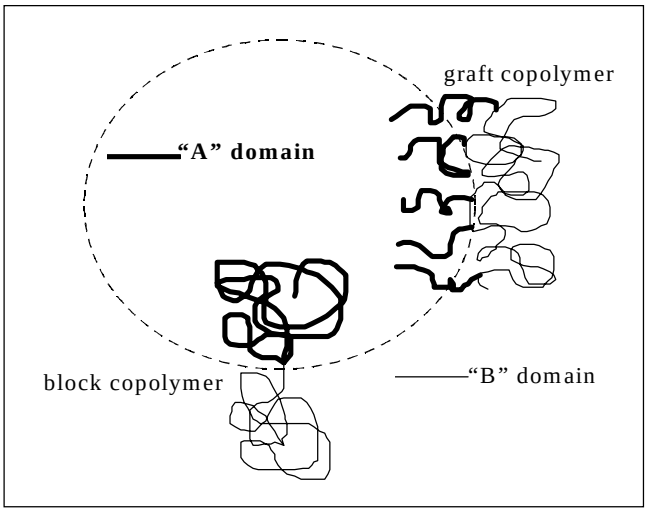

Figure 2-16. Compatibilization mechanism of block and graft copolymers.

Block copolymers consist of alternating sections of two or more monomers. Figure 2-16 shows a diblock copolymer consisting of repeat units A and B. In a graft copolymer the chain backbone consists of one repeat unit with one or more grafts of a second repeat unit branching off the backbone. If the composition of these copolymers is such that each of the repeat units involved is chemically compatible (or identical) with a phase in the blend, the copolymers will tend to congregate at the domain interfaces with the orientation shown in Figure 2-16. This action allows entanglements between the copolymer and each phase, thus strengthening the bond between the two phases, lowering interfacial tension, and creating smaller domain sizes. Numerous blends of otherwise incompatible polymers have been formed and studied using this method. To be effective the block or graft copolymer must be located at the domain interface.

While thermodynamics may dictate such an arrangement, the process of migration to the interface may be limited kinetically. Even in the melt, macromolecules are much less mobile than smaller molecules. Also, considering the relatively short time span most materials spend in the melt state when being processed, it easy to imagine that the copolymers may not have sufficient time to diffuse to the interfacial region in most applications. This problem can be circumvented if the copolymer is formed in-situ at the interface.

2-5-3. In-situ compatabilization of polypropylene, nylon-6 blends.

The in-situ formation of a block or graft copolymer in polymer blends is often accomplished by using two mutually reactive species to form the copolymer under the elevated temperature and mobility conditions of the melt. To provide reactive sites, a functionalized version of one of the components is often added

to the blend. This functionality should be capable of under going a reaction with the other species, while not being so heavily functionalized that it becomes incompatible with its parent polymer. An excellent example of such a system was used in this study. The compatabilization of nylon-polypropylene blends using a maleic anhydride functionalized polypropylene has been studied by numerous researchers. A portion of this work is summarized below.

2-5-4. In-situ compatabilization of polypropylene, nylon-6 blends - chemistry.

It is generally believed that the reaction between the maleic anhydride (MA) grafts and the nylon-6 (N6) occurs at the amine ends of the N6 chains when in-situ compatabilization is occurring in the melt. To help visualize this, the chemical structures of the materials involved are given below in Figure 2-17.

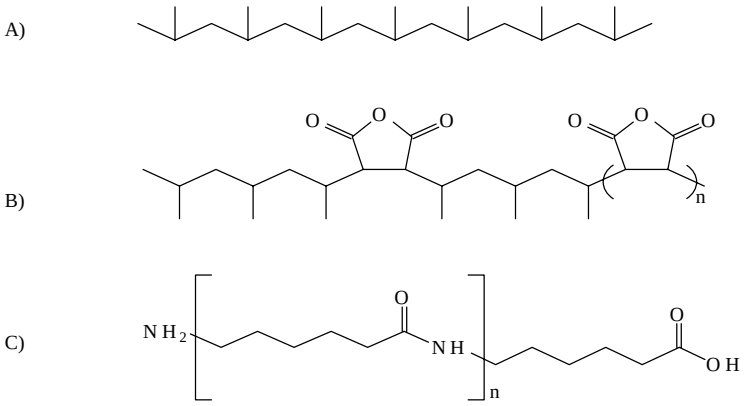

Figure 2-17. Chemical structures of materials used in blend systems: A) polypropylene, B) maleic anhydride functionalized polypropylene, C) Nylon-6

It should be noted that the structure presented for the maleic anhydride functionalized polypropylene (PP-g-MA) represents a possible arrangement of the maleic anhydride groups. The exact location and distribution of the groups is still the subject of debate. The likely mechanism for copolymer formation will consist of the following steps as shown in Figure 2-18.

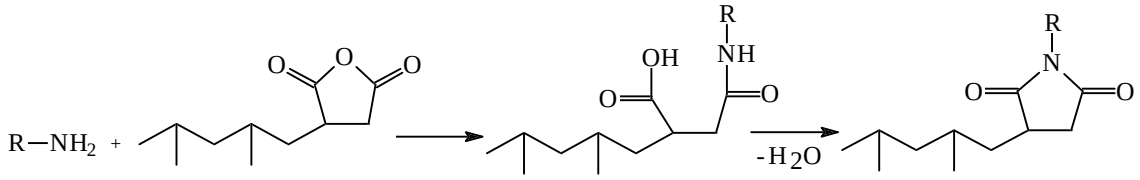

Figure 2-18. Formation of copolymer and possible ring closure.
According to Al-Malaika (ref. 28), the second reaction in this sequence is likely to occur due to the high temperatures (> 200°C) in the melt. Direct evidence of this reaction has been difficult to obtain.

It might be inferred that the maximum ratio of MA groups to amine end groups which can react is 1:1. This is not the case. Polyamides are capable of

undergoing hydrolysis which scissions the chains, reduces molecular weight, and creates new amine and carboxyl end groups. The process of hydrolysis is illustrated in figure 2-19.

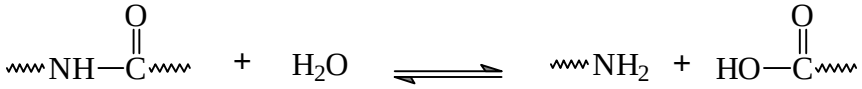

Figure 2-19. Hydrolysis equilibrium leading to chain scission and formation of additional end groups.

Through hydrolysis, the new reactive amine end groups created allow for additional linking with maleic anhydride groups. Amide groups within the chain are believed to be much less reactive than those at the chain ends. The proximity of water molecules formed in the compatabilization reaction may make this process more likely to occur near the interface between the two materials (ref. 28).

One final note should be made regarding the different behaviors of asymmetric (N6) versus symmetric nylons (N6,6) during compatibilization with PP-g-MA. It has been by Paul and coworkers that a symmetric nylon chain may form two grafts with PP-g-MA while an asymmetric nylon can only form one (ref. 31). The monomers which are used to produce these polymers explain this behavior. Assymetric chains, which are formed from a single monomer, will always be produced with one amine end group. Symmetric chains, which are polymerized from diamines and dicarboxylic acids, may have two, one, or no amine end groups.

2-5-5. In-situ compatabilization of polypropylene, nylon-6 blends - properties.

One of the earliest studies of the compatabilization of polypropylene, nylon-6 blends was done by Ide and Hasegawa (ref 21). Blends were prepared in an extruder with varying levels of PP, PP-g-MA and N6. These blends were then extracted with xylene to remove the PP portion, and the mass of the remaining portion determined. Figure 2-20 shows their results. In this plot, [N] represents the ratio of maleic anhydride groups to amino groups. It can be seen that as MA content increases ([N] increases) that the non-extractable portion of the blend increases, suggesting that a chemical link has formed between the PP-g-MA and N6 which cannot be solvated.

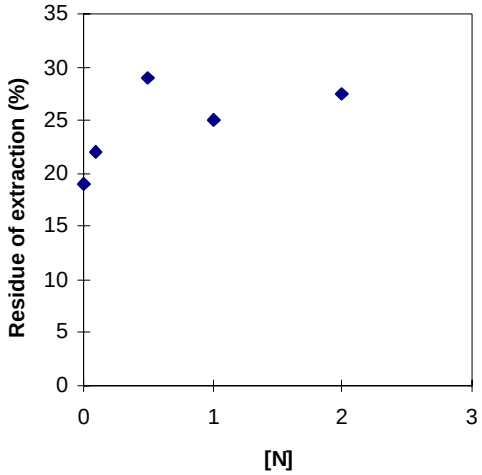

Figure 2-20. Effect of maleic anhydride content on extraction residue content (adapted from ref. 21).

The plot also shows that above [N] values of 0.5 or higher the amino end groups of N6 have effectively been saturated, resulting in a maximum in the amount of residue. Ide and Hasegawa also showed that the melt indices of the compatabilized blends were lower than non-compatabilized blends, suggesting an increase in viscosity.

More extensive characterization of the effect of copolymer formation on the viscosity of these blends has been done by Marco et. all (ref 22). In this study viscosity measurements of 70/30, PP/N6 blends were made using a capillary rheometer for various levels of MA content. Figure 2-21 gives a sampling of the results.

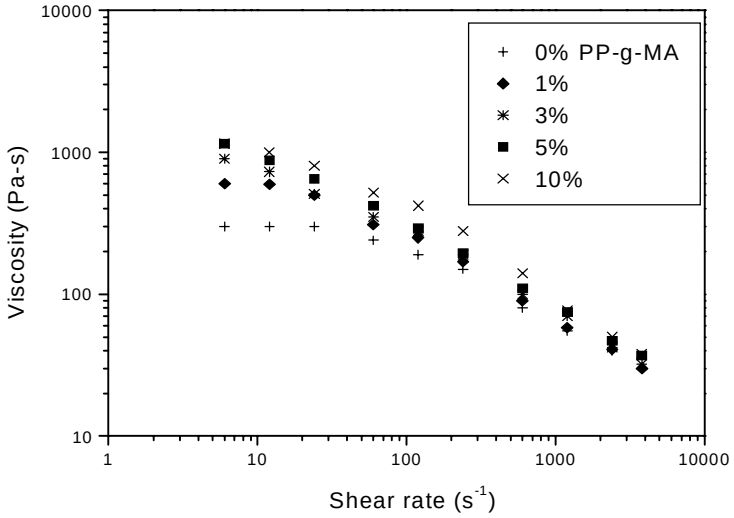

Figure 2-21. Viscous response of blends of PP/PA6 with varying maleic anhydride content (ref 22).

The viscosity of the grafted PP is typically lower than both the PP and N6 components of the blend. Therefore, if no compatabilization was occurring, a decrease in the viscosity of the blend should result from increasing the graft polymer content. The opposite effect is observed. Increasing viscosity with increasing MA content may be a function of the increased compatibility of the materials in the blend and the formation of a high molecular copolymer consisting of PP-g-MA and N6.

The mechanical properties of a blend also give an indication of the degree of compatibility between components. One such study of these effects has been done by Duvall et. all (ref 23). A blend of two incompatible materials will tend to be very brittle. A blend which shows a high degree of compatibility should display mechanical properties which are intermediate to the two materials. Figure 2-22 displays this trend.

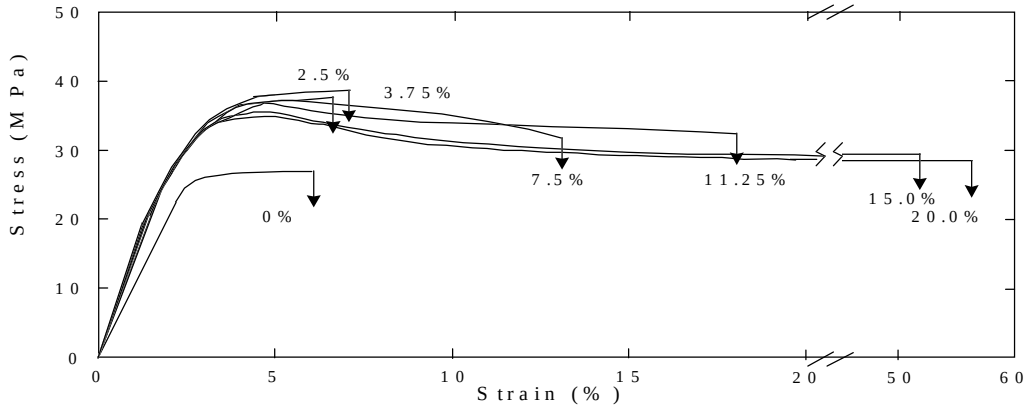

Figure 2-22. Effect of MA content on tensile properties of a PP/N6-6 blend using a PP-g-MA with "low" grafting levels - 0.2 wt% MA(ref 23).

It should be noted that this study was done with a nylon 6-6. The same general trends would be expected to hold for blends using N6 rather than N6-6. This plot clearly shows that as the compatabilizer content increases, the material fails at larger strain levels, showing a decrease in brittleness. This behavior suggests increased compatibility between the PP and N6-6 phases.

Maleic anhydride content is not the only variable which will affect the properties of these blends. The molecular weight of the grafted PP must be sufficient to allow for entanglements with PP chains. Additionally, increasing the number of grafts on the PP backbone will change the nature of the molecule. It is likely that at high grafting levels the presence of numerous polar maleic anhydride groups on the chain will cause the grafted polymer to become less compatible with polypropylene. These effects can be seen in Figure 2-23.

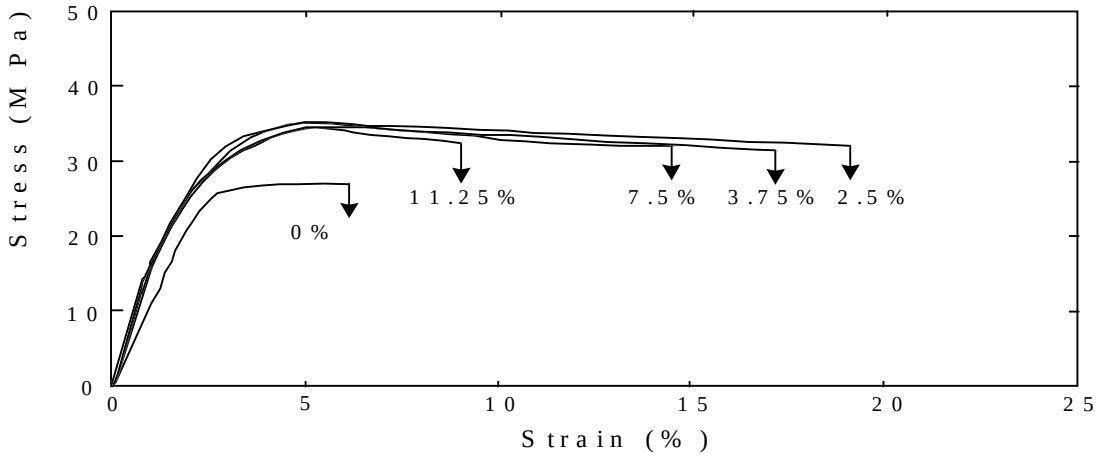

Figure 2-23. Effect of MA content on tensile properties of a PP/N6-6 blend using a PP-g-MA with "high" grafting levels - 2.7 wt% MA(ref 23).

From figure 2-23 it can be seen that the strain to break of this blend decreases as the amount of grafted polypropylene used increases, although the compatibilized blends still show larger values than the uncompatibilized blend. This trend suggests that while the graft copolymer formed does increase compatibility, the strength of the interphase between PP and N6-6 in these blends is affected by the nature of the PP-g-MA portion of the copolymer.

To this point much of the discussion has focused on indirect observations of the compatibilizing effect of the in-situ formed copolymer of PP-g-MA and N6 for compatibilizing PP/N6 blends. More direct evidence of compatablilzation is provided by microscopy studies. Paul and coworkers have done an excellent study of the effect of PP-g-MA on the morphology of PP/N6 blends (ref 24). Figure 2-24 shows Paul's results for the effect of MA content on blend morphology.

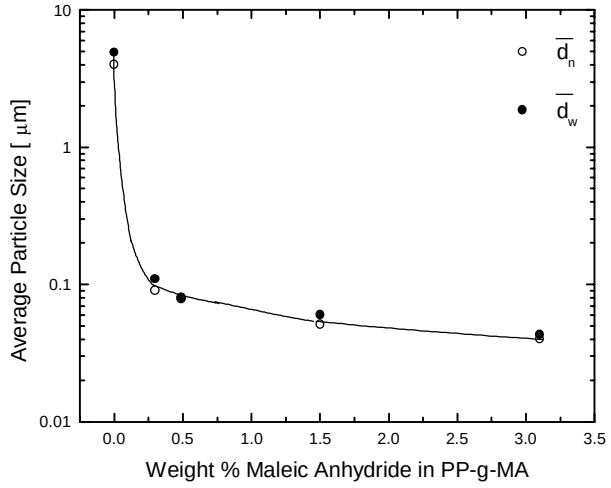

Figure 2-24. Effect of MA content on average domain size of dispersed PP-g-MA phase in a N6 matrix (ref 24).

These results are reminiscent of Ide and Hasegawa's results which also showed a plateau at high MA contents. As expected, increasing the amount of compatibilizer decreases the domain size.

Studies of the fracture toughness of the interface formed between sheets of PP containing PP-g-MA with N6 have been conducted by Boucher et. all (ref 25, 26), and Bidaux et. all (ref 27). In these studies sheets of PP and PP-g-MA were bonded to sheets of N6 at various bonding times and temperatures. A blade was then forced along the interface causing the PP and N6 sheets to separate. The force required and the size of the plastic deformation zone ahead of the crack allow calculation of the interfacial toughness. Boucher et. all has demonstrated the effect of chain mobility on copolymer formation using this method as shown in Fig. 2-25.

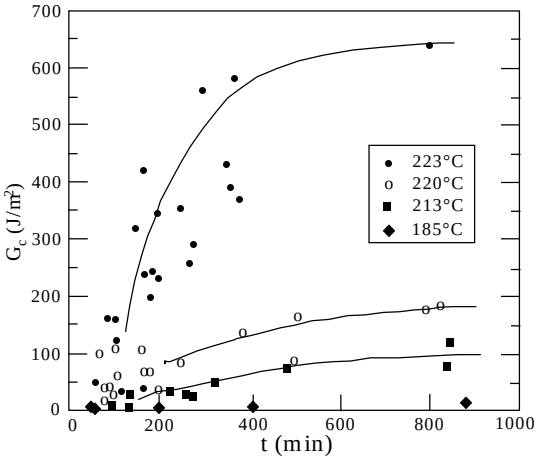

Figure 2-25. Effects of annealing time and temperature on fracture toughness, G_c, of the interface (ref 26).

Examining these results it can be seen that the greatest amount of compatibilization occurs at the highest temperature. In this plot, 223°C is the only temperature at which both the PP-g-MA and the N6 are in the melt state. Some copolymer appears to form even when only the graft polymer is in the melt state, but the formation of copolymer greatly increases when both components have increased mobility. These results suggest the important concept that compatabilization is brought about by the interdiffusion of the PP-g-MA and N6 leading to the reaction of the amine end groups with the maleic anhydride grafts and the formation of entanglements between the ends of the copolymer with each phase.

2-6. Production of Maleic Anhydride Functionalized Polypropylene.

The emphasis to this point has been on the effects of maleic anhydride content on the properties of blend systems. A brief mention has been made regarding

the effects of PP-g-MA structure on blend properties. A short discussion of the method used to produce PP-g-MA may shed some light on a weakness of this compatabilization approach.

There are three reported methods for the production of PP-g-MA: solid state reaction, solution grafting, and melt grafting. The most commonly used method commercially is melt grafting. In this process polypropylene, maleic anhydride and an organic peroxide are simultaneously processed through an extruder. Heat inside of the extruder leads to the thermal decomposition of the peroxide, forming radicals. These radicals may then abstract a tertiary hydrogen atom from polypropylene forming a macro-radical. This macro-radical may react with a maleic anhydride or lead to chain scission of the polypropylene. Unfortunately, the chain scission reaction is very fast. It is for this reason that the production of PP-g-MA involves a large reduction in molecular weight of the starting PP. In a study by De Roover et. all (ref. 29) the degradation of PP during the melt functionalization process was followed as shown in Figure 2-26.

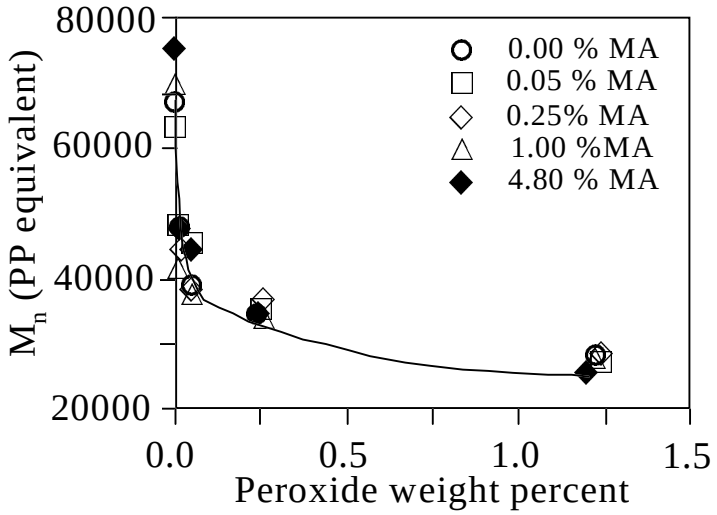

Figure 2-26. Change in M_n as a function of peroxide and MA content (ref. 29).

Increasing levels of peroxide are necessary to increase the amount of maleic anhydride grafted to the chain. Therefore, increasing maleic levels will lead to larger amounts of degradation, resulting in a low molecular weight material.

The exact mechanism of graft formation after radical production is still being debated, as is the exact nature and location of the maleic anhydride grafts along the backbone. There are conflicting views among researchers whether or not maleic anhydride may homopolymerize under melt reaction conditions to form short oligomeric grafts. De Roover et al. has presented evidence suggesting that homopolymerization is possible (ref. 30). Further work needs to be done in this area to determine the location and nature of the grafts as they have a profound effect on the compatibilization product.

3. Experimental

3-1. Materials

Materials from several different suppliers were used in this study. Nylon-6 was purchased from BASF, grade BS300 ([η] = 2.7 dL / g in sulfuric acid, 25°C). BASF 700D, a high amine end content nylon was also used in limited amounts. Non-functionalized polypropylene of 18 melt flow index (ASTM D1238 - 230°C / 2.16 kg) was obtained from Aristech. In a few instances, 12 and 35 melt flow index (ASTM D1238 - 230°C / 2.16 kg) Aristech polypropylenes were also used. Maleated polypropylenes were obtained from a number of industrial suppliers. The exact products used cannot be specified for proprietary reasons therefore these materials will be referred to using PP-MA-#, in which each material has its own unique number to be used consistently throughout. All of but one maleic

anhydride material was polypropylene based, PE-MA represents a polyethylene based material.

Color was incorporated into the fibers using CAMAC standard materials for both polypropylene and nylon-6. The exact composition of these materials cannot be disclosed. The color component was hopper blended in pellet form with the other materials prior to spinning. The coloration used consists of inorganic pigments with a suitable carrier for incorporation into the nylon-6 or polypropylene phases

During the production of polypropylene sheath fibers Lurol 6468 spin finish was used. In the production all other fibers Lurol nfs5338 (a nylon spin finish) was used. These products were obtained from Goulston Tech.

3-2. Materials Handling

The following information pertains to spinning operations. Nylon-6 was obtained directly from the supply used at CAMAC for daily spinning operations. Moisture contents were kept below 600 ppm. Non-functionalized polypropylene materials were stored under warehouse conditions with no special precautions. Functionalized polypropylene materials were stored in heat sealable lined bags to prevent moisture uptake.

In laboratory experiments, nylon-6 and functionalized polypropylenes were stored under vacuum with desiccant. Any further conditioning steps for a given experiment will be addressed with the discussion of the particular experiment.

3-3. Fiber Spinning

All fibers were spun on CAMAC's bicomponent spin line. The spinning equipment consisted of two extruders each of 1" diameter and L/D ratio of 30. Each extruder fed a metering pump which was followed by a six element static mixer. The two streams were routed through a temperature controlled head block, and then into the spin pack. The spin pack, purchased from Hills Inc., produced 64 filaments. Replacement of flow plates and the spinneret face allowed the production of fibers of circular or trilobal cross-section with side by side, core - sheath, or off center core - sheath configurations. Upon exiting the spinerette the fibers were subjected to an air quench, and descended the stack, approximately 15 feet. Prior to the first godet, one of the above mentioned spin finishes was applied. The first godet served to tension the fibers descending the stack while the next two godets were used to draw the fibers. A draw ratio of 3:1 was utilized. Finally, the fibers were taken up on a winder. The line was capable of throughputs of approximately 14 kg/hr. The target size for fibers produced was 10-12 denier. Fibers used in carpet samples were texturized in a

separate step prior to tufting using a Hills draw texturing machine. No additional drawing was incorporated in this step, but the fibers were crimped and air tacked together.

3-4. Compounding

In all cases the color component was blended in pellet form with the nylon or polypropylene in the respective extruder's hopper. In most instances, the functionalized polypropylene was also hopper blended in pellet form with the non-functionalized polypropylene. Some runs were conducted, and blends prepared for other tests, by first melt mixing the two polypropylene based components. This blending was done using an APV twin screw extruder (19mm screws, 3 kg / hr capacity), whose extrudate was pelletized.

3-5. Optical Microscopy

Cross sections of fibers were obtained using a Hund Wetzlar optical microscope and the following procedure. An entire fiber bundle was wrapped several times around a c-shaped metal block and taped into place. A second c-shaped block was then placed along the first such that a block with the fibers running through the center was formed. These two halves served as a mold and were secured together with a rubber band as shown in Fig 3-1.

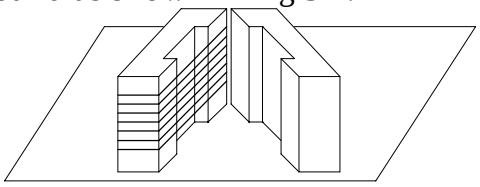

Figure 3-1. Schematic of mold used to mount fiber bundles in wax prior to cross-sectioning.

A mixture of 70% paraffin canning wax and 30% Eastotac® (a hydrocarbon wax from Eastman Chemical Co.) at 65°C was poured into the mold, filling the cavity. The wax was allowed to cool and then removed from the metal blocks, leaving a wax cube with fibers running through the center. This block was then microtomed at room temperature into sections approximately 10 microns thick. These sections were placed on glass slides, heated to melt the wax, cooled, and then dipped in Varsol (a combination of hydrocarbon based solvents produced by Exxon), just prior to observation under the microscope. The heating step served to secure the sections to the glass slide while the Varsol was used to temporarily solvate the wax so that it would be transparent under the microscope. A video capture system allowed micrographs of the cross-sections to be recorded.

3-6. Capillary Rheometry

A Kayeness Inc. capillary rheometer was used to obtain rheological data of the process materials and blends. The data obtained was not Bagley corrected as only one die (L / D = 20) was available. However, the data was Rabinowitsch corrected. After loading, the pellets were held in the barrel for three minutes to allow complete melting. After this time the plunger began its descent providing two measurements at each shear rate. All rheometer experiments were conducted twice to check for consistency. Some difficulty was encountered in measuring the viscosity of the high maleic content materials (PP-MA-2 and PP-MA-3), due to their extremely low viscosity at the temperatures of interest. The moisture content of nylon materials was determined prior to rheometry experiments using CAMAC's in house vapor pressure test method.

3-7. Compression Molding

A Dake hot press was used to prepare films for use in DSC and mechanical testing experiments. Films were produced by placing pellets between a sandwich consisting of two metal shims, two teflon sheets, and a picture frame type mold. The pellets were allowed to completely melt prior to the application of pressure. The time and temperature of molding varied depending on the experiment (usually 3-5 min. at 200 - 260°C) but the pressure was consistent at 5,000 psia. Films were removed from the press and allowed to air cool. These films would then be stored under vacuum with desiccant or conditioned as desired.

3-8. Differential Scanning Calorimetry (DSC)

A Seiko systems model 220 DSC was used to characterize the crystallizability of the materials used. A typical experiment used a nitrogen purge, a heating rate of 10°C / min, and a sample size of roughly 10 mg. Samples were cut from previously prepared compression molded films as described in section 3-7, and placed in sealed aluminum pans. It was assumed that the heat of fusion of polypropylene was not affected by the presence of maleic anhydride groups, a value of 209 J / g was used (ref.78).

3-9. Scanning Electron Microscopy (SEM)

SEM micrographs were obtained using a Cambridge Stereoscan 200 with an accelerating voltage of 15 kV. Samples were sputter coated with a layer of gold approximately 15 nanometers thick. Micrographs of fracture surfaces were obtained for two sets of conditions, room temperature fractures from Instron

tested specimens, and samples hand fractured after 15 minutes submersed in liquid nitrogen.

3-10. Tensile Testing

The mechanical properties of films prepared with blend compositions similar to those used in fiber production were investigated using an Instron model 4400R**.** Various testing rates were experimented with, the most common being 10mm / min. Ten to twelve samples were tested for each composition. Dog bone specimens were prepared from films produced via compression molding. These films were cut into the appropriate shape using a dog bone shaped die and press. In some mechanical tests the films were first heated to 115°C to soften the material prior to cutting. This was done because blends with a high content of PP-MA-2 were very brittle at room temperature, making the cutting of specimens impossible without producing cracks. When this was done, all materials, regardless if they were brittle or not, were also heated to 115°C prior to cutting to provide all samples with identical thermal histories. All dog bones were kept under laboratory conditions at least 24 hours prior to testing.

3-11. Thermogravimetric Analysis (TGA)

TGA analysis was performed using a Seiko systems TG / DTA 220 to provide a first check for material degradation. It was feared that the maleated polypropylenes may not be thermally stable at the temperatures required to process nylon. Isothermal experiments at 255°C were conducted under both air and nitrogen atmospheres. Experiments from room temperature to 450°C, ramped at 10°C / min were also conducted under air and nitrogen atmospheres.

3-12. Wide Angle X-Ray

X-ray diffraction patterns were obtained to verify that both components of the fiber were crystallizing and under going some orientation during the spinning process. A fiber bundle was aligned so that all fibers were parallel with the fiber axis vertical. A Warhaus camera was used to expose x-ray film with CuKα radiation (λ=1.54Å) at 40 kV for three hours at room temperature. Positives were developed and are presented as data.

3-13. Fourier Transform Infrared Spectroscopy (FTIR)

FTIR experiments were conducted on a Nicole 510 FT-IR spectrometer to verify the differences in maleic content levels among materials and to prove that maleated polypropylenes do indeed take up moisture from their surroundings. Films were prepared of approximately 1 micron in thickness. Each scan represents 200 samplings, and scans were produced in duplicate. No corrections

for water or carbon dioxide have been made to the spectra. That is, the data is essentially raw with only the background subtracted out.

3-14. Carpet Production

Carpet samples were tufted by an outside firm using fibers spun at CAMAC. The carpets were made from a minimum of five pounds of fiber and were supplied in strips approximately 2 feet wide and 10 feet in length. The carpets are a single level loop pile construction with a polypropylene backing, and a face material density of approximately 20 oz./yd^2.

3-15. Wear Testing of Carpet Specimens

Wear tests were conducted by CAMAC to qualitatively determine the degree of adhesion between the components and the suitability of the fibers as carpet material. A rectangular sample of carpet 25.5" by 8.25" was cut. This sample was used to line the inside of a drum, into which a hexapod (heavy metal object with six rubber "feet") was loaded. The drum was then rotated 50,000 times to simulate the conditions of foot traffic, under accelerated conditions. The sample was removed, vacuumed, to remove loose material, and then visually evaluated. Photographs of samples were taken to provide a permanent record of the results.

3-16. Acid Red Stain Testing

To test the resistance of the fibers to acidic stains, CAMAC conducted acid stain tests. An acidified solution of red dye was prepared using the following quantities of materials; 0.10g of FD+C (Food, Drug and Cosmetics) red #40 was added to 1000 ml of distilled water. Citric acid was then added to produce a pH of 2.8 (approximately 0.55g). A 2" diameter ring was placed on the carpet and filled with 20 ml of the solution, which was then worked into the carpet. The stain was allowed to set for 24 hrs. prior to washing with water. After the carpet was rinsed to a point where wash water appeared clear, the carpet was cleaned with an extraction vacuum cleaner and then allowed to dry for another 24 hrs. After this time the sample was visually inspected. Photographs of samples were taken to provide a permanent record of the results.

3-17. Coffee Stain Testing

Carpets were stained with coffee, by CAMAC, to evaluate their coffee stain resistance. A coffee solution consisting of 60 g of Ultra Roasted Decaffeinated Folgers ground coffee was added to 1000 ml of tap water. The coffee was brewed between 165-180°F in a coffee maker, at which point 20 ml was applied to the carpet specimen. The rest of the test procedure is identical to section 3-16, acid red stain test.

4. Results and Discussion

This chapter is divided into sections which roughly follows a chronological description of the work completed. The chapter begins with a discussion of some the difficulties encountered in the spinning of bicomponent nylon - propylene fibers, and the work done to understand the processing (extrusion conditions) and material characteristics (rheology and thermal stability) required to produce such a fiber. Further concerns of the suitability of materials used in this project for carpet applications (crystallizability and mechanical properties of blend systems) are then discussed. Finally, data from wear and stain testing of carpet samples are presented and the results are discussed in terms of the properties which were elucidated in previous sections.

4-1-1. Production of bicomponent fibers - side by side fibers

Though the eventual goal of this research was to produce a core-sheath bicomponent fiber of nylon-6 and polypropylene, initial processing runs were

done to produce bicomponent fibers of a side by side configuration. The reason for this decision was two fold. Due to the inherent lack of symmetry of the side by side configuration in comparison to that of a concentric core-sheath fiber it was felt that any problems which may arise from the mismatch of material viscosities would be amplified and thus easier to study in a side by side fiber. This was proven to be the case as the data which follows will indicate. Secondly, the hand drawing and cross-sectioning of side by side fibers allowed for a rapid and direct indication, via the observation of fiber splitting, of the relative quality of adhesion between the nylon-6 and polypropylene phases.

4-1-2. Production of Bicomponent Fibers - Extrudate exit angle

A value of four is commonly quoted as the maximum viscosity ratio, at a particular shear rate, under which bicomponent spinning may be achieved. This relationship was found to hold for the materials and processing conditions used. Table 4-1 provides the typical operating conditions used in the production of fibers. Table 4-2 lists the typical drawing conditions used. All fibers described from this point on should be considered to have been produced under these conditions unless stated otherwise.

Table 4-1. Typical bicomponent fiber processing conditions.

	Nylon extruder	Polypropylene extruder
Pressure	1000 psia	1000 psia
Metering pump speed	20.5 rpm	20.5 rpm
Barrel temperature- zone 1	243 °C	221 °C
Barrel temperature- zone 2	243 °C	221 °C
Barrel temperature- zone 3	249 °C	238 °C
Barrel temperature- zone 4	249 °C	238 °C
Head block*	260 °C	260 °C

* Head block is common to both extruders

Table 4-2. Typical bicomponent fiber drawing conditions.

Godet	Speed	Temperature
Denier	726 rpm	no temp. control
Draw roll 1	750 rpm	38 °C
Draw roll 2	2,250 rpm	26 °C

From table 4-1 it can be seen that the melt streams within the spin pack should be in the neighborhood of 260 °C. Figure 4-1 provides capillary rheometry data of several of the materials used in fiber production at 254 °C.

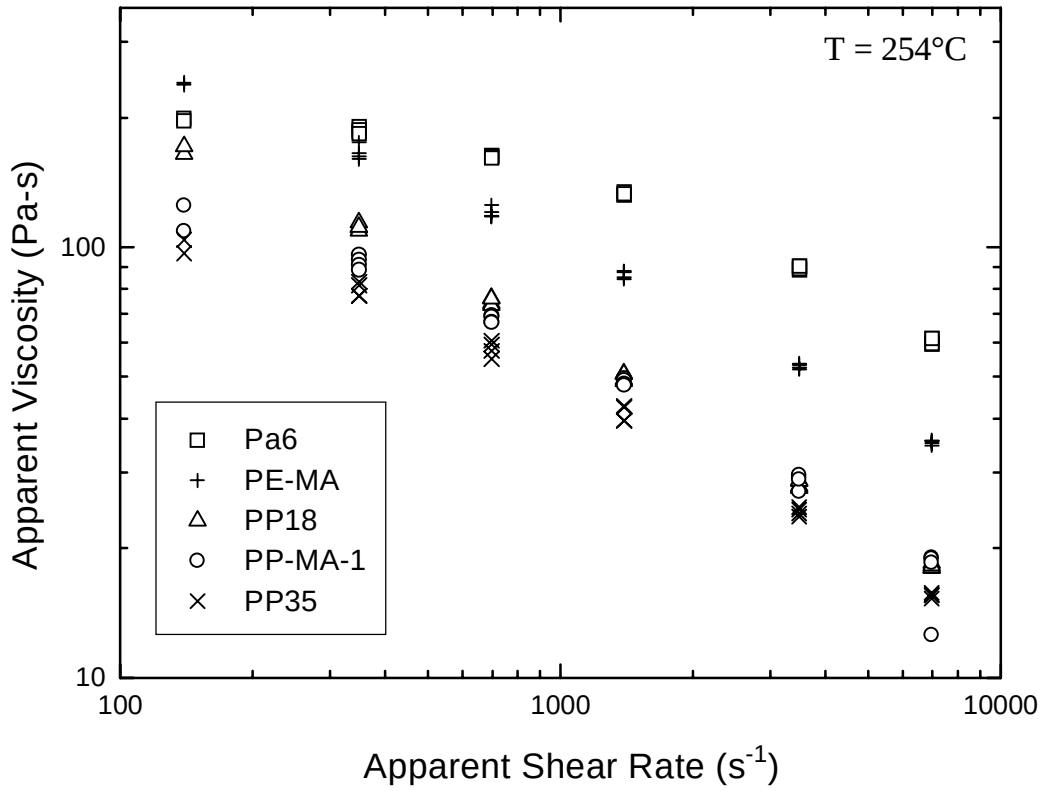

Figure 4-1. Capillary rheometry data of various process materials utilized, as determined at 254°C.

From the capillary rheometry data presented in Fig 4-1, it can be seen that at 254°F, the viscosity of nylon-6 (PA6) is substantially greater than most of the materials used. PP18 and PP35 are 18 and 35 melt flow index polypropylenes respectively. This terminology for non-functionalized polypropylenes will be used throughout this section. PE-MA refers to an ethylene based maleic anhydride grafted copolymer while PP-MA-1 refers to a polypropylene based maleic anhydride grafted copolymer. An estimate of the shear rate at the wall of the spinneret capillary based on the material throughput yields a value of 4,840 s^{-1}. Thus, comparing viscosity values at this shear rate in Fig 4-1 for PP-MA-1, 21 Pa-s, and nylon-6, 75 Pa-s, yields a ratio of 3.57, which falls within the bounds of a 4 to 1 viscosity ratio. For the spinning of these materials in a side by side configuration, a substantial amount of dog-legging (non-zero extrudate exit angle) was observed. However, the angle of exit was not so severe as to produce problems with material touching the face of the spinneret upon exit. This viscosity ratio does, however, provide an approximate bench mark found in this study. Viscosity ratios substantially larger than this were impossible to spin due to excessive dog-legging. Viscosity ratios slightly larger than 3.57 were found to be problematic at times, suggesting that this value represented the edge of the processing envelope for this bicomponent system.

Care should be taken when considering the above rheometry data in relation to the quoted value of the spinneret shear rate. The capillary region of the spinneret is much shorter than that used in a capillary rheometry experiment. Also, the entrance of the capillary in the spinneret is the sight of two converging melt streams which provides an added complication. It is very likely that the polymer melt exiting the spinneret has not yet achieved a steady state flow pattern and that the entrance and exit effects may be substantial. Viscosity values which are related to the processability of these materials are only approximations to the actual conditions during spinning.

4-1-3. Production of Bicomponent Fibers - Interface movement

A second important consideration is that the above quantities are calculated for the shear rate at the wall of the capillary, the region at which the shear rate will be its greatest. Figure 4-1 shows that as the shear rate decreases, while the magnitude of the differences in viscosity may increase between the materials, the ratios of the viscosities begin to decrease. For example, at a shear rate of 140 s^{-1}, PP-MA-1 has a viscosity of 140 Pa-s, while nylon-6 has a viscosity of 200 Pa-s, leading to a viscosity ratio of 1.43. This suggests that while the outer edges of the fiber may be at the edge of the processing envelope, the interior of the fiber, where shear rates are lower, is relatively stable. A dramatic example of the importance of the varying shear rate across the capillary observed during the course of this research is shown in Fig 4-2.

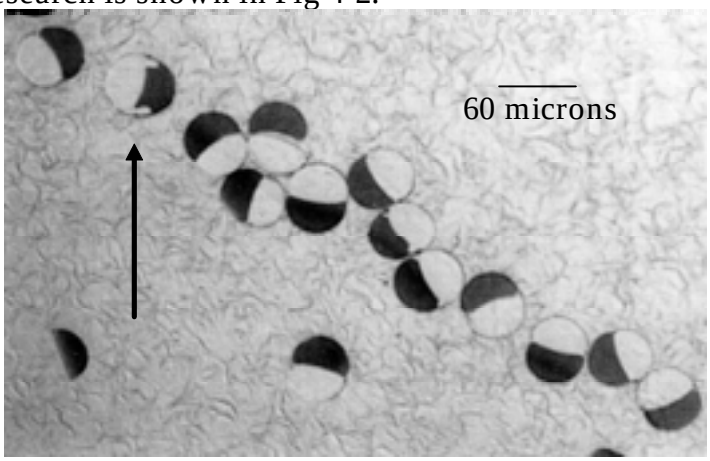

Figure 4-2. Cross section of a PE-MA / PA6 fiber demonstrating viscosity crossover.

Figure 4-2 is a typical photo of a fiber cross section used in this research. In all cases, unless specified otherwise, the darker phase of the fiber represents the nylon-6 portion. As stated earlier, colorant was added to the nylon-6 extruder during spinning to aid in the differentiation of the two phases. When referencing the composition of a fiber, the composition of each individual phase will be given, separated by a slash. Thus, Fig 4-2 of a PE-MA / PA6 fiber

represents a fiber which is 100% PE-MA in the non-nylon phase, and 100% nylon-6 in the nylon phase (the weight percentage of the colorant is not considered). Unless otherwise stated, it may be assumed that the two phases were metered at equivalent gear pump speeds. Examination of Fig 4-2 reveals that in the center of the fiber the darker phase, nylon-6, is concave. This suggests that the nylon-6 is attempting to wrap around the PE-MA, and hence must have a lower viscosity. However, this behavior is reversed at the outer portions of the fiber, where it can be observed that the PE-MA is attempting to move to the region of greatest shear suggesting that it has a lower viscosity. This behavior is referred to as interface movement. Returning to Fig 4-1, this behavior is fairly simple to explain. Comparing the viscosity curves for the two materials it can be seen that at high shear rates (corresponding to the outer edge of a fiber) PE-MA has a lower viscosity. But, at low shear rates (corresponding to the interior region of a fiber) the nylon-6 has a lower viscosity. At a shear rate of approximately 250 s^{-1} the viscosities cross over. The PE-MA / nylon-6 system was the only one observed to show this particular behavior in this study. It would be expected that two dissimilar materials would attempt to minimize the surface area of contact between themselves, and hence produce a flat interface to minimize the surface free energy. However as Fig. 4-2 shows the driving force to minimize the interfacial surface free energy is dominated by the system's desire to flow in the lowest energy state possible. That is the state in which the least amount of viscous dissipation occurs. The phenomena of interface movement was observed in most other fibers produced with a side by side configuration to some degree. Figure 4-3 represents a typical example.

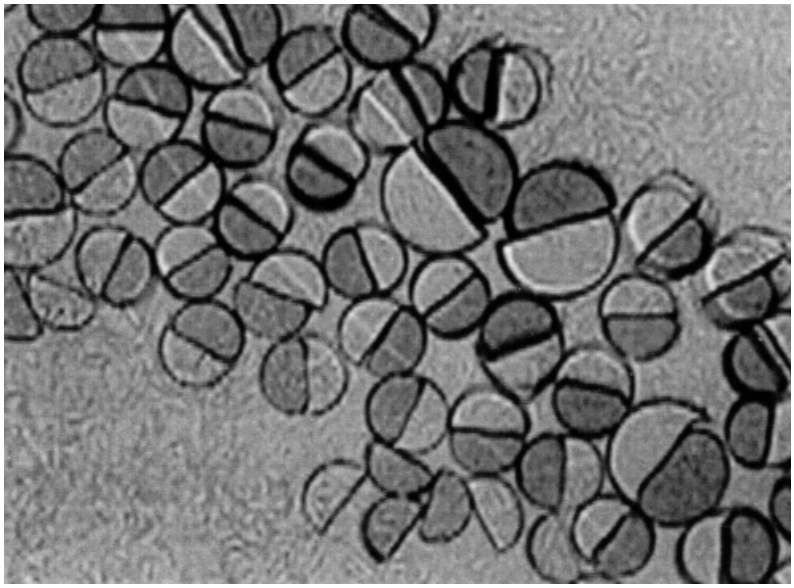

Figure 4-3. Typical level of interfacial rearrangement during side by side spinning. Fiber shown is 90%PP18, 10%PP-MA-1 / PA6.

The magnitude of the rearrangement in most cases was not large, probably due to the shortness of the spinneret capillary which gives the material very little time to reposition. In the spinning of a round core-sheath fibers, interface movement was not a problem because the lower viscosity component was the sheath material, as shown in Fig 4-4. From Fig 4-4 it appears that visually there is a degree of "square" character to what should be circular fibers. It is believed that this is further evidence of the relatively short time span in which the material is given to rearrange or possibly in this case, relax. The nature of the spin pack design is such that the sheath is deposited around the core at four points along the core's periphery, thus forming the apparent four corners of a square.

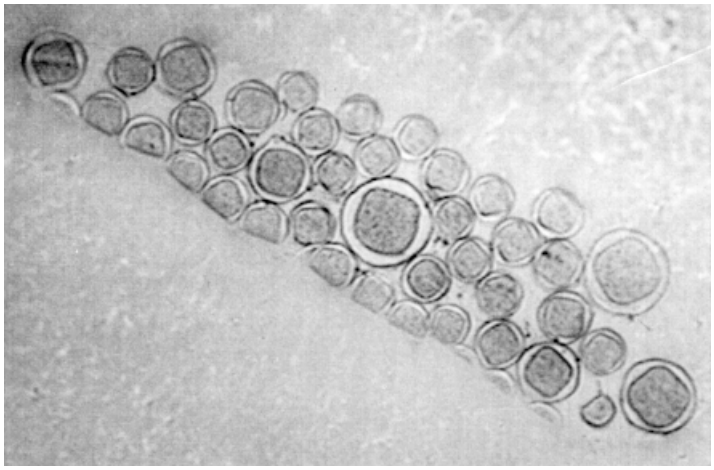

Figure 4-4. Typical configuration of a core-sheath fiber spun with the lower viscosity component as the sheath. The fiber shown is a 60% core of PA6 / 40% sheath of 33%P18, 67% PP-MA-1.

In a few instances the higher viscosity component was spun as the sheath material, with no interface movement as shown in Fig 4-5. Again, this is likely due to the short length of the capillary section. Once the importance of matching the viscosities was understood at the beginning of the research, few problems with regards to dog-legging or interface movement were encountered. The only additional problems occurred when the viscosity ratio was pushed to the limits in an attempt to produce a polypropylene component with as high a maleic anhydride content as possible.

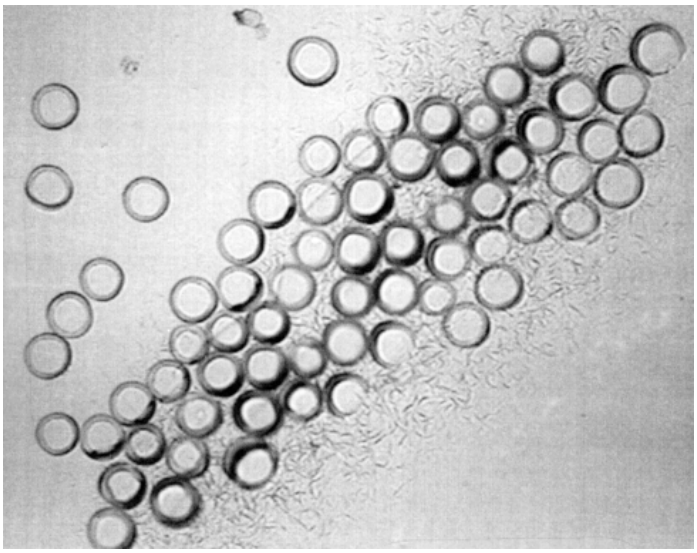

Figure 4-5. Typical configuration resulting from a core-sheath fiber spun with the lower viscosity component as the core. The fiber shown is a 60% core of 33% PP18, 67% PP-MA-1 / 40% sheath of PA6.

4-1-4 Additional Rheology

Figure 4-1 presented data for many of the materials studied during the course of the research. Early during the project PP35, due to its low viscosity, was dropped from the list of possible materials in favor of PP18. Even though PE-MA showed favorable rheology, it too was dropped from the project because it is an ethylene based material. It was felt that the blending of polyethylene and polypropylene would add complexity and have insufficient mechanical properties at the elevated temperatures occasionally experienced in a carpeting application. Often times the heat build up beneath the casters of a chair due to friction may raise the temperature enough locally to be problematic even for polypropylene fibers. While the PP-MA-1 material displayed acceptable properties, in an effort to better the economics of the fiber, cheaper maleated materials were sought. Maleated polypropylenes from several different suppliers of a lower cost were obtained: PP-MA-2 ,PP-MA-3, PP-MA-4, PP-MA-5, and PP-MA-6. Each of these maleated polypropylenes is produced via the same reactive extrusion process that was described in the introduction. Thus, increasing maleic contents lead to decreasing molecular weight in these materials. The one possible exception is the PP-MA-1 material which is believed to be functionalized in a solution grafting process, allowing it to retain a larger molecular weight and contain high amounts of grafted maleic anhydride. Figure 4-6 contains the rheology of the maleic anhydride functionalized materials; PP-MA-1, PP-MA-3, and PP-MA-2. Special care should be taken when interpreting the data in Fig. 4-6. Due to their very low viscosities, the PP-MA-2 and PP-MA-3

materials could not be tested at the same temperatures as the other materials. Therefore, the data presented in Fig. 4-6 was taken at a temperature 64°C lower. As stated above, the melt functionalized materials are expected to be of a lower molecular weight due to the degradative nature of the melt grafting process, this is shown by their very low viscosities. Also indicative of low molecular weight materials is the extension of the Newtonian plateau to greater shear rates. This behavior can also be noted in the melt functionalized materials.

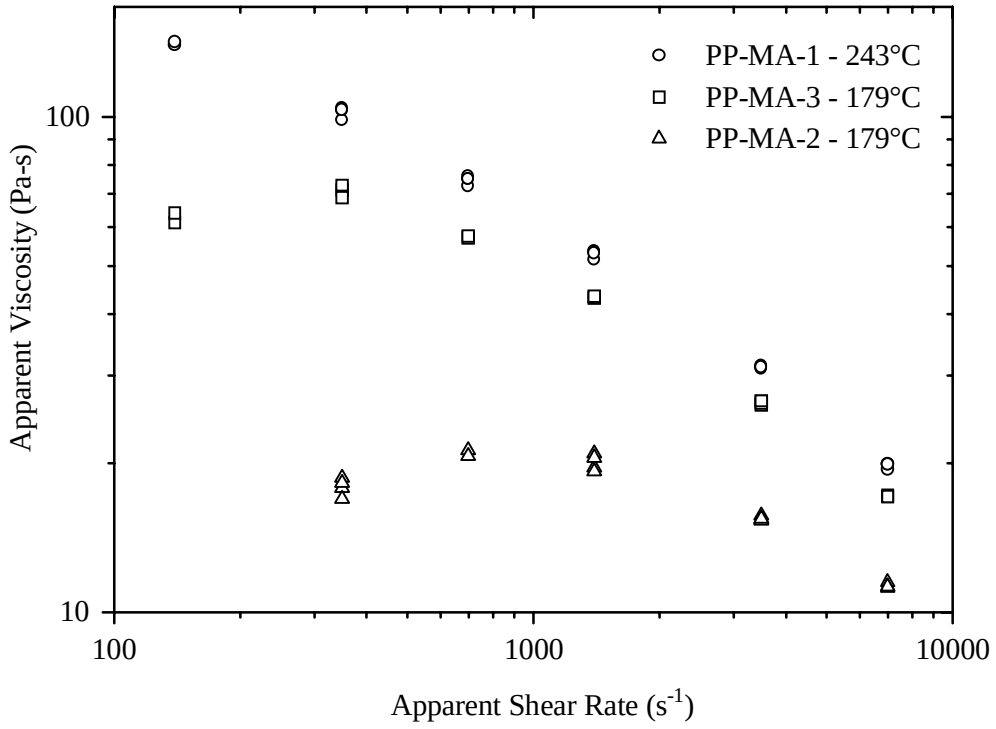

Figure 4-6. Capillary rheometry data of selected maleated polypropylenes. Note that data for PP-MA-2,3 materials was obtained at 179°C in comparison to 243°C for the PP-MA-1 material.

Additional information can be extracted from the rheometry data if one compares viscosity values for a material at a fixed shear rate for varying temperatures. This analysis will yield the activation energy for flow at that shear rate, giving an indication of the temperature dependence of the viscosity. In most instances this analysis is conducted within the Newtonian plateau region. But, because the Newtonian range of shear rates is not encountered in this project, higher shear rates were used and thus shear rates corresponding to the non-Newtonian region were analyzed. Values of the activation energy were found at shear rates of 140 s^{-1} and 6980 s^{-1}. Figures 4-7 and 4-8 contain additional capillary rheometry data taken at temperatures complimentary to fig 4-1, 243°C and 266°C respectively.

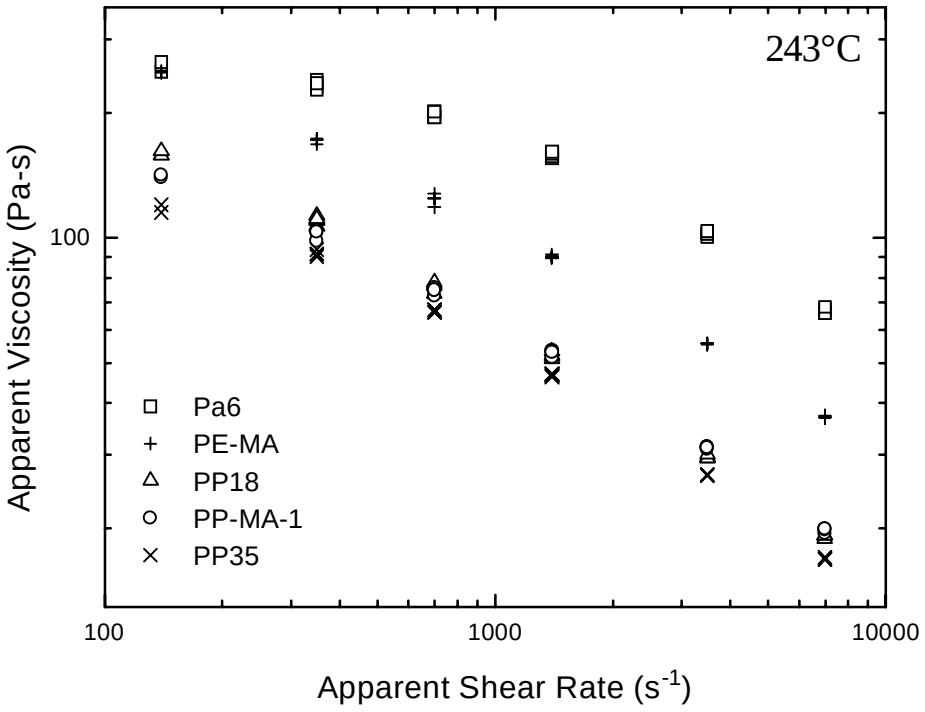

Figure 4-7. Capillary rheometry data of selected process materials at 243°C.

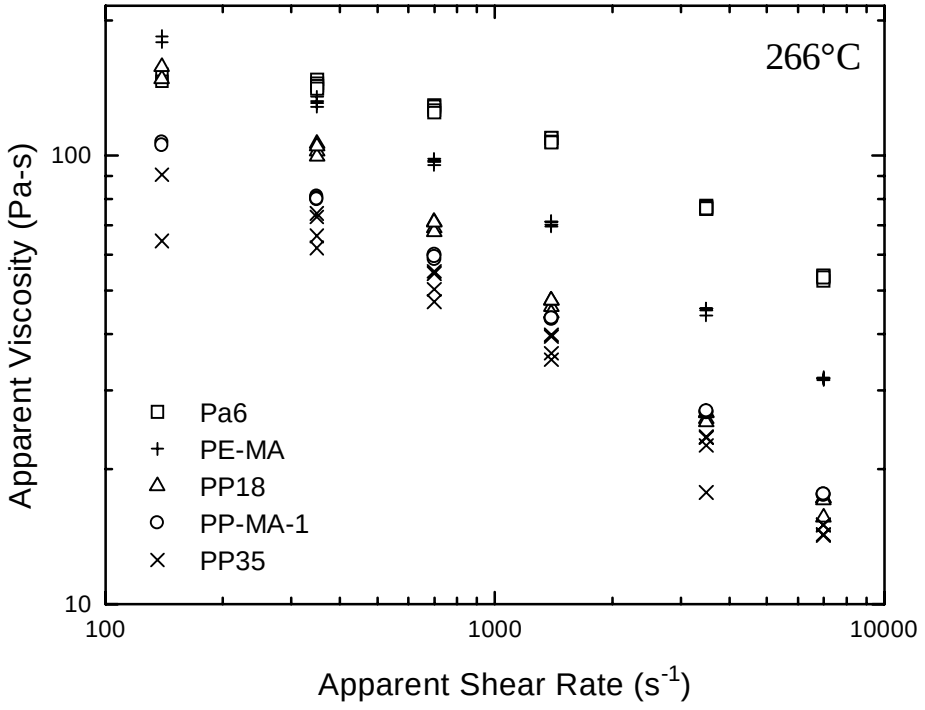

Figure 4-8. Capillary rheometry data of process materials at 266°C.

Using the rheological data from Figs 4-1,7, and 8 activation energy plots can be plotted, as shown in Fig. 4-9. Figure 4-9 is the plot used to obtain the activation

energies at a shear rate of 6,980 s^{-1}. Figure 4-10 contains the data used to determine activation energies at a shear rate of 140 s^{-1}.

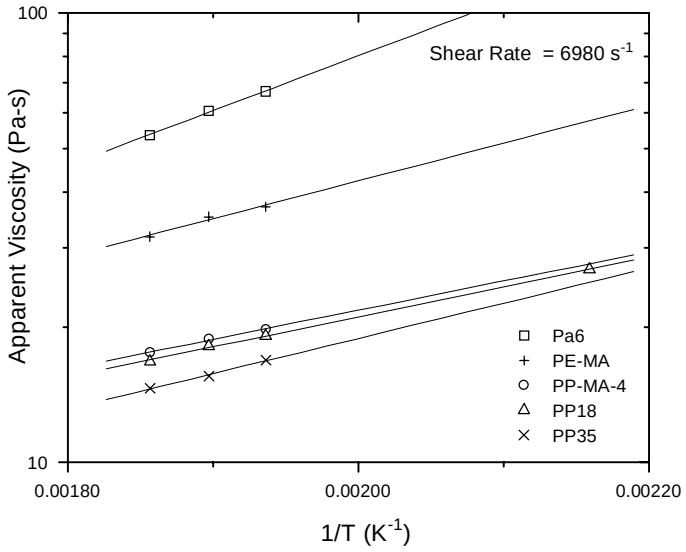

Figure 4-9. Plot used to determine the activation energy of flow at a shear rate of 6980 s^{-1}.

The temperature range over which this data spans represents only 22°C, with the exception of the PP18 which contains an additional data point at 190°C.

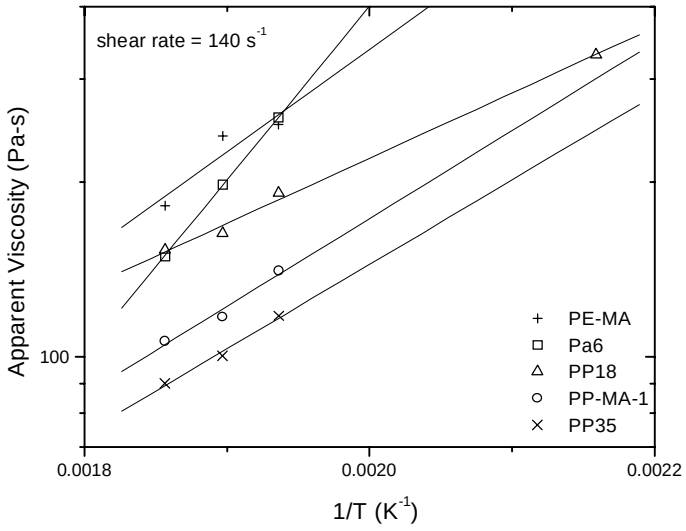

Figure 4-10. Plot used to determine the activation energy of flow at a shear rate of 140 s^{-1}.

Slight amounts of scatter can be seen in the data for the lower shear rate plot at 140 s^{-1} which may affect the results, though the 6980 s^{-1} shear data follows the

appropriate linear response. Table 4-3 summarizes the results of estimating the flow activation energy from these plots.

Table 4-3. Summary of flow activation energy data at two shear rates (6,980 s^{-1} and 140 s^{-1}) for process materials.

Material	Flow activation energy Shear rate = 6,980 s^{-1}	Flow activation energy Shear rate = 140 s^{-1}
Pa6	2.4 kcal / mol	5.9 kcal / mol
PP18	1.3 kcal / mol	2.2 kcal / mol
PP35	1.5 kcal / mol	2.8 kcal / mol
PE-MA	1.7 kcal / mol	3.5 kcal / mol
PP-MA-1	1.3 kcal / mol	3.0 kcal / mol

The most obvious trend from the data shows that at higher shear rates the viscosities of the materials become less sensitive to changes in temperature, as typical for non-Newtonian materials. Additionally, it can be seen that nylon-6 is the material most sensitive to changes in temperature. Therefore, the use of temperature as a tool to better match viscosities will have more of a pronounced effect on nylon-6. It must be recalled that both polymer streams experience the same temperature within the spin pack so that their temperatures cannot be varied independently. Considering the following equations, a relationship which gives an indication of the effect of temperature on the processing envelope has been developed.

$$\eta_i = A_i \exp\left[\frac{E_i}{RT}\right] \tag{4-1}$$

η = viscosity
A = pre-exponential factor
E = Flow activation energy
R = gas constant
T = temperature
i = n for nylon-6, p for propylene

At a given shear rate (at the capillary wall for example), eq. 4-1 will give the temperature dependence of each material. Knowing that the largest practical viscosity ratio for spinning fiber in this project was observed to be 3.57, the temperature boundaries for processing two materials can be determined (assuming the nylon-6 to be the most viscous component).

$$3.57 = \frac{\eta_n}{\eta_p} = \frac{A_n \exp\left[E_n / RT\right]}{A_p \exp\left[E_p / RT\right]} \tag{4-2}$$

Rearranging equation 4-2 and solving for the temperature yields eq. 4-3.

$$T = \frac{\left(E_n - E_p\right)}{R\left[\ln\left(3.57\left(A_p / A_n\right)\right)\right]} \qquad (4\text{-}3)$$

Thus, knowing the temperature dependence of viscosity for each material and the maximum viscosity ratio for spinning allows the maximum temperature for spinning to be estimated. Of course, this is a theoretical value based on the viscosity ratio alone. Other factors such as machine throughput, melt strength, and thermal stability of materials may set the practical temperature for spinning. Using DSC, the melting point of the nylon-6 used in this study, 224°C, sets a lower bound of roughly 238°C on the temperatures which may be used. The temperature of 260°C used in this study is well above this value because it represents a more practical limitation which was set by the extrusion equipment to produce an acceptable throughput. It should also be recalled that the temperature sensitivity decreases as the shear rate increases. Much of the material in the spinneret capillary will be experiencing shear rates comparable to the 4840 s^{-1} value given earlier, where the differences in flow activation energies are smaller. The use of temperature to match viscosities in this project served as fine tuning while the choice of appropriate propylene component was the most important criteria.

Flow activation energy is a property dependant on the local nature of the chain. Therefore the flow activation energy should be independent of molecular weight. Comparing, in Table 4-3, the values for PP18 and PP35, two polypropylenes of differing molecular weight, a discrepancy can be noted. Especially at the lower shear rate, a large difference exists. The reason for this discrepancy is unknown. The values for PP18 appear to be artificially low in comparison to the other polypropylene materials, PP35 and PP-MA-1.

As an aside it should be mentioned that the elongational viscosity was also observed to play an important role in the process of bicomponent fiber spinning as one would expect. It was noted that fibers consisting of a known low shear viscosity, and hence likely a low elongational viscosity, did not have sufficient melt strength to be spun into a fiber. That is to say that the tension in the spin line exceeded the stress which the fiber in melt form could withstand, leading to breakage prior to the denier roll. No specific studies of elongational viscosity behavior were conducted. These behaviors are exemplified the most by PP-MA-2 which has the highest amount of maleic anhydride grafting, and as such should have a lower molecular weight, in comparison to PP-MA-3. While the addition of maleic groups along the chain will increase the molecular weight slightly, the action of chain scission will be have a greater effect.

4-1-5. Production of Bicomponent Fibers - Spin pack hydrodynamics

Early in the project, in addition to the traditional problems associated with bicomponent spinning described above, problems were encountered in obtaining fibers of a uniform composition. Figure 4-11 illustrates the fibers resulting from this difficulty.

The use of trilobal fibers at times during this project represents a compromise between the direction of the graduate student and the industrial sponsor, who made this research possible. While the systematic study of a variable under the simplest of conditions would be ideal from a scientific stand point, this method does not necessarily provide the quickest path to proving viability. As the desired end product of this research was a bicomponent nylon-6, polypropylene fiber suitable for carpet applications (where a trilobal configuration would be beneficial), compromises were made to serve the needs of both parties. Returning to the discussion, Fig 4-11 shows two distinct populations of fibers. One population consists totally of nylon-6 material while the other consist mainly of PP-MA-1 with a small amount of nylon-6. It should be restated that this fiber was spun with equal volumetric flow rates of each material with a side by side configuration. In a process which is admittedly poorly understood by the author, the manufacturer of the spin pack, Hills Inc., suggested that this problem may arise from the improper start up of the spinning operation. Hills Inc. suggested that the flow of the lower viscosity component be established in the spin pack before introducing the higher viscosity component.

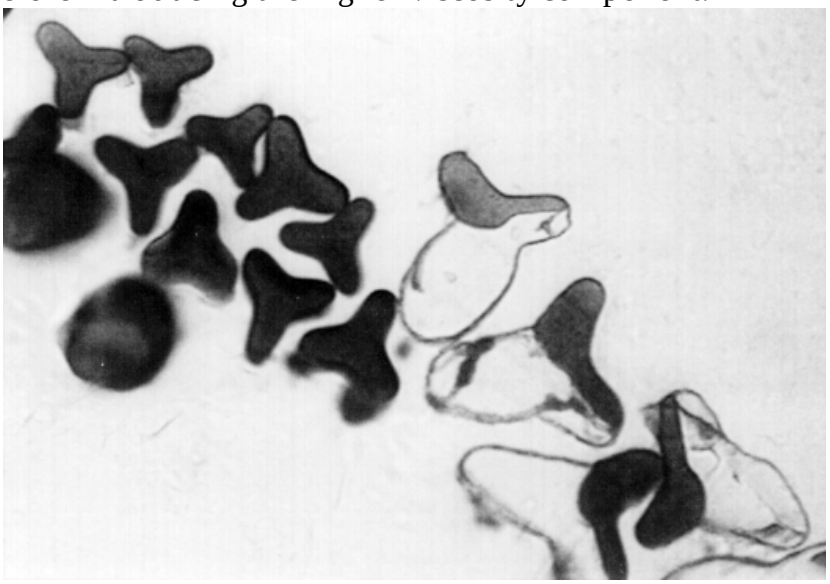

Figure 4-11. Uneven distribution of components across the spin pack. The fiber shown is a PP-MA-1 / PA6 trilobal fiber that has not been drawn.

This procedure is meant to prevent the higher viscosity component from initially "crowding out" the lower viscosity component. While the exact cause of this

problem was not determined, using the procedure suggest by Hills Inc. did alleviate the problem of uneven material distribution.

4-1-6. Production of Bicomponent Fibers - Fiber size distribution

The revised start up procedure did not alleviate all of the problems associated with uneven fiber size. Figure 4-12 show a typical example of this problem. The figure clearly shows the presence of a large fiber. In order to determine if this problem was arising from uneven drawing of the fibers or from a spinneret hole receiving excess material, cross sections of an individual fiber were taken along its length. Figure 4-13 shows the results of one such test.

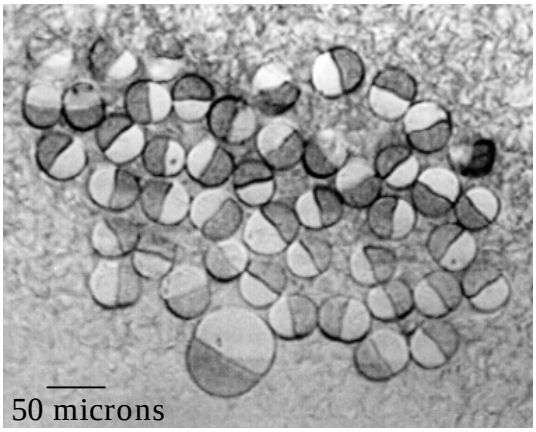

Figure 4-12. Typical maldistribution of fiber sizes. The fiber shown is a 33% PP18, 67% PP-MA-1 / PA6 fiber.

Figure 4-13 clearly shows that a single fiber is showing a variation in diameter along its length. This strongly suggests that a problem existed with the drawing step. Apparently the spin line is experiencing fluctuations in tension. The source of this problem, material or equipment related, was not determined. The phenomena of draw resonance has been predicted for high speed bicomponent spinning operations. All fibers spun in this research were done using a low speed winder.

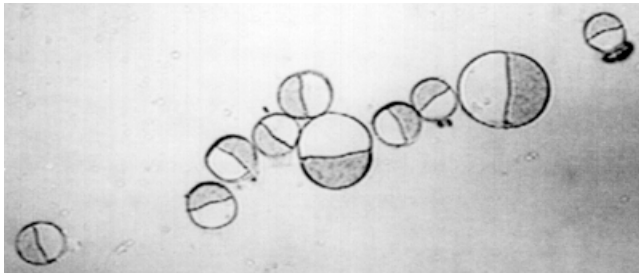

Figure 4-13. Results from taking cross sections of an individual fiber at different points along its length.

4-2-1. Thermal Stability of Materials During Processing

The spinning of a bicomponent fiber requires that both materials withstand temperatures suitable for processing of the higher melting material. In the production of a bicomponent nylon-6, polypropylene fiber this requires the polypropylene to withstand nylon-6 processing temperatures in the spin pack. For this study it was required that the polypropylene component be stable at a temperature of 260°C. Additional concerns about the thermal stability of maleic anhydride functionalized polypropylene were also addressed. One cannot forget that these materials have already been processed once in their lifetime during the melt functionalization process. This section begins with Thermogravimetric analysis (TGA) of the PP18, PP-MA-1, and PP-MA-2 materials. Further studies using a capillary rheometer are presented. Lastly, cross sections of fibers spun from previously melt blended materials are also presented as further evidence of stability.

4-2-2. Thermal Stability of Materials During Processing - TGA

Thermogravimetric studies of the degradation behavior of three of the polypropylene materials were conducted under nitrogen, or an air atmosphere. Two experiments were conducted for each atmosphere, the first experiment followed weight loss for isothermal conditions (255°C), while the second experiment followed the weight loss during a temperature ramp of 10°C / min from room temperature to 450°C. The ramped experiments' weight loss curves are accompanied by the differential temperature data relative to an empty reference pan. Figures 4-14 and 4-15 give the results for the isothermal experiment under nitrogen and air atmospheres respectively for PP18, PP-MA-1, and PP-MA-2. Note that the scales are not the same for each figure and that the plot begins five minutes into the experiment.

The temperature of 255°C was chosen because it approximates the highest temperatures experienced by the materials during processing. Comparison of the y-axis scales of Figs 4-14 and 4-15 show the expected dependence of weight loss on the presence of oxygen. Under an air atmosphere degradation occurs more rapidly and to a greater extent.

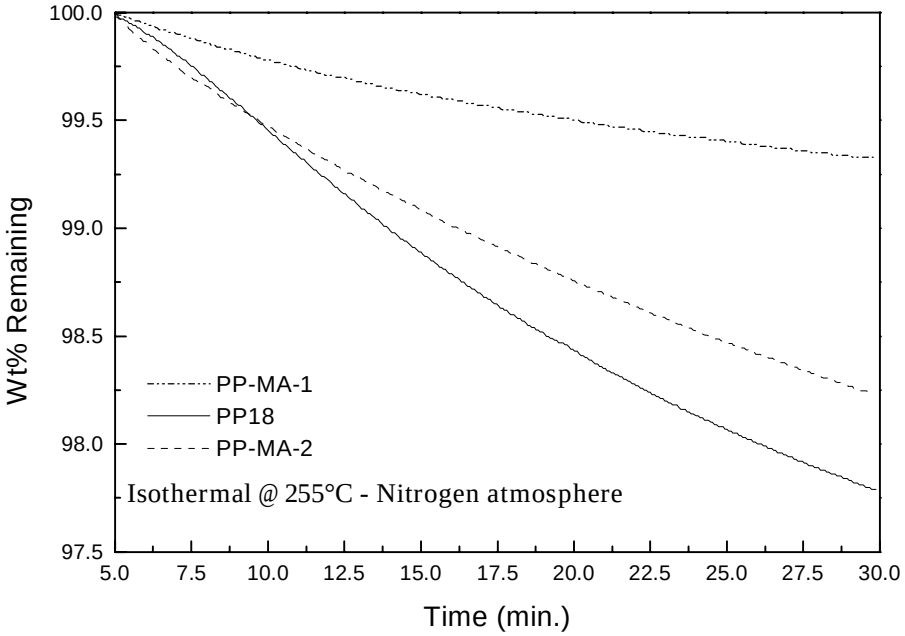

Figure 4-14. Isothermal degradation of materials under a nitrogen atmosphere. Note that plot begins five minutes into the experiment.

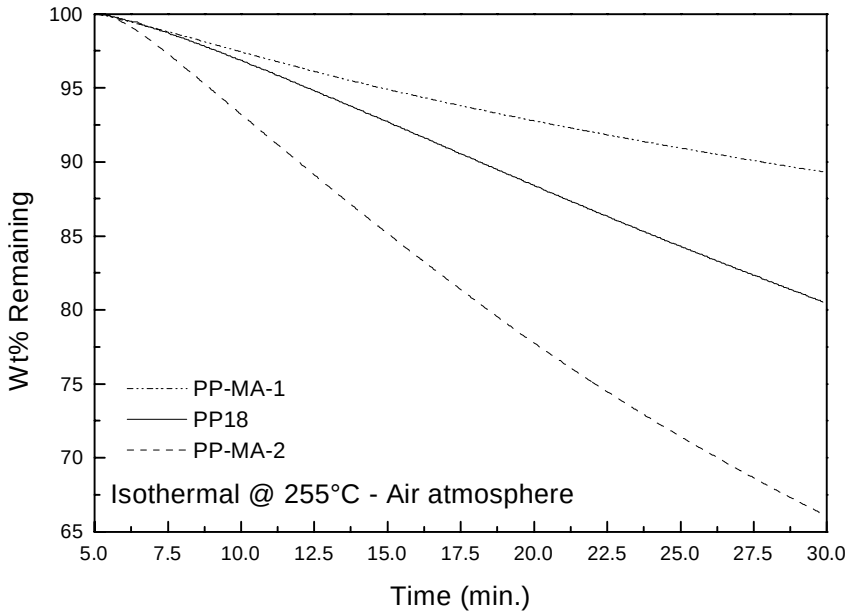

Figure 4-15. Isothermal degradation of materials under an air atmosphere. Note that plot begins five minutes into the experiment.

There were initial fears that the presence of the maleic anhydride functionality may decrease the thermal stability of the materials or that there may be a volatile component consisting of ungrafted maleic anhydride present. From these plots no definite trend can be assigned. In both plots it appears that the PP-MA-1 material is the most thermally stable, yet the PP18 and PP-MA-2 materials swap positions depending on the atmosphere. Care should be taken when attempting to draw inferences from this data. Each material is produced industrially for various applications. It is likely that the stabilizer packages used in each material are different. The important information to be ascertained from these plots is that under a nitrogen atmosphere (the conditions present in the extruder) the materials underwent less than 5% weight loss after 30 minutes. A minimum of nine minutes of exposure to an air atmosphere at elevated temperatures was required to bring about a 5% reduction in weight. These time spans are much longer than the those experienced during actual processing.

Figures 4-16 and 4-17 present data for the temperature ramp experiments. As stated earlier these figures contain both weight loss and normalized differential temperature data.

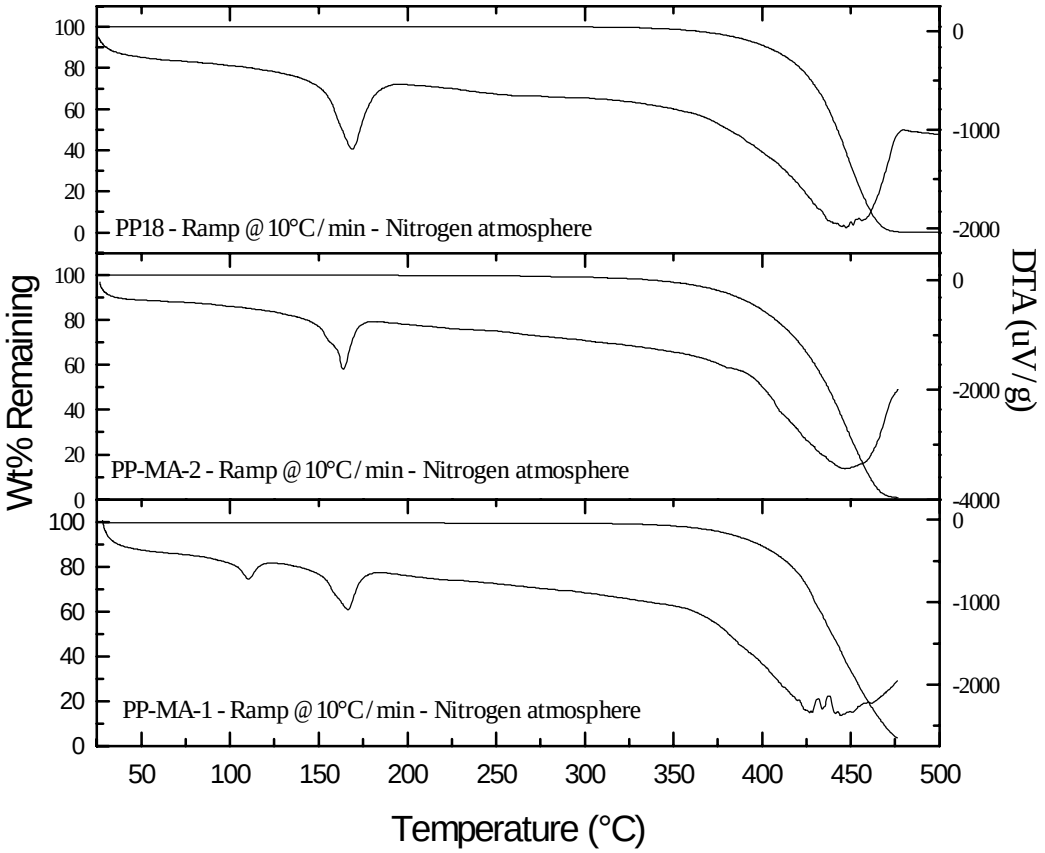

Figure 4-16. Degradation of materials under a nitrogen atmosphere, ramped at 10°C / min. In each plot the upper curve represents the weight loss data while the lower curve contains the DTA signal.

Interestingly, it can be seen that under an air atmosphere, Fig. 4-17,the degradation becomes so exothermic that the equipment cannot maintain the 10°C / min heating rate. The weight loss curves can be seen to move from right to left briefly as the TGA attempts to return to the programmed time temperature profile. This phenomena also creates the apparent tilt to the DTA signal.

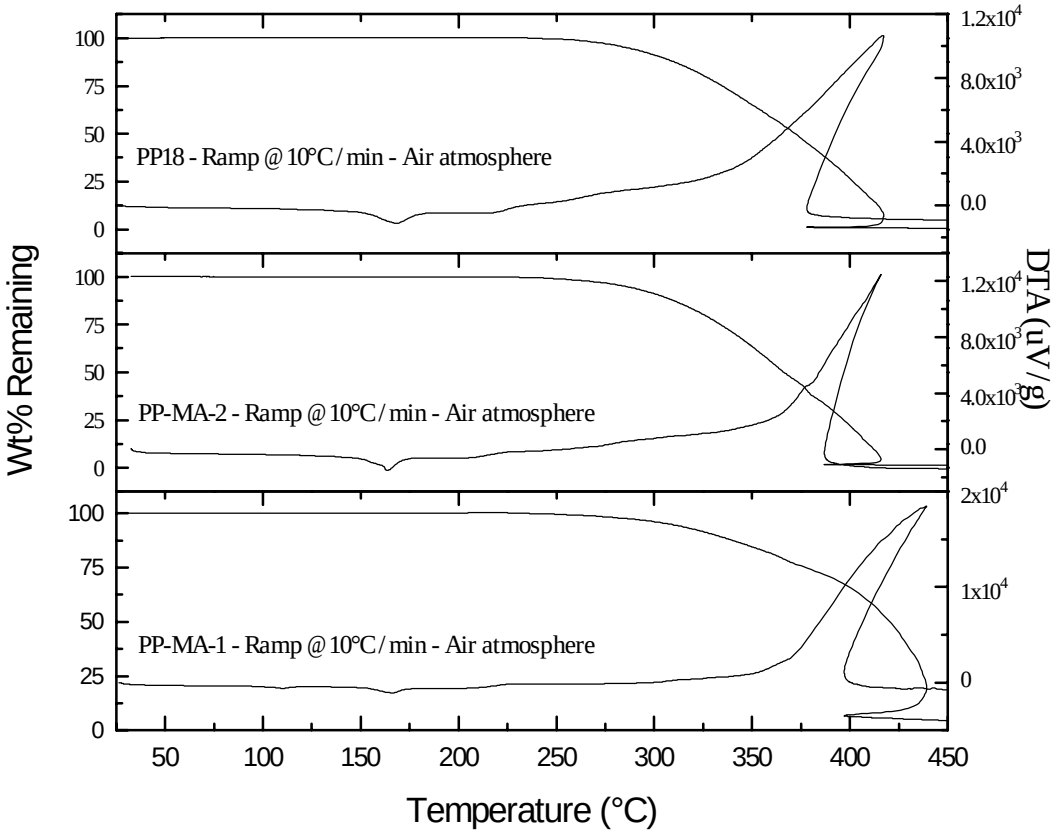

Figure 4-17. Degradation of materials under an air atmosphere, ramped at 10°C / min. In each plot the upper curve represents the weight loss data while the lower curve contains the DTA signal. Note slope in DTA signal and reversal of weight loss curves are due to deviations from the programmed 10°C / min heating rate as described in the text.

The most noticeable difference among the materials can be seen at temperatures below 200°C in the DTA signals. This portion of the DTA curve relates to the crystallization behavior of the materials, more of which will be discussed later using DSC. Using the temperature at which a weight loss of 5% has occurred as an indicator of the onset of degradation, examination of the plots reveals no definite trends. As expected the temperature at which degradation is much higher under a nitrogen atmosphere. Table 4-4 summarizes the results of the isothermal and ramp experiments. Of most importance is the fact that serious degradation does not occur until at least 25°C above the processing temperature

under an air atmosphere and at over 100°C in excess of the processing temperature under a nitrogen atmosphere.

Table 4-4. Summary of TGA results for PP18, PP-MA-1, and PP-MA-2

	iso - 255°C 5% Weight loss time (min.)		iso - 255°C Wt% Remaining after 30 min.		ramp - 10°C / min. Temperature (°C) at 5% weight loss	
	Air	N_2	Air	N_2	Air	N_2
PP18	11.8	>30	80.20%	97.80%	286	384
PP-MA-1	13.3	>30	88.70%	99.30%	309	378
PP-MA-2	8.9	>30	66.20%	97.80%	284	364

4-2-3. Thermal Stability of Materials During Processing - Capillary Rheometry

The use of TGA to follow the degradation behavior of a material does not necessarily tell the complete story. Degradation as a result of chain scission may occur during processing. This type of degradation does not lead to an observable weight loss, and may be missed by TGA. Above the critical molecular weight for entanglement most polymers show a dependence of zero shear viscosity on molecular weight to the 3.4 power, thus the use of rheology should be a very sensitive method for following chain scission. For this reason experiments were conducted in which material was sheared once in the rheometer and then placed back in the rheometer and tested.

A slight decrease can be noted for these materials. If the mechanical action of shearing was leading to substantial degradation, it would be expected that the severity of the viscosity change would be greater for the lower temperature experiment. Both experiments show similar behavior. Using the 3.4 power approximation for the relationship between viscosity and molecular weight yields changes in molecular weight of about two percent. Both Figs 4-18 and 4-19 show that PP18 alone or blended with PP-MA-1 show very little degradation.

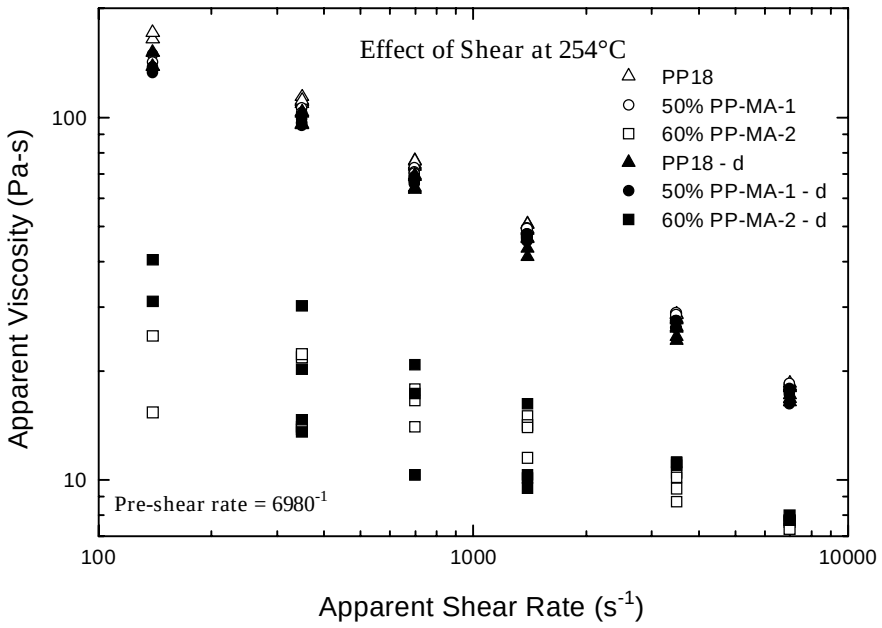

Figure 4-18. Capillary rheometry data for materials initially sheared at 6,980 s^{-1} and 254°C. Data collected at 254°C. The -d refers to samples which have been sheared once in the rheometer prior to testing.

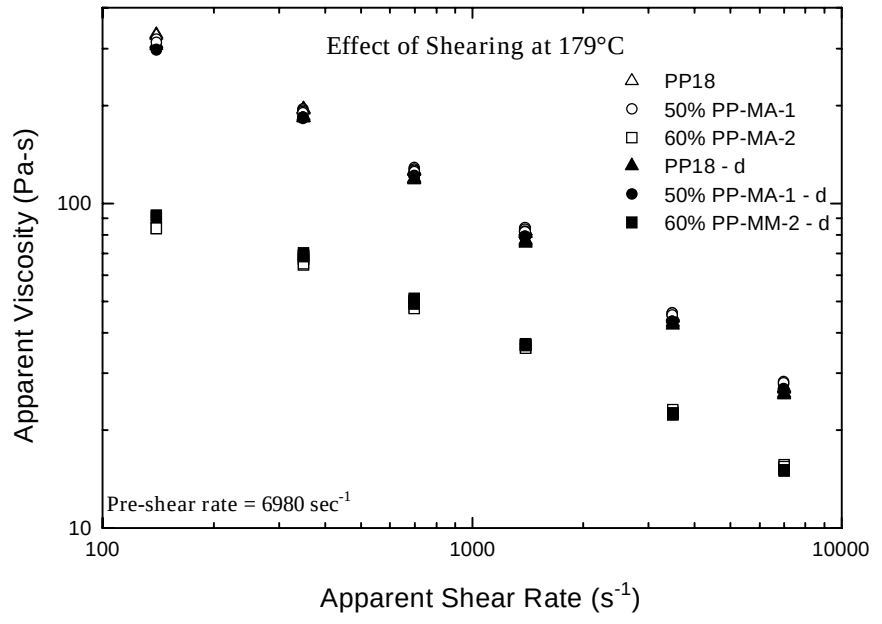

Figure 4-19. Capillary rheometry data for materials initially sheared at 6,980 s^{-1} and 179°C. Data collected at 179°C. The -d refers to samples which have been sheared once in the rheometer prior to testing.

4-2-4. Thermal Stability of Materials During Processing - Melt Blending

A final, qualitative indication of the processing stability of these materials and their blends can be seen in the following micrographs. Concerns over the quality of the blending achieved within the single screw polypropylene extruder with mixing element when hopper blending materials were addressed by conducting fiber spinning runs in which the polypropylene component had been pre-blended in a twin screw extruder as a separate step. Thus, these trials represent the production of fibers which have already been processed once prior to spinning. Figure 4-20 contains the micrographs of two samples prepared via hopper blending, while Fig 4-21 shows the cross-sections of fibers produced under identical conditions for materials which were previously melt blended in the twin screw extruder. Twin screw extrusion was carried out at 200°C, with the extrudate being quenched in a water bath and subsequently pelletized.

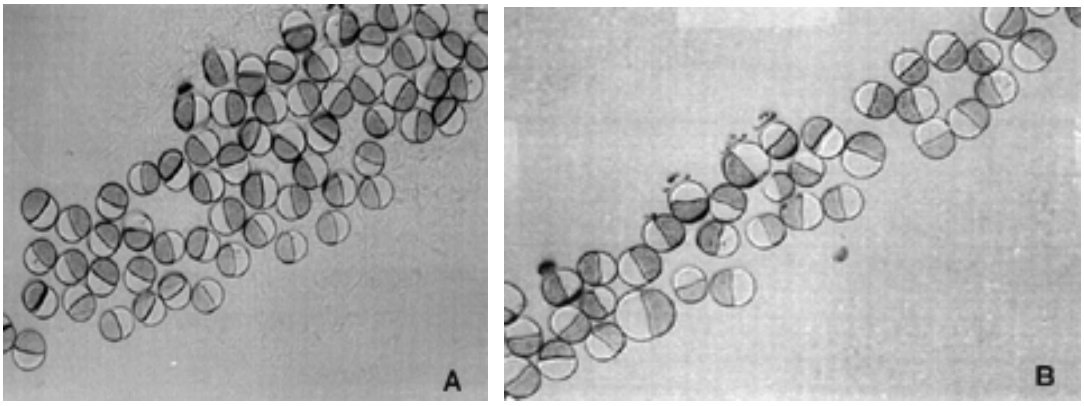

Figure 4-20. Cross-sections of fibers produced by hopper blending of polypropylene materials. A) 5% PP-MA-2, 95% PP18 / PA6, B) 50% PP-MA-1, 50% PP18 / PA6.

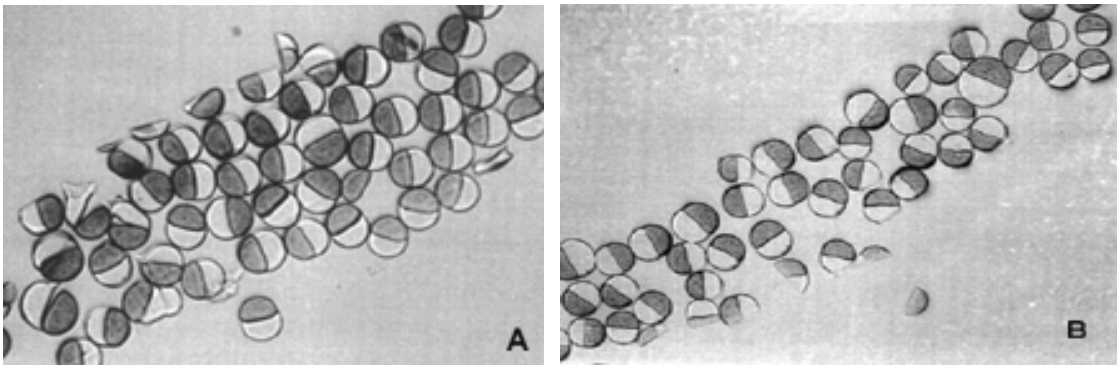

Figure 4-21. Cross-sections of fibers produced by melt mixing of polypropylene materials prior to spinning in a twin screw extruder. A) 5% PP-MA-2, 95% PP18 / PA6, B) 50% PP-MA-1, 50% PP18 / PA6.

Recalling that chain scission should have a large effect on viscosity, qualitatively one could use the phenomena of interface movement to determine if any gross

changes in the viscosity have occurred by comparing the shapes of the interfaces. Comparing similar materials from Figs 4-20 and 4-21 it can be seen that there is no apparent affect on the shape of the interface due to the extra processing step involved with melt blending the polypropylene component prior to spinning.

4-3-1. Crystallization Behavior of Project Materials and Blends

Both nylon-6 and polypropylene are semicrystalline polymers. The amount of crystallinity present in the final fiber will be a function of the material and process variables. A high crystalline content in carpet fibers helps to make the fibers more resistant to matting, capable of retaining properties at elevated temperatures, and resist staining. Because the ability of a polymer to crystallize depends on its molecular symmetry, there were concerns that the random addition of maleic anhydride along the backbone could greatly disrupt this symmetry, leading to a material with a low crystalline content. To address this concern, DSC was used to partially characterize the crystallization behavior of the project materials.

4-3-2. Crystallization Behavior of Project Materials - Melt Functionalized Materials

The nature of the melt functionalization process which produces this series of materials leads to random scission of the backbone. The placement of the functional group is not well controlled with maleic groups being placed randomly on the chain (though usually at the ends) in single or multiple units (polymaleic anhydride grafts). A disruption of the crystallization behavior would not be unexpected. Figure 4-22 contains a series of three functionalized polypropylenes along with PP18. A steady decline in the melting point of the materials can be seen as the level of functionalization increases. This behavior can be explained by the melt functionalization process. An increase in functionalization will break up the symmetry of the polypropylene backbone which will lead to less perfect crystals and less crystallinity. Examination of the peaks in Fig 4-22 also shows a broadening of the melting endotherms as the maleic content increases, until two distinct peaks appear.

The exact nature of this phenomena is not yet fully understood. The presence of two peaks suggests that there are two crystal populations present in this material. Attempts to observe separate melting and crystallization events using optical microscopy were unsuccessful. Further insight may be obtained by examining the crystallization behavior of these materials as shown in Fig 4-23. Within the functionalized materials a trend towards greater crystallization temperature can be seen. The PP18 homopolymer does not follow this trend.

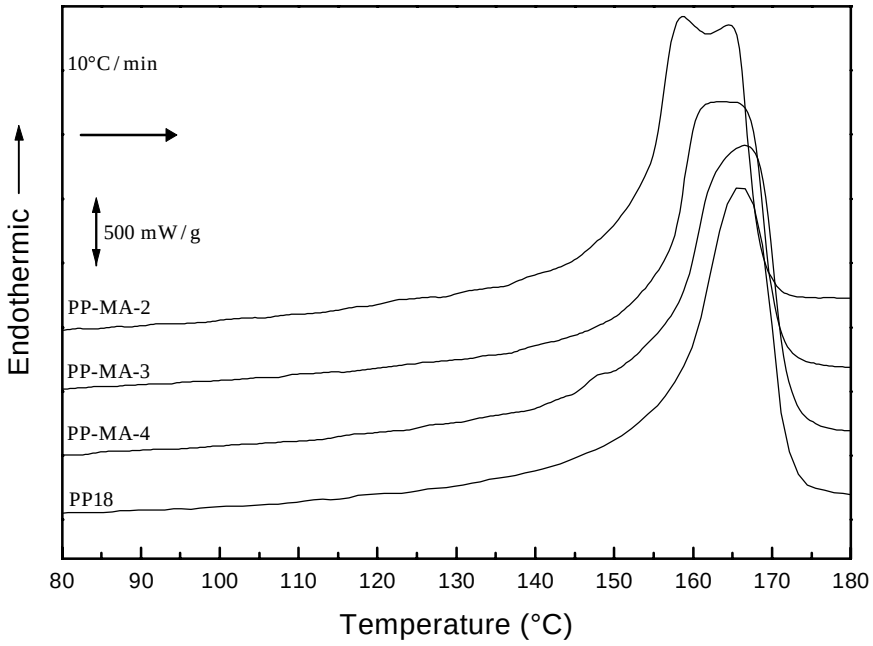

Figure 4-22. Melting behavior of melt functionalized materials. Degree of functionalization increases moving vertically.

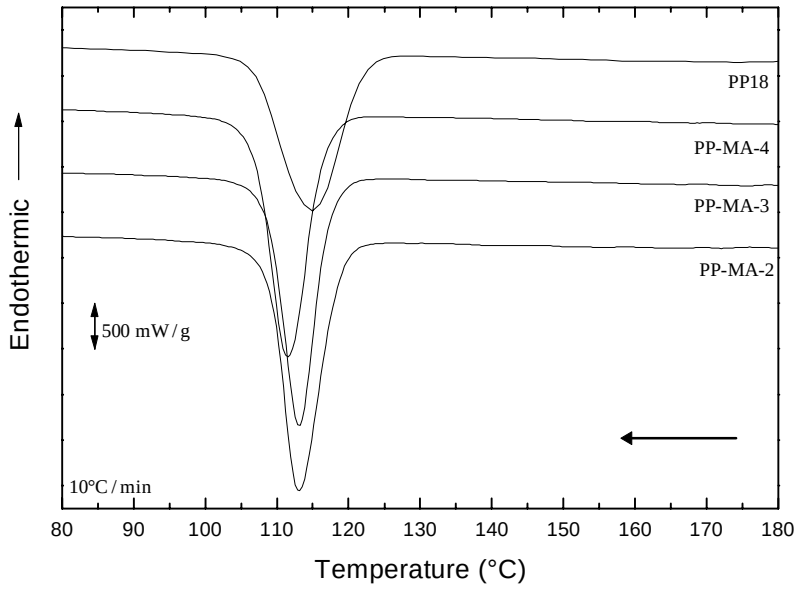

Figure 4-23. Crystallization behavior of melt functionalized materials. Degree of functionalization decreases moving vertically.

The most interesting feature is that the PP-MA-2 material does not show a double crystallization peak to compliment the apparent double melting peak. This suggests that one crystalline population forms during cooling.

The exact method used to make these materials is not known. Some manufacturers of maleic anhydride polypropylenes will blend a heavily functionalized material with polypropylene to produce a pellet with an overall intermediate content of maleic anhydride. An examination of the individual chains within a pellet would reveal that there are two types of chains present, short , in heavily functionalized chains, and long chains with no maleic anhydride. It is possible in this material that the populations are sufficiently compatible to crystallize together when rapidly quenched. During a slow quench there may be sufficient mobility for the two populations to segregate, yielding to distinct crystalline populations. These conditions are present during the DSC scan.

The most important result from this study is to note that while the melting temperature may decrease as the level of functionalization increases, the change is relatively small. The addition of maleic anhydride to the polypropylene backbone is not severely affecting the thermal stability of the crystals formed. Additional information regarding the level of crystallinity will be considered in section 4-3-4.

4-3-3. Crystallization Behavior of Project Materials - PP-MA-1 and PE-MA

Further information about the composition of the materials used in this project can be obtained using DSC. The PE-MA material is an ethylene based material, thus its melting point should be much lower than the polypropylene materials used. Its DSC trace bears this fact out as shown in Fig 4-24, along with three other materials. The DSC trace confirms this. The lower melting peak occurs at a temperature which would be indicative of a low density polyethylene with a substantial amount of branching. Long chain branched molecules are known to greatly increase the elongational viscosity of a material, and thus a long chain branched polyethylene would be the logical choice to improve melt strength. The crystallization behavior of these materials is plotted in Fig 4-25. The DSC trace of PP18 is replotted for reference when comparing these materials to those in Figs 4-22 and 4-23. The PP-MA-6 material is a maleated polypropylene similar to the other melt functionalized materials, and shows similar melting behavior. The most interesting material is the PP-MA-1 material which shows both a low and high temperature melting peak. Information supplied by the manufacturer revealed that the PP-MA-1 material contains a small percentage of polyethylene for the purpose of increasing the material's melt strength.

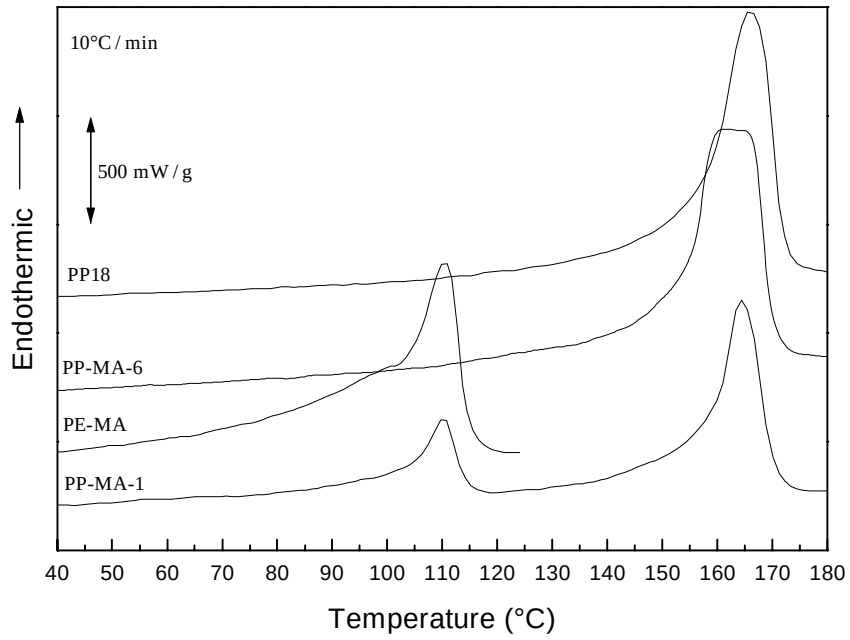

Figure 4-24. Melting behavior of process materials. Note the presence of lowering melting polyethylene content in the PE-MA and PP-MA-1 materials.

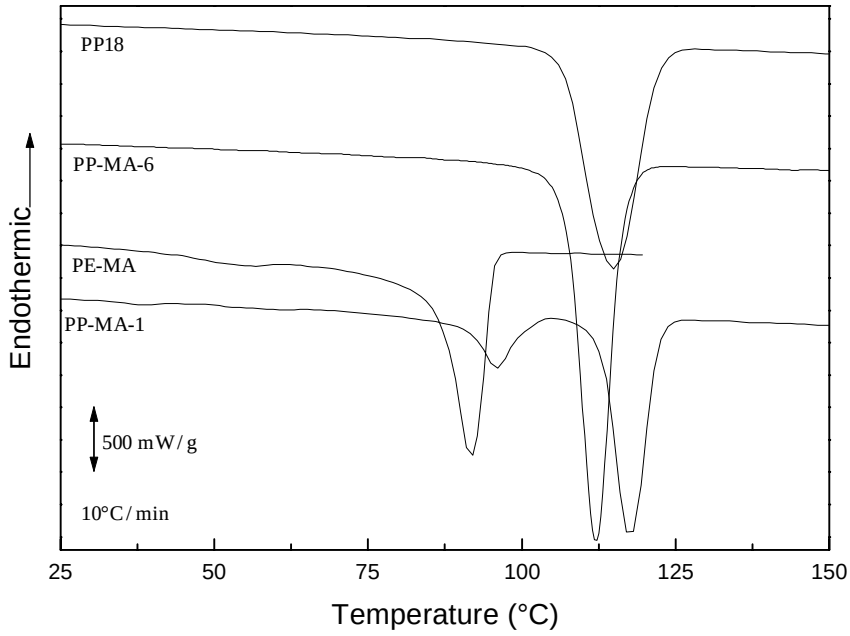

Figure 4-25. Crystallization behavior of selected functionalized materials. PP18 included as a reference.

No new behaviors are seen in Fig 4-25. As with the other maleated materials which are similar, the PP-MA-6 crystallizes at a slightly higher supercooling than PP18. The melting behavior of PP-MA-1 does raise some concerns. It is important that the material comprising a carpet have good thermal stability. Friction with sliding furniture can lead to localized heating. Polypropylene is well above its glass transition temperature at room temperature. Therefore a high crystalline content is necessary to provide mechanical stability at room temperature and above. The low melting point of polyethylene materials makes them unsuitable for carpeting applications due to the possibility of this localized heating. This is one of the reasons why the PE-MA material was dropped during the project. Fortunately, the melting point of polypropylene is sufficient high to allow its use in most carpeting applications. There is a concern that the presence of this low melting material in PP-MA-1 may weaken the material at elevated temperatures. The presence of a low melting component may also cause the fusing of fibers together during service, severely altering the carpet's original texture. There is hope that the fraction of crystalline polypropylene will be sufficient to allow the material to retain its properties at elevated temperatures. The higher crystallization temperature of the polyethylene component in PP-MA-1 as compared to PE-MA is not surprising considering that the presence of polypropylene crystallites may serve as nucleating sites for the polyethylene in the PP-MA-1 material.

4-3-4. Crystallization Behavior of Project Materials - Crystal Content.

Integration of the area beneath the DSC scans yields a value of the heat of fusion for these materials. Using this information along with the published value for the value of the heat of fusion for isotactic polypropylene yields the crystalline content. Table 4-5 summarizes these calculations along with the melting and crystallization temperatures for the various materials used in this project.

Table 4-5. Crystalline content of materials using DSC. Multiple entries refer to the lower and higher temperature peaks respectively. ΔH_f PP = 209 J/g, ΔH_f PE = 289.9 J/g. PP-MA-1 entry represents the percentage of crystalline PE and PP respectively.

Material	Tm (°C)	Tc (°C)	% Crystallinity
PP18	165.1	110	46.3
PP-MA-1	110, 164.2	96, 117.6	8.3, 31.1
PP-MA-2	158.7, 164.6	113.2	48.7
PP-MA-3	163.9	113.2	47.9
PP-MA-4	166	111.5	47.9
PP-MA-6	160.9	112.2	49.5
PE-MA	110.8	91.8	37.8

The melt functionalized series of materials yield crystallinity values which are approximately equivalent and slightly greater than the eighteen melt flow polypropylene. The overall crystalline content of the PP-MA-1 material is less than that of the other polypropylene materials. This may be an indication of its greater molecular weight relative to the melt functionalized materials or that the grafted maleic anhydride groups are more effective at disrupting the symmetry of the chain in comparison to the other molecules..

4-3-5. Crystallization Behavior of Project Materials - Blends.

While it was not expected that any unusual behavior observable by DSC would result from blending the functionalized and non-functionalized propylenes, DSC scans were obtained to verify the melting behavior of these blends. Figure 4-26 contains a systematic variation of PP-MA-2 content blended with PP18 and its effect on the melting behavior of the blends.

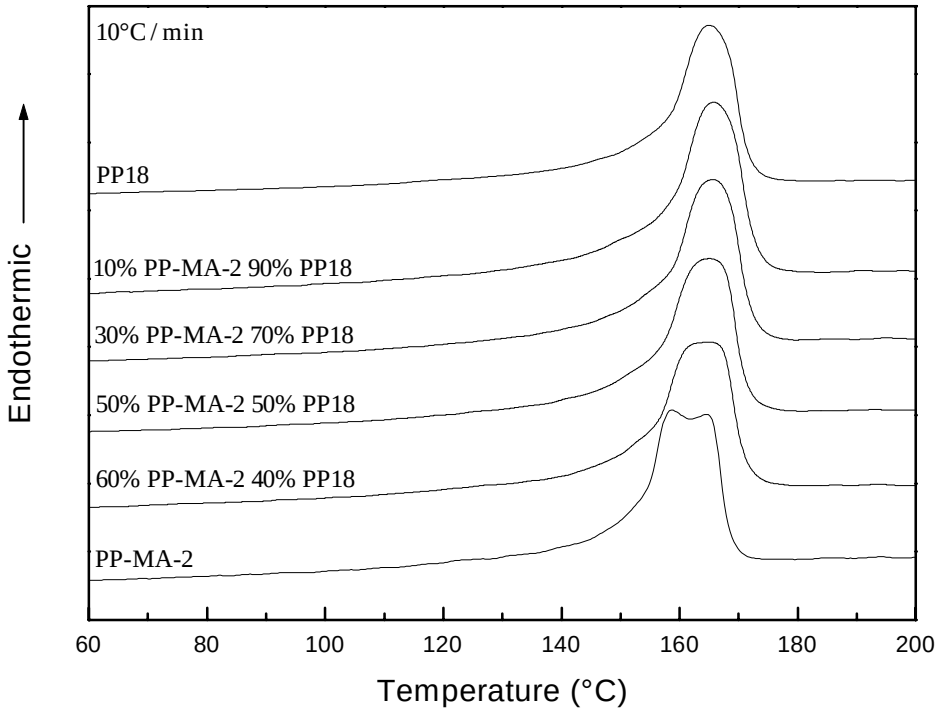

Figure 4-26. Melting behavior of blends of PP-MA-2 and PP18.

Once again, the double melting peak is observed for the pure PP-MA-2 material. Increasing contents of the PP-MA-2 material are shown to broaden the melting peak and lower the melting temperature. This is logical as the PP-MA-2 material is less symmetric and of lower molecular weight than the PP18. The corresponding crystallization behavior for these blends is shown in Fig 4-27.

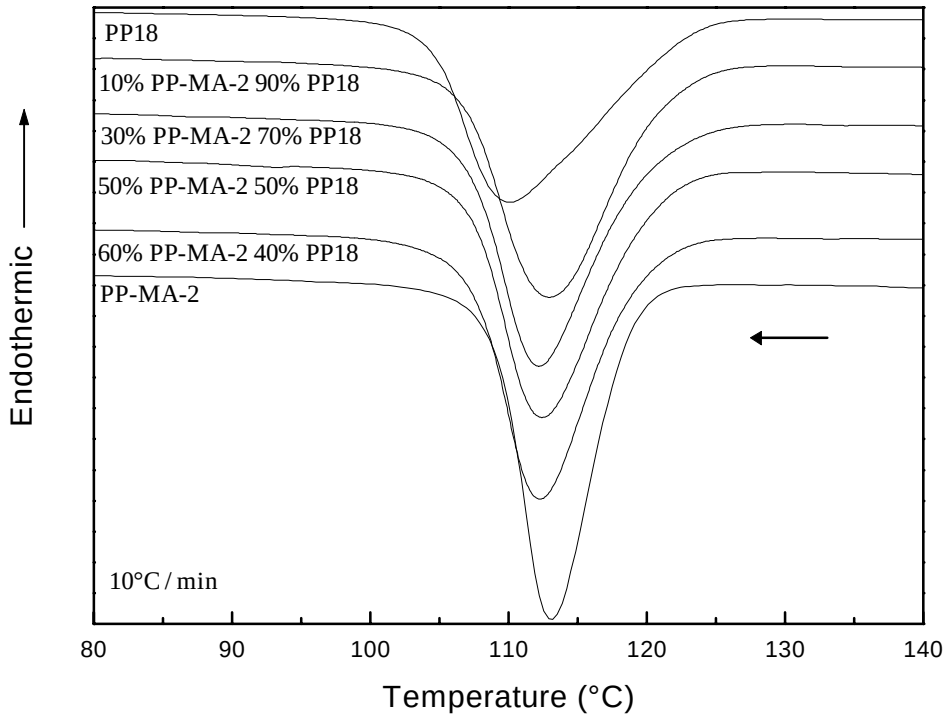

Figure 4-27. Crystallization behavior upon cooling from the melt of blends of PP-MA-2 and PP18.

The crystallization behavior of these blends follows expected trends. For blends of the two materials, the PP-MA-2 content raises the crystallization temperature of the blend relative to pure PP18. This suggests that the PP-MA-2 may be acting as a nucleating agent for PP18 crystallization. Close examination of the location of the blend peaks shows that the crystallization temperature of the blends is relatively constant regardless of PP-MA-2 composition. The melting and crystallization behavior of the PP-MA-1 material when blended with PP18 is shown in Fig 4-28.

At a composition of 50% PP-MA-1 the presence of the lower melting polyethylene peak can still be observed. Upon cooling the temperature span between the two crystallization peaks decreases relative to the span between the melting peaks, suggesting that the lower melting phase is nucleated by the higher melting phase.

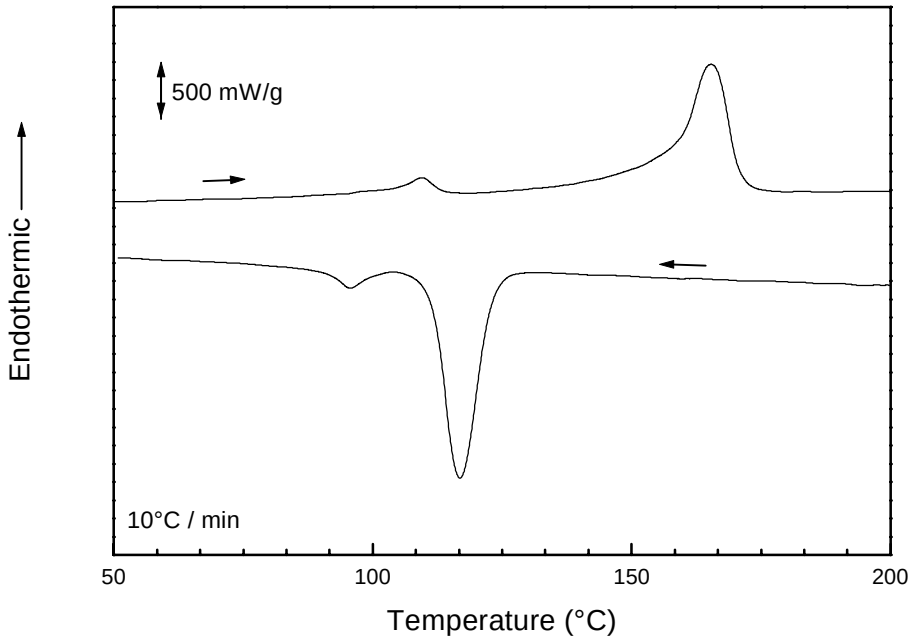

Figure 4-28. Melting and crystallization behavior of a 50% PP-MA-1, 50% PP18 blend.

4-4-1. Mechanical Properties of the Blend Systems.

A recurring theme of this project is the effect that the functionalization process has on the properties of the final material. These differences lead to different levels of performance in the final fiber product. The purpose of conducting tensile tests on blends of polypropylene with the functionalized materials was to determine if the low molecular weight of some of these materials would effect the mechanical properties of the system or, if the presence of a high content of maleic anhydride functionalization would lead to poor compatibility in these polypropylene blends, which could adversely effect mechanical properties. All data below represents tests conducted on dog bone samples of the specified blend, not on fibers.

4-4-2. Mechanical Properties of Blend Systems - Small to Intermediate Strain.

To fully appreciate the nature of the differences between the materials, a comparison of the properties over two strain ranges needs to be made. At very small strains the modulus gives an indication of the stiffness of the material. Figure 4-29 contains the modulus data for selected blends. The selection of these blends was made based on the results of fiber cross-sections. The high content PP-MA-2 and PP-MA-1 blends had shown the most promise from an adhesion

standpoint, and thus were the focus. Considering the low molecular weight of the PP-MA-2 material, a systematic variation of its content in blends was conducted because it was most likely to lead to poor mechanical properties. The PP-MA-5 material is made using the same process as the PP-MA-2 material, but contains a lower maleic anhydride content.

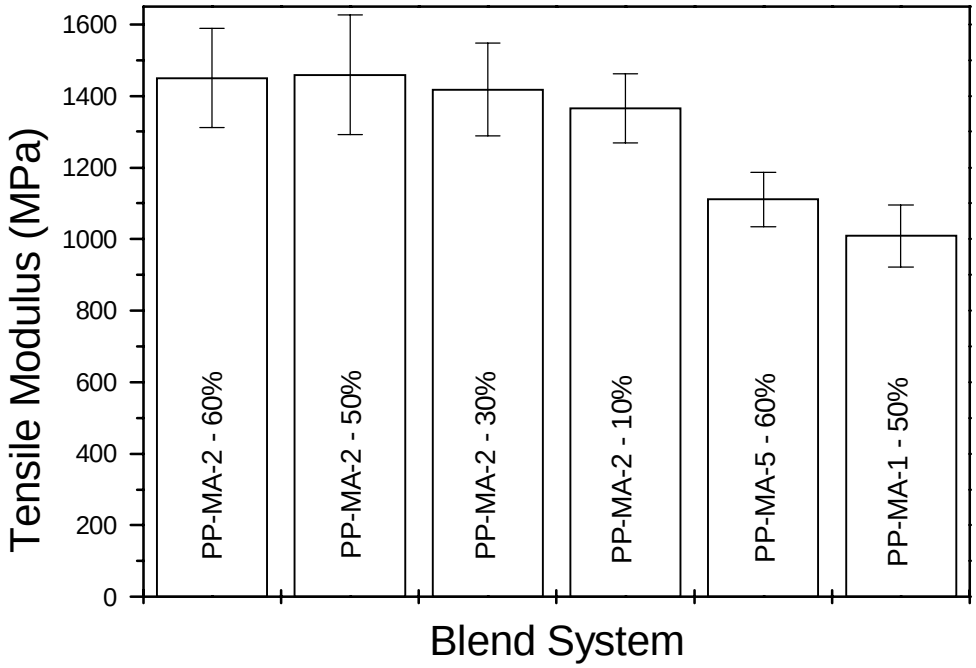

Figure 4-29. Tensile modulus of blend systems. Testing rate 10 mm / min. at room temperature using dog bone specimens.

The data in Fig 4-29 suggests that all of the blends of PP-MA-2 yield roughly the same modulus, while the PP-MA-1 material has the lowest modulus. Table 4-6 compares the relative levels of crystallinity obtained by DSC for each of these samples. A comparison of properties at larger deformations is given in Fig 4-30 by comparing the strain at maximum load of the blends. Each of the materials contains roughly the same level of crystallinity with the exception of the PP-MA-1 blend. The PP-MA-1 blend does appear to contain less crystalline content then the other blend, which may well account for its lower modulus.

Table 4-6. Crystalline content of mechanical testing specimens, prior to testing, using DSC. ΔH_f PP = 209 J/g, ΔH_f PE = 289.9 J/g (ref.78). The PP-MA-1 entry represents percentage which is crystalline PE and PP respectively.

Blend System	% Crystallinity
60% PP-MA-2, 40% PP18	48.5
50% PP-MA-2, 50% PP18	51.4
30% PP-MA-2, 70% PP18	48.6
10% PP-MA-2, 90% PP18	52.1
60% PP-MA-5, 40% PP18	46.8
50% PP-MA-1, 50% PP18	2.96, 41.0

The variation in crystalline content among the PP-MA-2 blends is probably due to error in determining the area underneath the melting endotherm of the DSC scan. The lower crystalline content in PP-MA-1 is not surprising because its consists of higher molecular weight material which will crystallize slower for a given thermal history relative to the melt functionalized materials. A trend begins to become apparent when considering this data. High quantities of PP-MA-2 act to stiffen the material, raising the modulus and producing a lower strain to maximum load. The PP-MA-1 blend goes to a larger strain before reaching its peak load. This behavior further suggests PP-MA-1 has a higher molecular weight relative to the melt functionalized materials, creating greater extensibility.

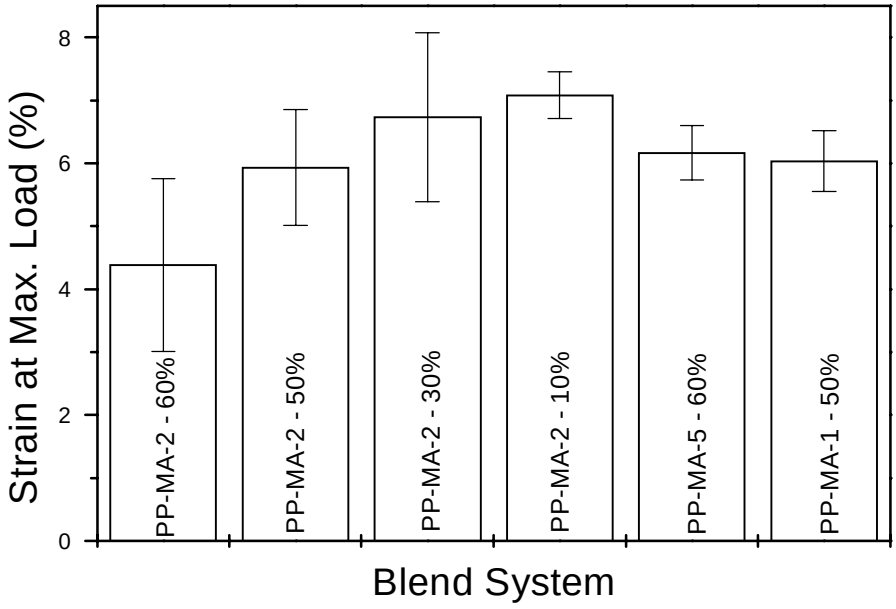

Figure 4-30. Strain at maximum load of blend systems. Testing rate 10 mm/min. at room temperature using dog bone specimens.

4-4-3. Mechanical Properties of Blend Systems - Ultimate Properties.

A comparison of the ultimate properties provides striking differences between these blends. The higher molecular weight of the PP-MA-1 material clearly shows, better ultimate properties than the melt functionalized materials. Figure 4-31 compares the toughness of these blends. It can clearly be seen that the blend with PP-MA-1 is much tougher (energy to fail) than any of the PP-MA-2 and PP-MA-5 blends. The high content PP-MA-2 blends have very poor toughness. Even at only ten weight percent these materials have less than half of the toughness of the PP-MA-1 blend.

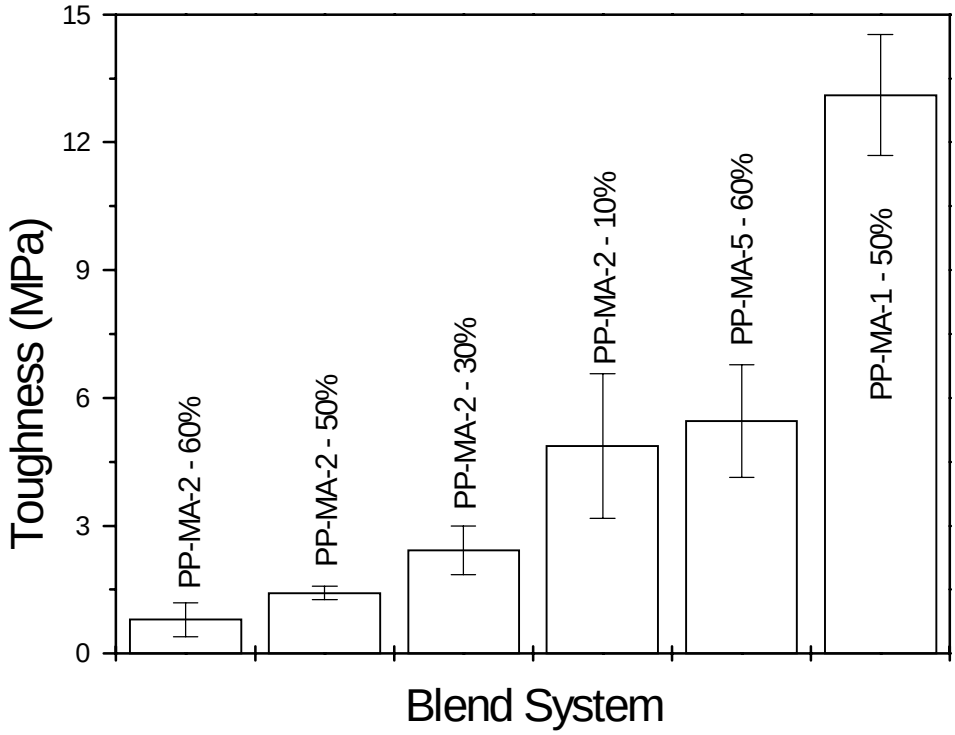

Figure 4-31. Toughness of the blend systems. Testing rate 10 mm / min. at room temperature using dog bone specimens.

The short chain nature of the PP-MA-2 leads to low extensibility. This point is further exemplified in Fig 4-32. A comparison of the strain to break properties shows that the differences in toughness came about largely due to the relative levels of strain each blend may achieve prior to failure. The PP-MA-1 material is capable of withstanding much higher strains.

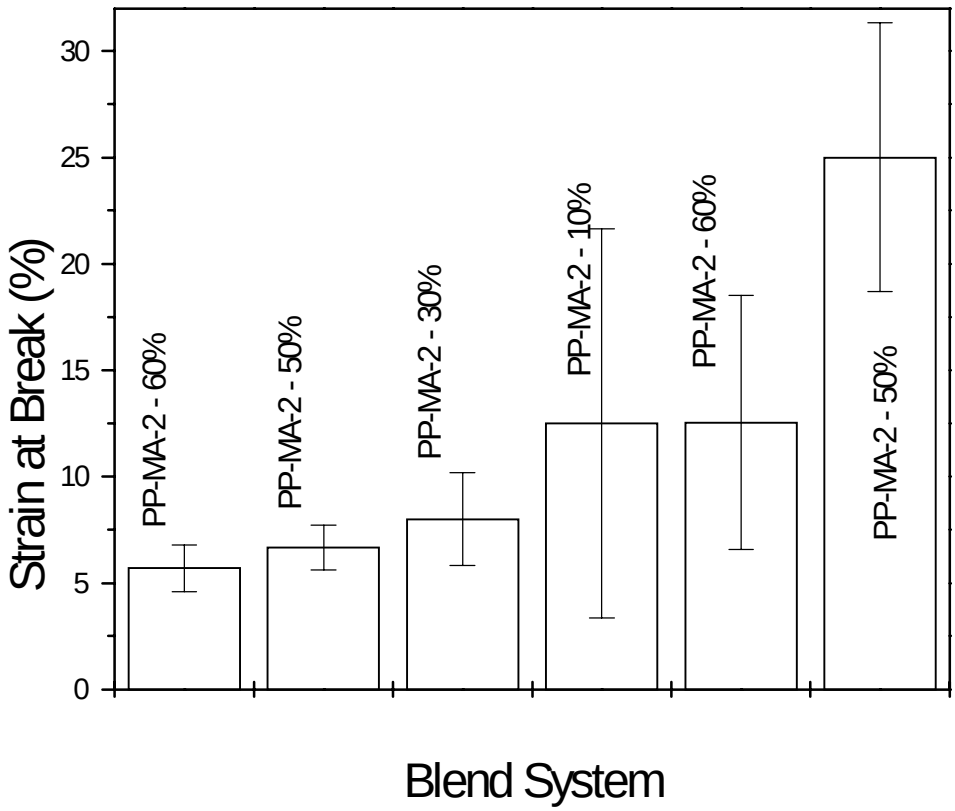

Figure 4-32. Strain at break of blend systems. Testing rate 10 mm / min. at room temperature using dog bone specimens.

The importance of this difference in the mechanical behavior of these materials will become more apparent when deducing the differences in carpet wear performance between these blends. Blends which show roughly equivalent adhesion to the nylon-6 phase in fibers through cross-sectioning will not necessarily show similar wear resistance when tested as a carpet sample.

4-4-4. Mechanical Properties of the Blend Systems - An Aside on Morphology.

It is possible to account for the poor performance of the PP-MA-2 material when blended with polypropylene to be a result of incompatibility. As the level of functionalization increases, the polar nature of the molecule increases. This could eventually lead to a system in which the functionalized polypropylene shows poor compatibility with a non-functionalized polypropylene. Admittedly a weakness in this project may have come from a failure to fully appreciate this phenomena. Figures 4-33 contains SEM micrographs of blend specimens fractured after being cooled in liquid nitrogen.

A)

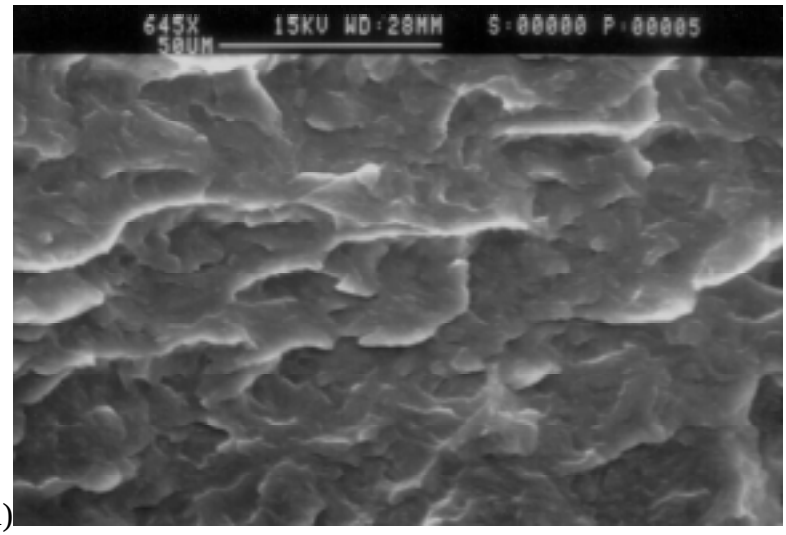

B)

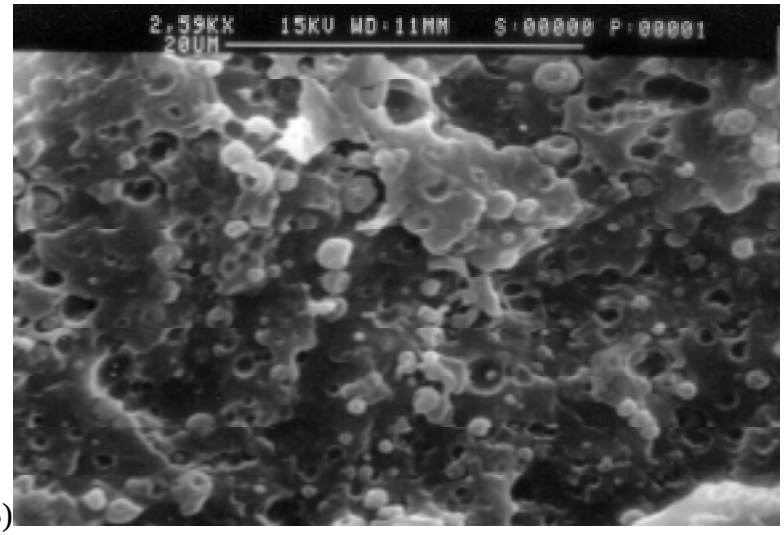

C)

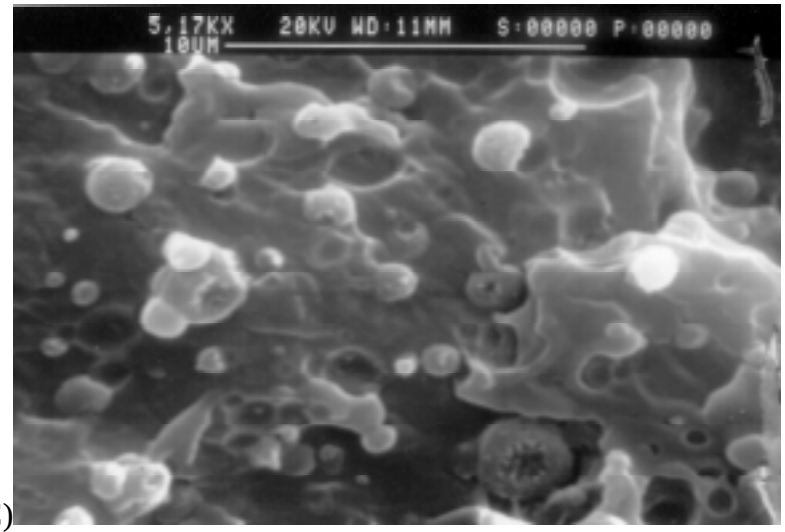

Figure 4-33 SEM micrographs of blends fractured after cooling in liquid nitrogen. A)60% PP-MA-2, 40% PP18: B,C)50% PP-MA-1, 50% PP18. Note, magnification levels vary among micrographs.

There is a startling difference between the blends. The PP-MA-2 material, at this scale level, appear to be nearly homogeneous, while a distinct phase separated morphology can be observed in the PP-MA-1 blend. This behavior counters the notion that it is poor miscibility in the PP-MA-2 systems that is likely contributing to poor large strain properties. It is likely that the small domains in the PP-MA-1 material consist polypropylene material which is sufficiently functionalized (made sufficiently polar) to render it incompatible with PP18.

4-5-1. Qualitative Interfacial Adhesion of Fibers.

Lacking a test with the sensitivity to determine the interfacial adhesion of the polypropylene component to the nylon-6 component in an individual fiber, relative differences in the quality of adhesion for various formulations were determined qualitatively by examining cross-sections of the fibers using optical microscopy. The cross-sectioning process was used to select blends which showed the most promise, reducing the number of samples which needed to be tufted into carpet samples, to determine their wear properties. Often times the quality of the adhesion could be determined without cross-sectioning. Fibers which had very poor interfacial adhesion would separate when drawn by hand. What follows is a rough chronological account of the fibers spun which show the project's evolution towards fibers of sufficient interfacial adhesion. Any variation from the processing conditions noted in Table 4-1 will be noted.

4-5-2. Qualitative Interfacial Adhesion of Fibers - PP-MA-1 Blends and PE-MA .

The initial runs using the PP-MA-1 and PE-MA materials proved to be very promising. These materials were spun without blending in any polypropylene initially. This made them difficult to process, as the melt exiting the spinneret tended to lack strength. Figure 4-34 is a cross-section of a PE-MA / PA6 bicomponent fiber displaying reasonable adhesion.

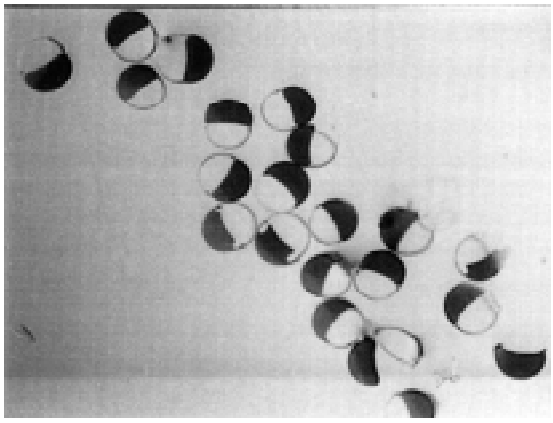

Figure 4-34. Cross section of a PE-MA / PA6 fiber displaying reasonable adhesion and viscosity cross over, head block temperature 288°C.

As mentioned earlier, despite the fact that the PE-MA material displayed promising interfacial adhesion, the material was dropped from the project because it was polyethylene based. Early attempts were conducted at elevated head block temperatures with the hope of increasing the kinetics of the compatabilization reaction. Figure 4-35 Is a cross-section of an PP-MA-1/PA6 fiber.

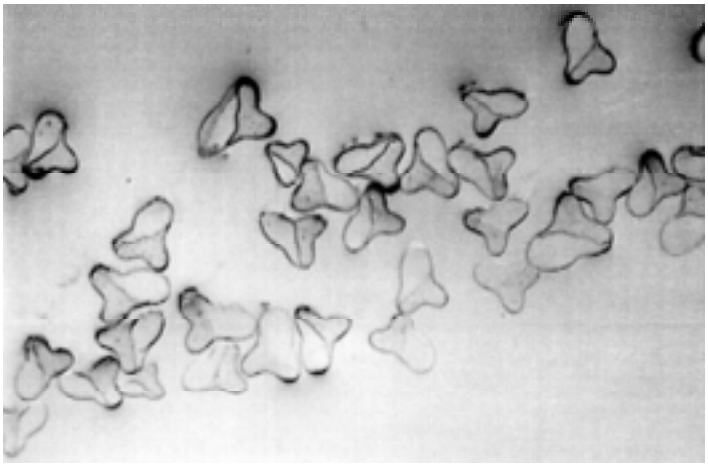

Figure 4-35. Cross section of a PP-MA-1 / PA6 fiber with excellent adhesion, head block temperature 288°C.

The quality of the adhesion in these fibers is excellent. Not a single separation is observed. This, however, did not mark the end of the project as an early success. The PP-MA-1 material is by far the most expensive of the functionalized polypropylenes used in this project. The economics of using a wholly PP-MA-1 polypropylene component were not acceptable. Focus was then shifted to producing a bicomponent fiber using the PP-MA-1 material which would be closer to being economically feasible. Figure 4-36 represents the earliest of such attempts by blending the functionalized material with a non-functionalized polypropylene. Numerous failures are observable in these fibers. One can also see from these and the previous cross-sections the problems associated with obtaining an even cross-section at the elevated head block temperature, due to viscosity differences. Additional experimentation was done to better understand the rheology of these blend systems as shown in Fig 4-37.

In the range between ten to fifty weight percent of the PP-MA-1 it can be seen that there is only a slight depression in the viscosity as the PP-MA-1 content increases. This difference becomes negligible at high shear rates. Recall from Fig 4-1 that the viscosity curves of the two pure materials were nearly equivalent.

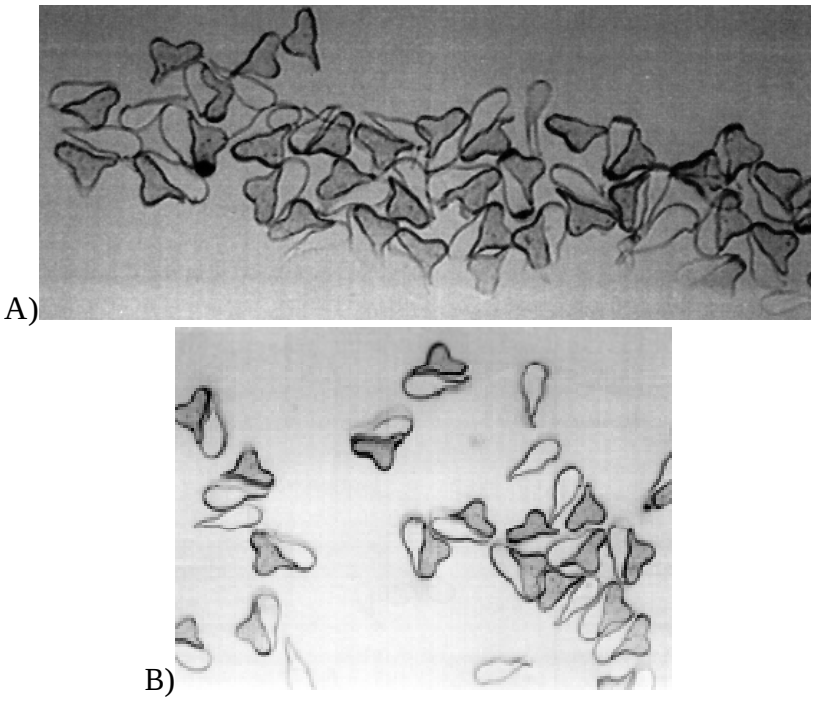

Figure 4-36. Cross sections of fibers using blends of PP-MA-1 and PP18 to reduce the materials cost of the bicomponent fiber. A)10% PP-MA-1, 90% PP18 / PA6. B) 20% PP-MA-1, 80% PP18 / PA6. Head block temperature 288°C.

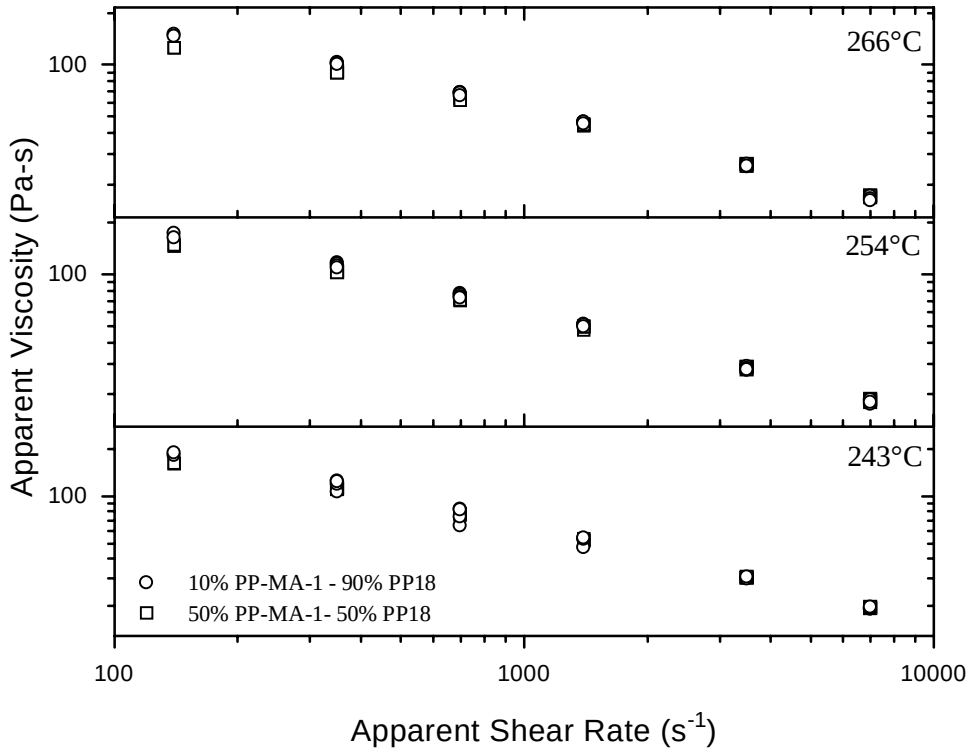

Figure 4-37. Viscous response of PP-MA-1, PP18 blend systems at temperatures and shear rates comparable to spinning conditions.

Despite the economics of the situation, it was decided to increase the PP-MA-1 content for purposes of hopefully finding a rough minimum of the level needed to obtain adequate adhesion as the unblended PP-MA-1 had shown that quality adhesion could be obtained with this material. A content of 67% PP-MA-1 was used in the fibers shown in Fig 4-38. These fibers display excellent adhesion as no failures can be found. As mentioned earlier problems were encountered with the distribution of fiber size that were never fully understood. With these results enough data had been collected to provide a feel for the amount of PP-MA-1 necessary to provide adequate adhesion, as determined by cross-sectioning. How this level of adhesion related to actual carpet wear performance was still unknown. Therefore, it was based on these results that the first samples were spun for carpet wear testing. The results of the wear tests will be presented in section 4-6.

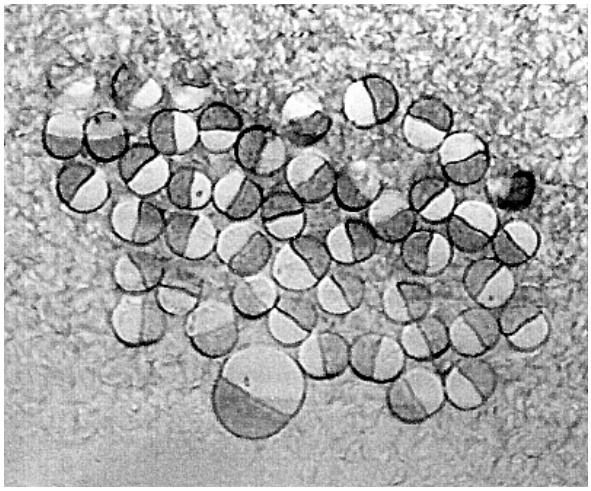

Figure 4-38. Cross section of fibers consisting of 67% PP-MA-1, 33% PP18 / PA6 produced with the goal of approximating the minimum level of PP-MA-1 necessary for adequate adhesion.

4-5-3. Qualitative Interfacial Adhesion of Fibers - Blends of Melt Functionalized Materials.

Just after the initially promising results with the PP-MA-1 material a second avenue towards bettering the economics of the fibers was investigated. It is believed that the PP-MA-1 material is manufactured using a special solution grafting process which does not degrade the polypropylene as severely as the melt functionalization process. The manufacturer will not release this proprietary information, but it is believed that this is also the reason for PP-MA-1's much greater cost than other maleic anhydride functionalized materials. To reduce costs melt functionalized polypropylenes from several different suppliers were obtained for testing. The rheology of selected blends of the PP-MA-3 and PP-MA-2 materials is shown in Fig 4-39.

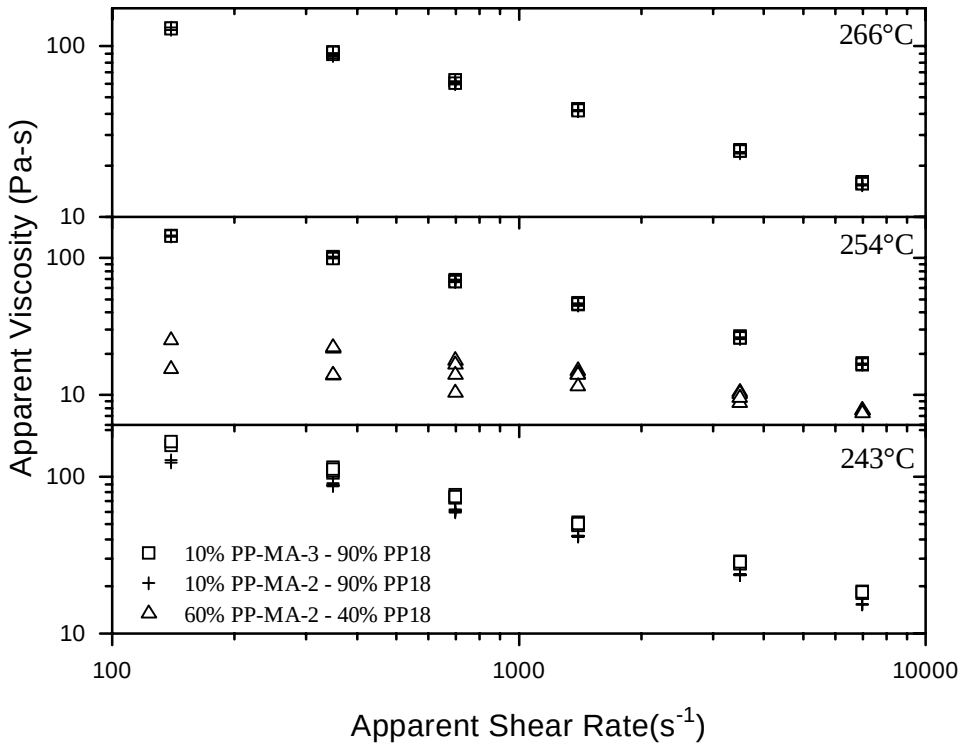

Figure 4-39. Viscous response of blends of PP-MA-3 and PP-MA-2 with PP18 at temperatures and shear rates comparable to spinning conditions. Note the data at 254°C contains an extra blend and a slightly different viscosity scale.

The pure component rheology of these materials was given previously in Fig 4-6. Figure 4-39 reveals no surprising trends. The lower maleic anhydride content material yields a blend of higher viscosity due to its greater molecular weight. Because the viscosities of the pure components is so different, a substantial effect on the blend viscosity can be noted at high functionalized polypropylene contents (60%PP-MA-2 at 254°C) in contrast to the PP-MA-1 system. Thus, while it is possible to vary the PP-MA-1 content without greatly affecting the processability of the system, the same does not hold for the heavily melt functionalized materials. In fact, the 60wt% PP-MA-2 system represents the greatest content which only could be spun with great difficulty. Figure 4-40 presents micrographs of the first trials using the melt functionalized materials at 10% loading levels.

A)

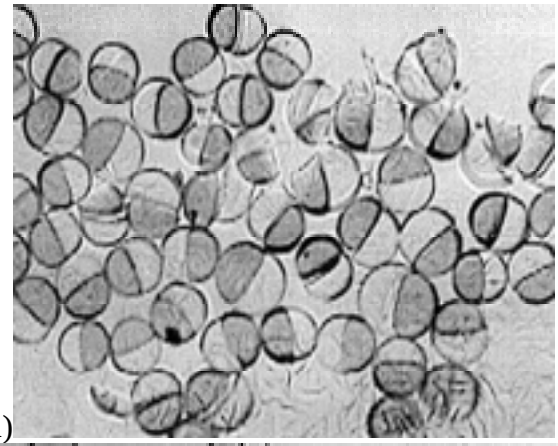

B)

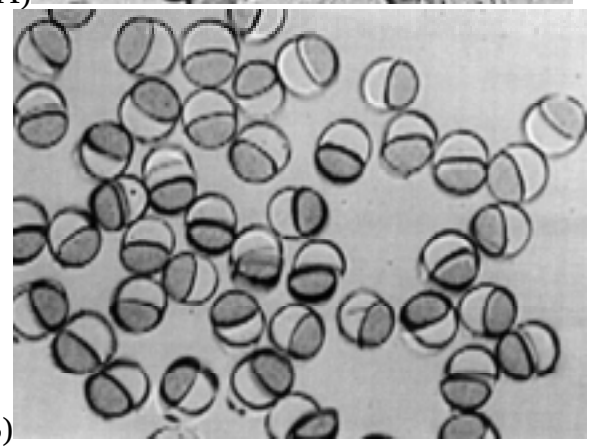

Figure 4-40. Cross sections of fibers produced using melt functionalized polypropylenes. A)10% PP-MA-3, 90% PP18 / PA6 B)10% PP-MA-2, 90% PP18 / PA6. Head block temperature 288°C.

Close examination of the micrographs reveals that both materials are exhibiting considerable adhesion, with the PP-MA-2 material being slightly better. To determine if lower PP-MA-2 contents would provide the same level of adhesion additional fibers were spun as shown in Fig 4-41.

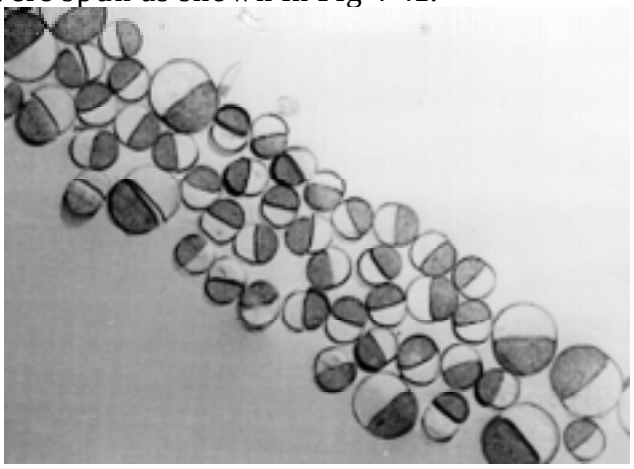

Figure 4-41. 5% PP-MA-2, 95% PP18 / PA6 fiber cross section showing adhesion similar to that of the 10% blend.

The adhesion shown by the 5% PP-MA-2 content fiber was found to be similar to the 10% PP-MA-2 content fiber. These results were very encouraging from an economic standpoint. It was thus decided that these materials would also be tested as carpet samples though their adhesion was not quite that of the PP-MA-1 material.

4-5-4. Qualitative Interfacial Adhesion of Fibers - Mixing of Blends.

It was hypothesized that the lack of adhesion in the blended samples could be occurring because the mixing provided by the single screw extruder, with a static mixing element, was insufficient to adequately disperse the two materials when blending the components as pellets in the hopper.

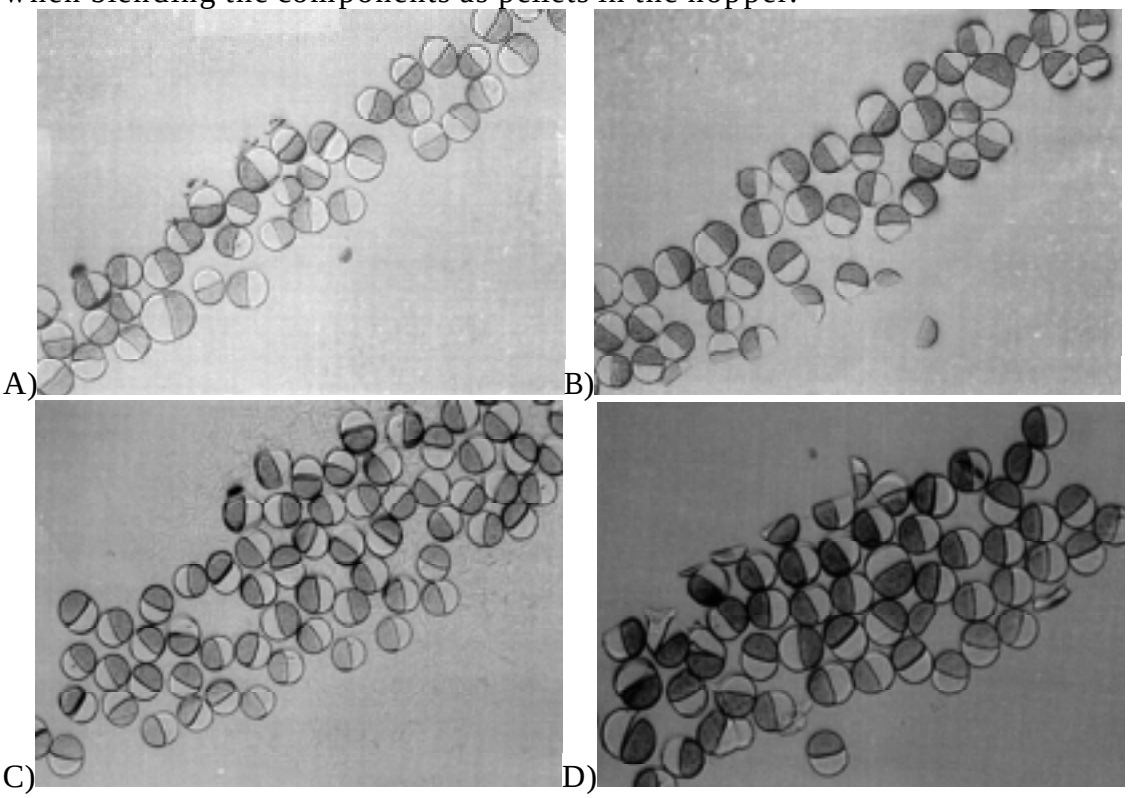

Figure 4-42. Comparison of fiber cross sections processed by hopper blending versus pre melt blending in a twin screw extruder. A) 50% PP-MA-1, 50% PP18 / PA6, hopper blended. B) 50% PP-MA-1, 50% PP18 / PA6, twin screw blended. C) 5% PP-MA-2, 95% PP18 /PA6, hopper blended. D) 5% PP-MA-2, 95% PP18 /PA6, twin screw blended.

An experiment was conducted in which fibers spun by hopper blending the materials were compared to fibers spun using materials which had been previously melt blended in a twin screw extruder. Figure 4-42 compares the fibers for an PP-MA-1 blend and an PP-MA-2 blend.

No differences in the adhesion of the PP-MA-1 blends can be seen between micrographs A and B. The fragments present in micrograph B are fibers which were not microtomed perpendicular to the fiber axis. Likewise, no differences can be noted for the PP-MA-2 system. Using these results it was deemed that the mixing provided by the static element in the single screw extruders was providing adequate mixing of the two materials.

4-6-1. Wear Testing of Carpet Samples.

To provide a measure of the quality of the fibers being produced wear testing was conducted on samples which had been textured and then tufted into carpet samples. These results not only give an indication of how these fibers would perform under actual use conditions, they are also helpful in differentiating the levels of adhesion for different composition. Figure 4-43 is a photograph of a carpet sample which has undergone a 50k cycle accelerated wear test. Comparing the upper and lower edges of the photograph to the center, the wear track produced during the wear test can be seen clearly. In this and all other wear specimens presented, an indication of the seriousness of the wear produced by the test can be obtained by comparing the center of the sample to the edges.

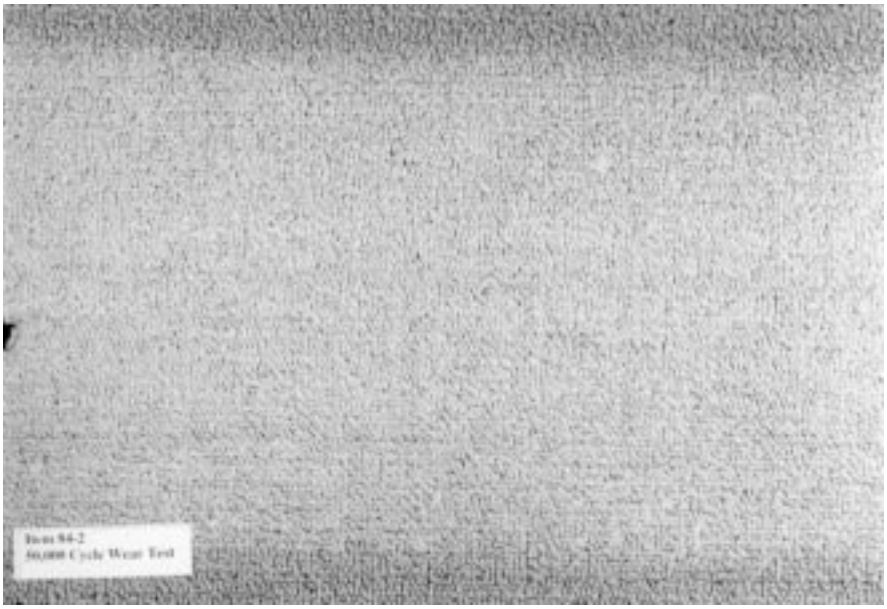

Figure 4-43. Wear tested carpet: 60% core, 40% sheath. Core - PA6, Sheath - PP18.

Care should be taken when comparing photographs. Unfortunately the photos do not always capture all of the details which are visible when examining the actual sample. Several photographs are slightly overexposed further reducing the amount of information these pictures can convey. The sample in Fig 4-38 shows relatively poor wear behavior. This is not surprising since no functionalized polypropylene has been used to enhance the adhesion between

the two components. Interfacial failures show a characteristic whitening of the carpet due to the scattering of light which occurs between the separated phases. Figure 4-44 is a wear tested sample that showed considerably better wear characteristics.

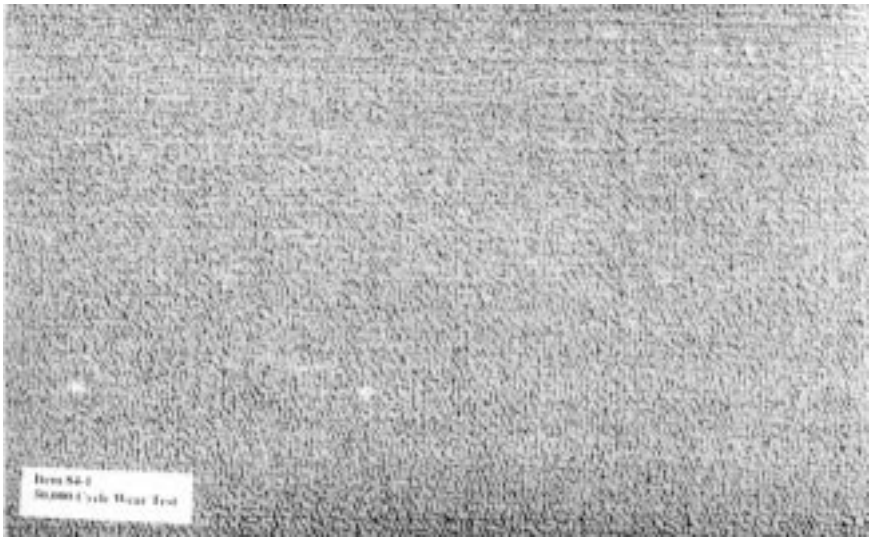

Figure 4-44. Wear tested sample showing good wear resistance. 60% core, 40% sheath. Core - Pa6, Sheath - 67% PP-MA-1, 33%PP18.

This sample does show some signs of wear. However the contrast between the center portion of the carpet and the lower edge is much less than the sample in which no compatabilizer was used.

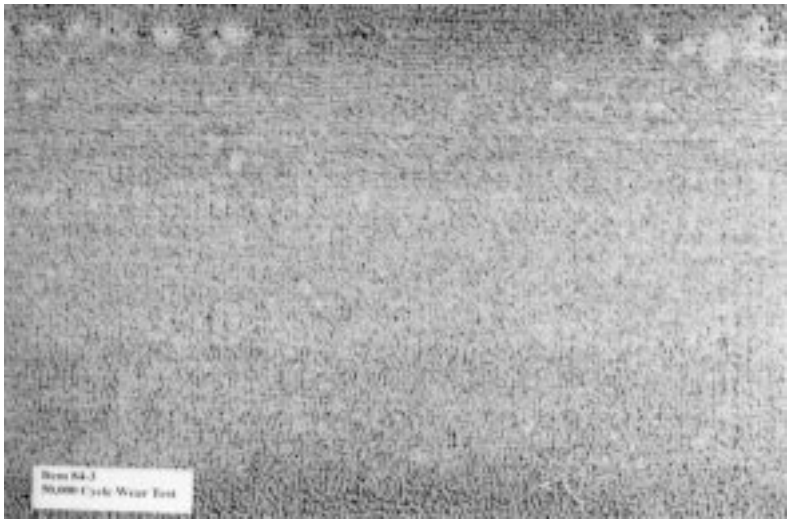

Figure 4-45. Wear tested carpet: 60% core, 40% sheath. Core - Pa6, Sheath - 10% PP-MA-2, 90% PP18.

These results suggest that the cross-section method of determining the relative level of adhesion may in fact relate to the real world performance of these materials. Regrettably Fig 4-45 shows that is not entirely true. Recalling Fig 4-

40, cross-sections of a 10% PP-MA-2, 90% PP18 fiber displayed fair adhesion. Figure 4-45 displays adhesion which is not much improved over the uncompatalbilized sample. The failure of the cross-sectioning method to predict the wear performance probably can be explained by the differences in mechanical properties between the PP-MA-1 and PP-MA-2 blends. The blends containing PP-MA-2 showed brittle behavior, lacking toughness. The cyclic deformations experienced during the wear test will require the fibers to absorb a great deal of energy repeatedly. There may be good adhesion produced in these systems between the nylon-6 and polypropylene phases, but the mechanical properties of the polypropylene phase is such that it cannot withstand the loadings experienced in a carpet application. The PP-MA-1 blends displayed much greater toughness and were more extensible, thus helping them maintain their structure during the constant shearing and crushing action of the wear test. Additionally, one can picture that with its higher molecular weight that the PP-MA-1 blends may produce a stronger, tougher interface due to a greater number of entanglements per compatabilizer chain. For the above reasons the melt functionalized polypropylenes were dropped in favor of the PP-MA-1 material despite its higher cost.

Because of this effect of the mechanical properties of the sheath on the performance of the fiber, tests were conducted which varied the amount of material used as the sheath component relative to the core. Figure 4-46 compares a 40% sheath fiber to a 30% sheath fiber.

A) 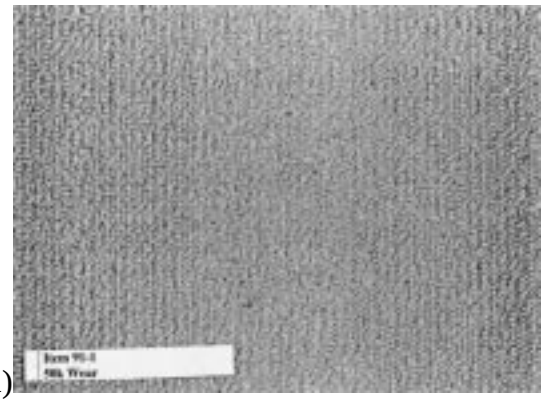 B) 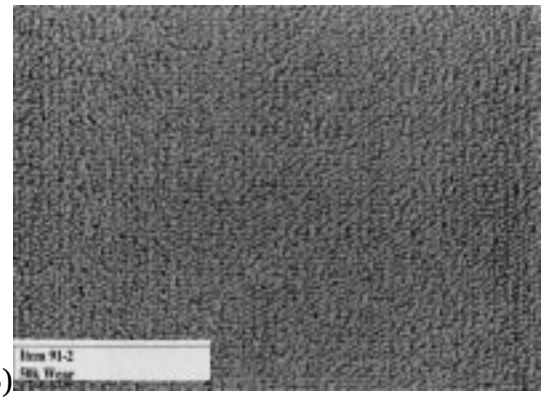

Figure 4-46. Effect of sheath thickness on wear properties. A) 40% sheath, 60% core B) 30% sheath, 70% core. Both fibers consist of a sheath of 50% PP-MA-1, 50% PP18 / core of PA6.

From the photographs it is difficult to compare the relative wear of these samples. Close observation does reveal that the contrast between the center and the edges of the samples is greater for the sample with the larger amount of sheath material. This is very plausible. Traditionally nylon carpets are considered to be very tough, with good resiliency. Less sheath material translates to more core material. Thus the sample with the thinner sheath has a

stronger nylon-6 backbone to support the fiber and absorb energy. Furthermore, the thinner the sheath, the farther out from the center of the fiber the interface between the two phases will exist. As the radius to the interface increases so does the area of contact between the phases, thus providing a greater amount of surface area for adhesion. Sheath ratios of less than 30% have not been tested as carpet samples. Figure 4-47 Illustrates the thinness of a 10% sheath.

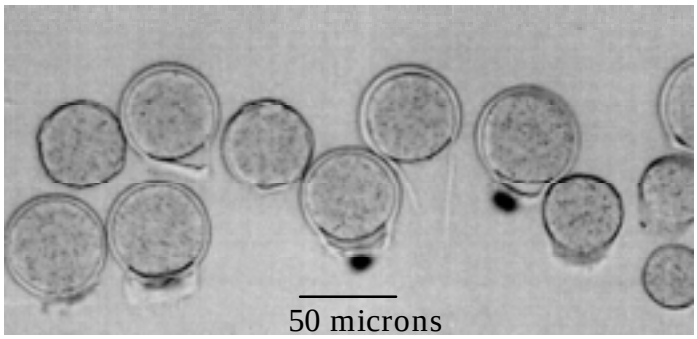

Figure 4-47. Cross section of fibers with 10% sheath of PP18 / 90% core of PA6 illustrating the radial thickness of the sheath component at low volume fractions.

While fibers of this cross-section will have a correspondingly larger surface area for bonding, there are two potential disadvantages. The economic benefit of producing a bicomponent polypropylene/ nylon-6 fiber is lost with decreasing sheath thickness, as polypropylene is much less expensive than nylon-6 from a raw materials standpoint. Secondly, as the polypropylene sheath becomes thinner, scuffing and other wear processes which remove material from the fiber, will expose the core more quickly.

4-6-2. Stain Testing of Carpet Samples.

The main purpose for producing a bicomponent fiber with a polypropylene sheath was to obtain a carpet with improved stain resistance. Therefore stain testing was conducted to determine if the fibers were meeting there intended goal. It was speculated that a high level of maleic anhydride may increase the polarity of the polypropylene phase and thereby decrease the inherent stain resistance of the olefinic material. A photograph of a carpet sample stained with coffee, prior to cleaning is given in Fig 4-48 along with a cleaned specimen.

Unfortunately again the photographs do not give a full appreciation of the performance. Looking for contrast along the edges versus the center of the sample shows a clear stain on the sample prior to cleaning. In contrast, the cleaned sample shows little variation in color. This performance can be considered very good and is indicative of the majority of the fibers produced with a sheath consisting of polypropylene based materials in this research.

A) 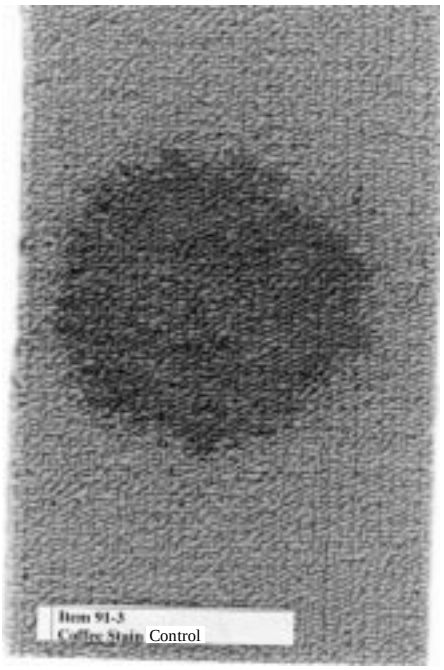

B) 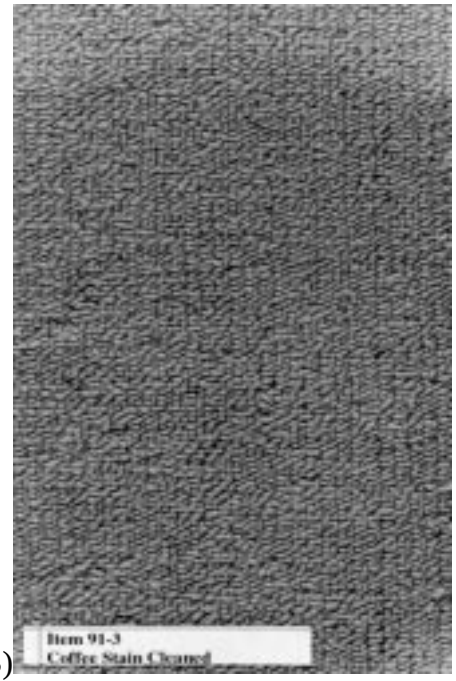

Figure 4-48. Coffee stain testing of carpet samples. A) after staining B) after cleaning. Both samples consist of a 40% sheath of 33% PP-MA-1, 67% PP18 / 60% core of PA6.

Additional stain tests were done with acid red dye. These tests not only show the ability of the polypropylene component to resist such stains, but also demonstrates that this resistance is dependant on the maintaining of the integrity of the interface between the phases. Figure 4-49 shows the results of the acid red dye test on representative samples. This figure clearly shows the ability of these fibers to resist staining from polar materials. It is nearly impossible to detect any stain on the cleaned sample. Further insight into the properties of this fiber during its service life can be obtained by first conducting a wear test and then performing the stain test. Ideally these fibers must be able to retain there stain resisting properties. Figure 4-50 shows the results of the wear test for this fiber, while Fig 4-51 shows the results of stain testing a sample after the wear test.

Figure 4-50 shows that the wear performance of this fiber is fair, while the previous figure had shown that it had excellent stain resistance. Examining Fig 4-51 shows that while the stain resistance is still very good, it has decreased somewhat. This suggests that wear which leads to failure of the interface allows for spaces into which the staining liquid may seep into the core of the fiber. Thus, the quality of the interface is not only essential to producing a fiber with excellent wear characteristics, it is also necessary to provide good stain resistance.

A) 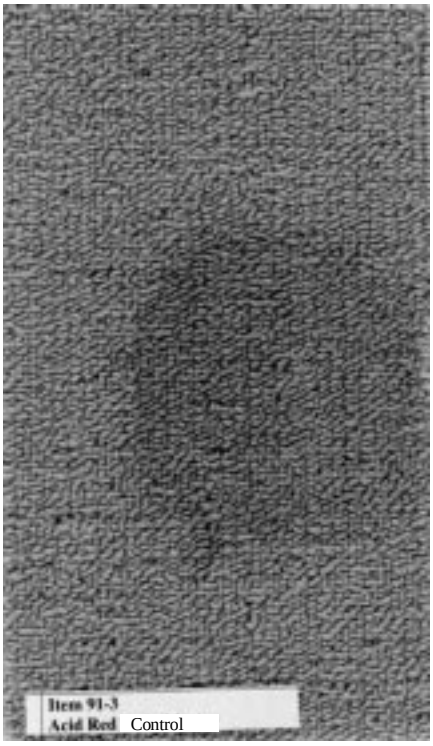

B) 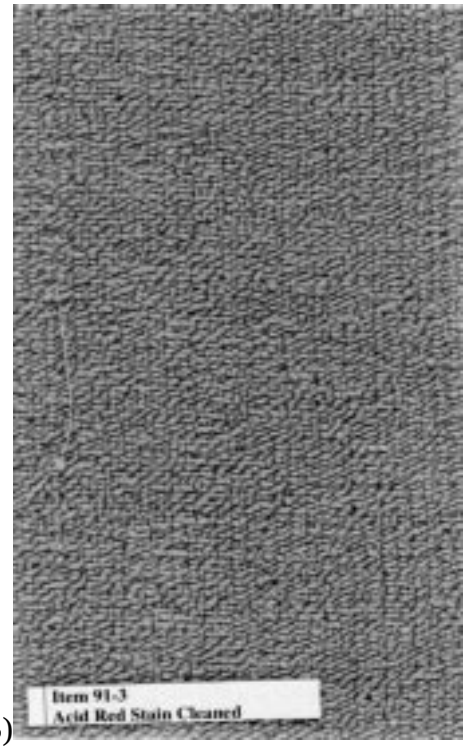

Figure 4-49. Acid red stain testing of carpet samples. A)after staining B)after cleaning. Both samples consist of a 40% sheath of 33% PP-MA-1, 67% PP18 / 60% core of PA6.

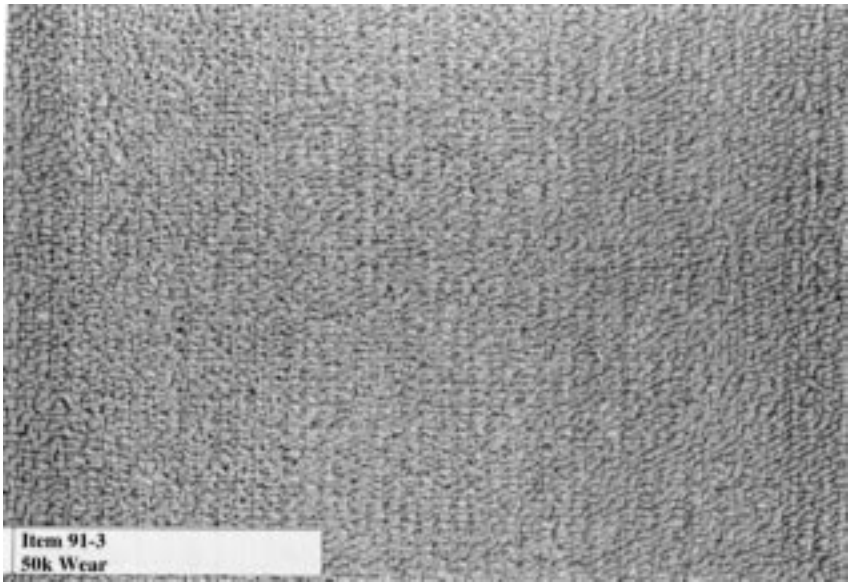

Figure 4-50. Wear test results for a 40% sheath of 33% PP-MA-1, 67% PP18 / 60% core of PA6.

A) 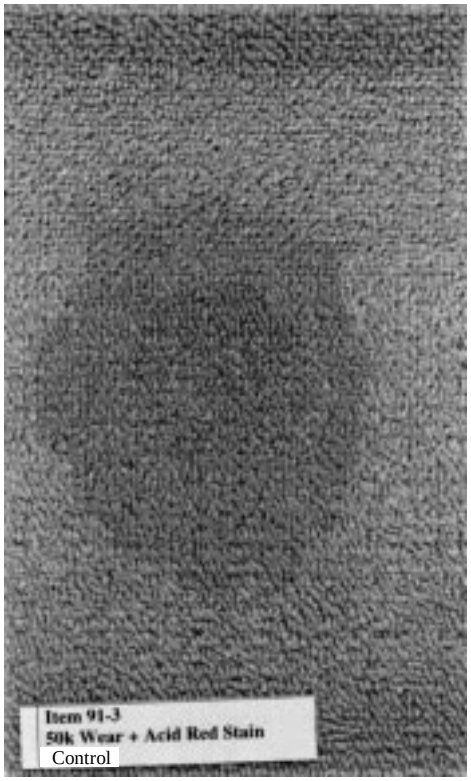

B) 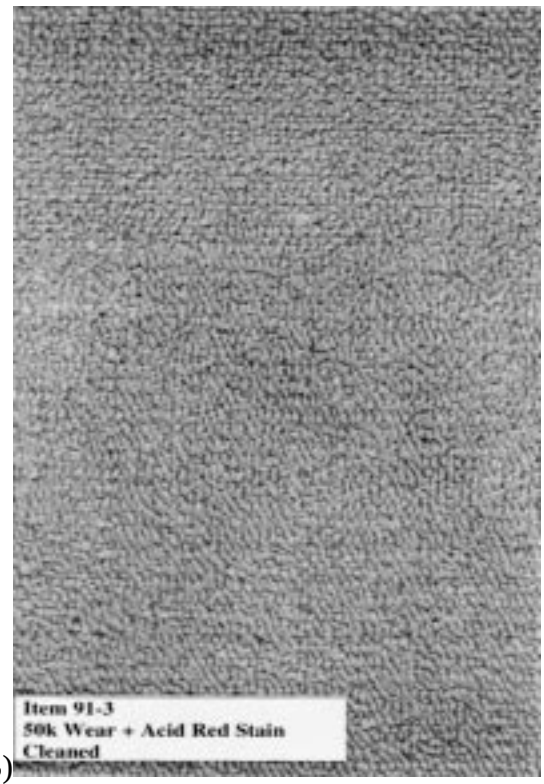

Figure 4-51. Results of stain testing after wear testing for a 40% sheath of 33% PP-MA-1, 67% PP18 / 60% core of PA6.

5. Conclusions

Bicomponent fibers consisting of nylon-6 and isotactic polypropylene were produced using a maleic anhydride functionalized polypropylene to form in-situ a compatibilizer between the components. The spinning of bicomponent fibers using these materials requires a viscosity ratio of approximately 3.57 between the components The viscosity ratio was also found to play a key role in the final cross-section of the fiber. TGA and capillary rheometry studies provided data suggesting that degradation of the polypropylene component was not severe despite the use of processing temperatures above traditional values.

Carpet samples produced using nylon-6 core / polypropylene sheath bicomponent fibers displayed stain resistance comparable to a wholly polypropylene carpet. The wear characteristics of these fibers were found to be strongly dependent upon the composition of the polypropylene phase. The

overall maleic anhydride content of the functionalized polypropylene was found to be critical in attaining adequate adhesion between the materials. Additionally, the molecular weight of the functionalized polypropylene was found to be crucial by contrasting the PP-MA-1 and the PP-MA-2 materials. Tensile testing of blends of the materials with a non-functionalized polypropylene showed that the high content of PP-MA-2 required to obtain adequate adhesion, as determined through cross-sections and optical microscopy, produced a brittle material. In the final carpet application the toughness of the polypropylene phase as well the maleic content were found to influence the wear behavior.

While carpets produced with the PP-MA-1 material displayed promising properties, the level of functionalized material required makes these fibers nonviable from an economic standpoint.

Recommendations for Future Studies

The data which would most aid progress in producing a nylon-6 / polypropylene bicomponent fiber that is economically viable would be a thorough study of the quality of adhesion obtained between the two materials as a function of maleic anhydride content and temperature. No such test was devised during the course of this research. Ideally, the method will allow testing of the interface of individual fibers. Such a test may require a specialized load cell capable of measuring very small forces.

Definitive proof of the difference in molecular weight between the PP-MA-1 and PP-MA-2 materials could be provided using GPC. Any testing would have to be based on the premise that the addition of the maleic anhydride group does not significantly affect the radius of gyration of the chain.

Additional work to elucidate the type of morphology formed in the interfacial region of the fibers may provide clues to possible avenues to pursue to enhance

adhesion between the phases. DeRoover (ref.29) has suggested that the presence of the β crystalline form of polypropylene near the interface in fracture energy studies significantly enhances the toughness of the interface. It would also be interesting to determine if the clearly phase separated morphology of the PP-MA-1 material is affecting the mode of failure around the interface. Finally, further considering the morphology of the system, very little work was done to characterize the state of orientation of the phases. Obtaining WAXS spectra of the fibers would provide insight to this question. Such a study may provide information that would allow the tailoring of self-crimping behavior should off-center core / sheath fibers be produced.

Appendix 1 - Syndiotactic / Isotactic Polypropylene

One of the properties that make bicomponent fibers unique is their ability to self crimp. Differences in elasticity of an assymetric fiber leads to an imbalance of stresses across the cross section of the fiber causing a twist to form along the length of the fiber. Based on this principle, fibers consisting of isotactic polypropylene and syndiotactic polypropylene were spun. Obviously these two materials are very similar chemically, so adhesion between the polypropylenes should not be problematic. Because of the difference in tacticity, the two materials crystallize into different structures at different rates. By taking advantage of this phenomena, a bicomponent fiber showing excellent crimp with excellent adhesion should be attainable. Fibers of this type were spun using a syndiotactic polypropylene supplied by Fina and the same isotactic polypropylene used throughout the research (PP18).

As with any bicomponent fiber spinning process the first key variable to consider is the viscous response of the materials. Figure A-1, presents capillary rheometry data of the syndiotactic polypropylene along with some isotactic data.

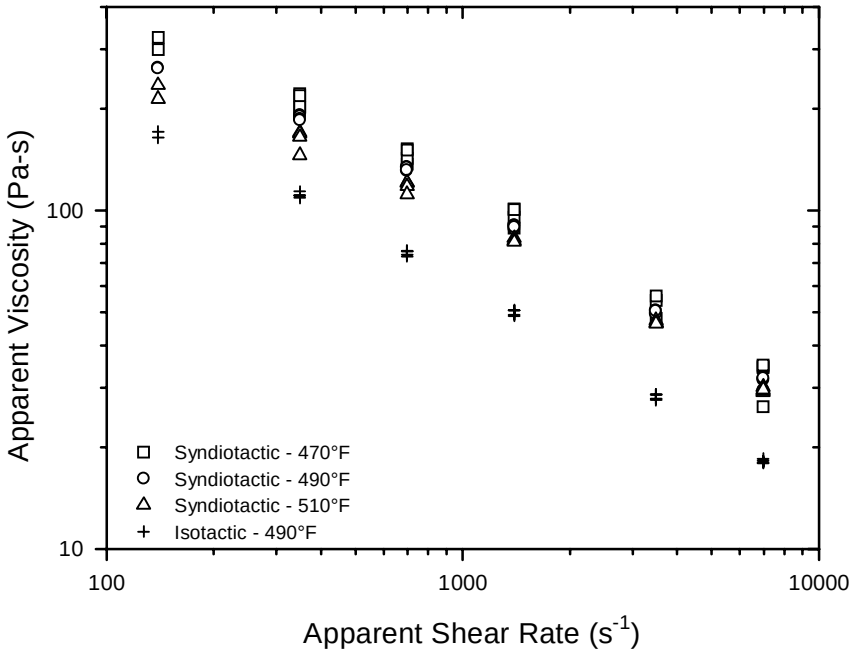

Figure A-1. Capillary rheometry data of syndiotactic polypropylene. Isotactic data at 490°F is provided for reference.

The plot clearly shows that this particular syndiotactic resin is more viscous than PP18. However, the difference is well within the 4:1 rule of thumb. Using this information fibers were spun with a side by side configuration. The cross-sections of these fibers are shown in figure A-2.

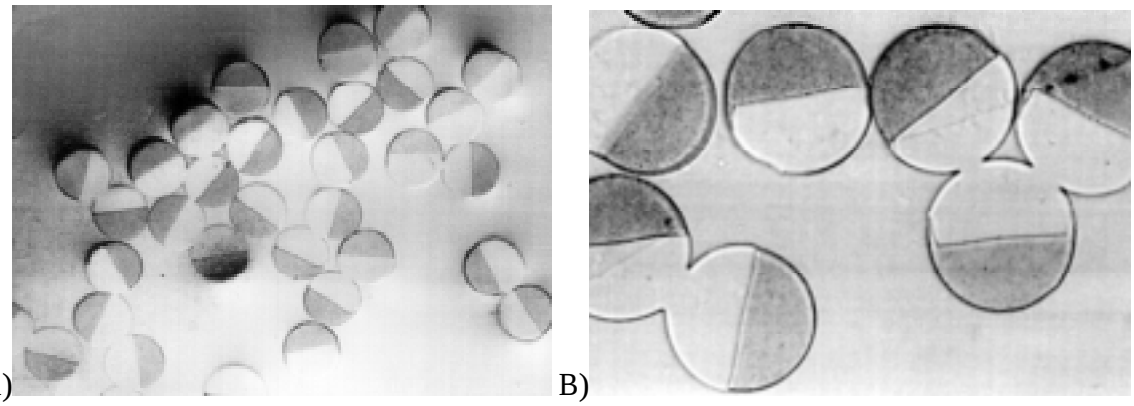

Figure A-2. Syndiotactic / isotactic polypropylene fiber. Dark phase consists of isotactic material. A)low magnification showing fiber symmetry. B) higher magnification showing fusing of syndiotactic component.

The cross-sections show that very little interface movement is occurring and that the adhesion between the phases appears to be excellent. At higher magnification it can be seen that in several instances adjacent fibers have fused together. This fusion occurs only between the syndiotactic components of adjacent fibers. This phenomena is a result of the lower melting point of syndiotactic polypropylene relative to the isotactic material. These fibers were processed at temperatures higher than necessary (the same conditions that were being used for the nylon-6 / polypropylene fibers described earlier). Thus, while tests were not conducted, it is likely that the unintentional fusion of adjacent fibers could be corrected quite easily.

These fibers show no crimping behavior as spun. But, upon drawing a very tight crimp is achieved. As mentioned above, the differences in the crystallization of the two propylenes lead to this phenomena. Figure A-3 shows a cross-section of the drawn fiber.

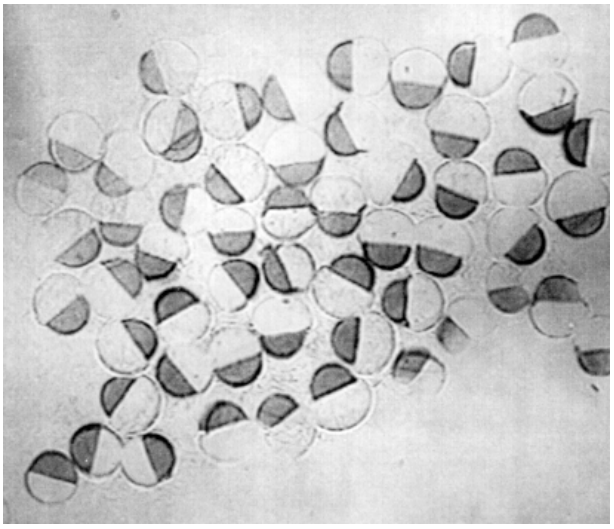

Figure A-3. Cross-section of drawn syndiotactic / isotactic polypropylene fiber.

Close examination of the micrograph reveals the two materials are responding to drawing very differently. The syndiotactic component appears swollen in comparison to the isotactic component. This is likely due to the greater elastic nature of the syndiotactic component. The syndiotactic component contains a lower crystalline content after spinning than the isotactic component. Thus, the syndiotactic material has a greater rubbery, amorphous character above T_g relative to isotactic polypropylene. Upon the release of the drawing stress, the syndiotactic portion of the fiber retracts more than the isotactic component, which leads to the high degree of crimping observed in these fibers. Taking an undrawn fiber and heating slightly without tension also produces a high degree of crimp with these fibers.

It was mentioned above that the crystallization behavior of the syndiotactic material differs from that of the isotactic material. Figure A-4 gives the syndiotactic resin's melting behavior as determined by DSC.

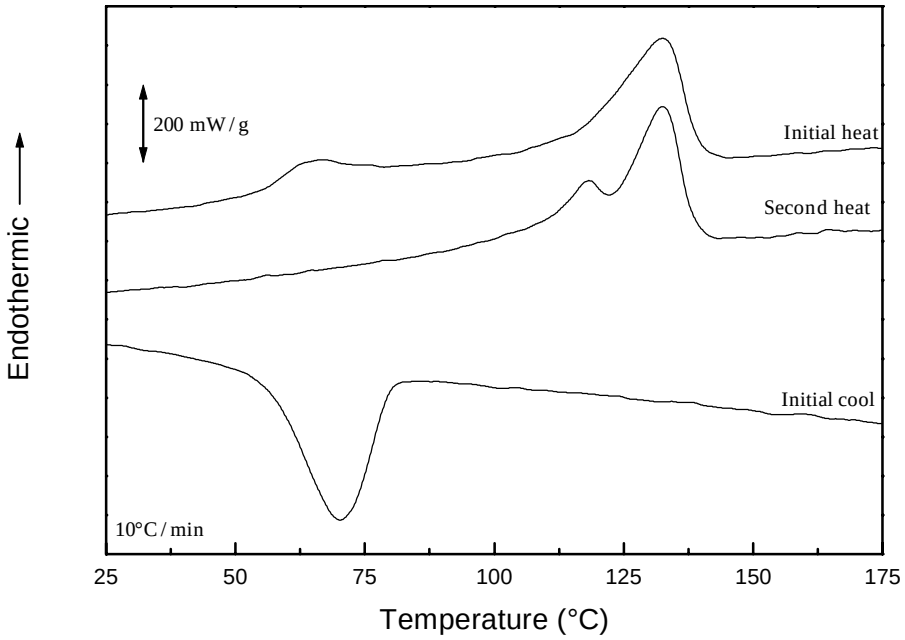

Figure A-4. DSC melting and crystallization behavior of syndiotactic polypropylene. Sample was heated (top scan), cooled (bottom scan), and reheated (middle scan).

The syndiotactic material displays interesting crystallization behavior. Upon heating an aged sample, a very low and broad melting population can be found. During the second heating, this melting endotherm is not observed. This suggests that while sitting at room temperature the material slowly undergoes additional crystallization. Most likely this behavior can be ascribed to defects in the syndiotactic configuration of the material. The resin most likely is not perfectly syndiotactic, containing short runs of atactic or isotactic material. These defects lower the crystalline content and perfection. At 132.5°C the melting point of the syndiotactic polymer can be seen to be much lower than that of isotactic polypropylene.

To further demonstrate the quality and permanence of the crimp obtained the fibers were placed in toluene at 70°C for ten minutes. The hot toluene is capable of dissolving the syndiotactic component but not the isotactic. The remaining fiber (isotactic only) was observed using SEM as shown in figure A-5.

A) 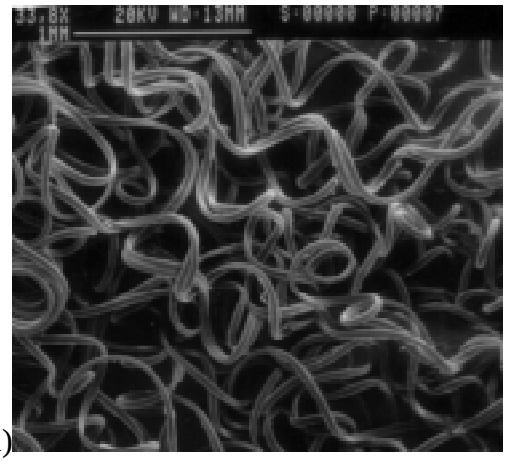 B) 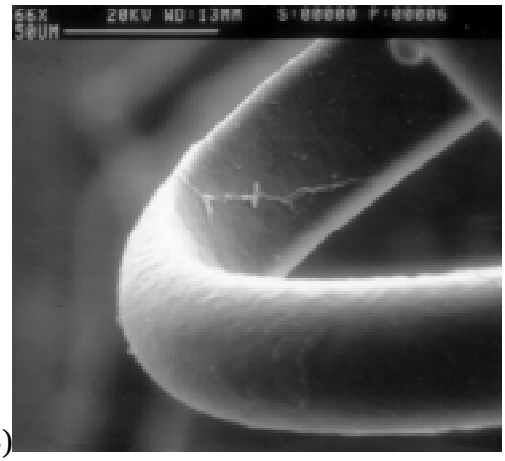

Figure A-5. SEM of isotactic portion of the fiber. Fibers maintain crimp after removal of syndiotactic component.

The figure clearly shows that the isotactic portion of the fiber maintains the crimped conformation even after removal of the syndiotactic component. The fibers appear flat on one side suggesting that only the syndiotactic component has been removed. To further prove that only the syndiotactic portion was removed, the FTIR spectrum of the dissolved residue was examined as shown in figure A-6.

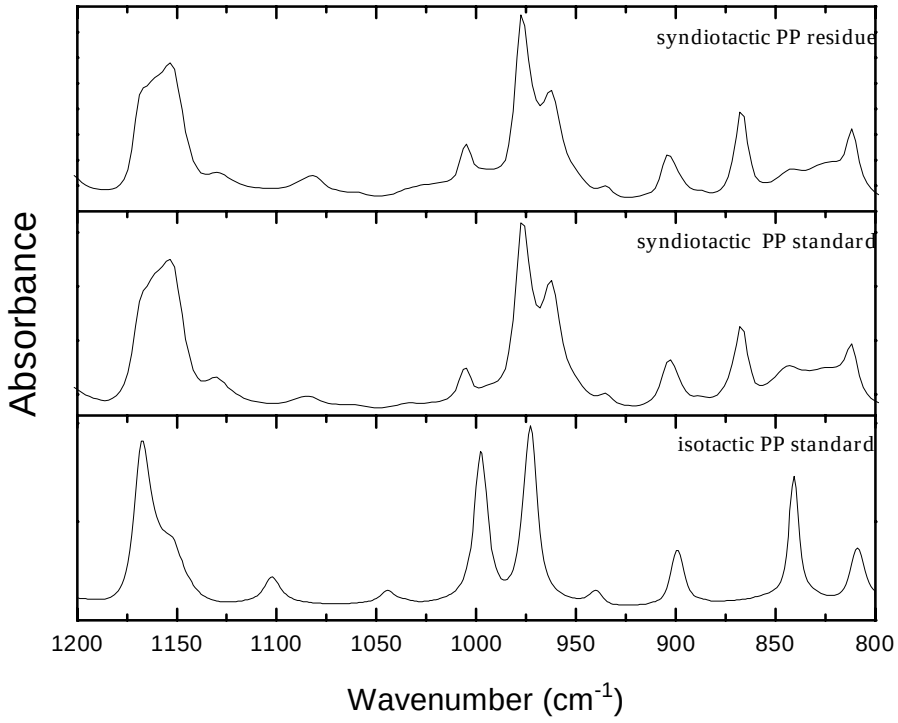

Figure A-6. FTIR spectra comparing isotactic polypropylene standard, syndiotactic polypropylene standard and syndiotactic polypropylene residue obtained from toluene after solvation. Standards obtained by compression molding pellets into a film prior to scan.

The spectra clearly shows that while the materials have many common vibrations, they are not the same material.

Finally, no study of fibers would be complete without an examination of WAXS patterns and orientation. Figure A-7 presents three WAXS patterns of a side by side syndiotactic / isotactic polypropylene fiber. The first pattern shows a fiber as spun, and shows very little orientation. The reflections from both the isotactic and syndiotactic components are evident. The second pattern was obtained from a fiber drawn online to a ratio of three to one. The amount of orientation has increased as evidenced by the increasing azimuthal dependence of the diffraction.

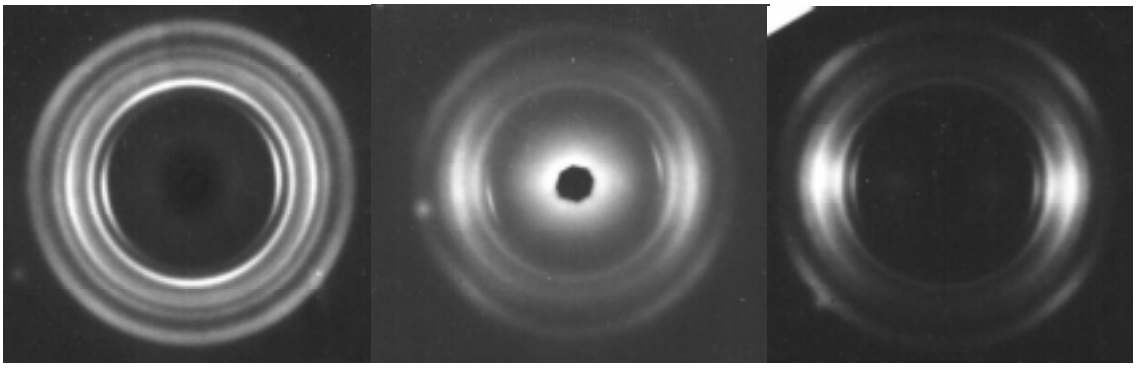

A) B) C)

Figure A-7. WAXS patterns of a side by side syndiotactic / isotactic polypropylene fiber. A) fiber as spun B) fiber drawn online, draw ratio of 3, C) fiber hand drawn to maximum extension before failure.

Finally, the last pattern is of an as spun fiber which was drawn by hand up to the breaking point. This fiber shows the greatest amount of orientation. The orientation functions for these fibers were not quantified.

A bicomponent fiber consisting of isotactic and syndiotactic polypropylene in a side by side configuration was spun to produce a bicomponent fiber with excellent self crimping characteristics. This fiber was spun successfully as shown by the data above. This fiber does posses certain limitations when contrasted with a wholly isotactic fiber. The melting point of the syndiotactic polypropylene is much lower than that of the isotactic material, lowering the maximum service temperature of these fibers. Finally the lower crystalline content of the syndiotactic will weaken the tenacity of these fibers relative to a wholly isotactic fiber. However, it is unlikely that failure at the interface of the two materials will be an added complication due to the chemical similarity of the two polypropylenes.

References

1. H. Brody, Synthetic Fibre Materials, John Wiley and Sons Inc., New York (1994).
2. Various authors, *International Fiber Journal*, pp. 20-59, June 1998.
3. Hills, W.H., U.S. Patent No. 5,162,074, November 10, 1992.
4. Han, C. D., *Journal of Applied Polymer Science*, **17**, 1289 (1973).
5. Han, C. D., *Journal of Applied Polymer Science*, **19**, 1875 (1975).
6. Southern, J.H, Ballman, R.L., *Journal of Polymer Science: Polymer Physics Edition*, **13**, 863 (1975).
7. Everage, A.E., *Transactions of the Society of Rheology*, **19** (4), 509 (1975).
8. White, J.L., Lee, B.L., *Transactions of the Society of Rheology*, **19** (3), 457 (1975).
9. Uhland, E., *Polymer Engineering and Science*, **17** (9), 671 (1977).
10. Everage, A.E., *Transactions of the Society of Rheology*, **17** (4), 629 (1973).
11. MacLean, D.L., *Transactions of the Society of Rheology*, **17** (3), 385 (1973).
12. Bagley, E.B., *Journal of Applied Physics*, **28**, 624 (1957).
13. Cogswell, F.N., Polymer Melt Rheology, Wiley, New York (1981).
14. Wilkes, G.L., *Journal of Chem. Education*, 58 (11), 880 (1981).
15. Rosen, S.L., Fundamental Principles of Polymeric Materials, 2nd ed., John Wiley and Sons Inc., New York (1993).
16. Bird,B.B, Armstong, R.C., and Hasseger, O., Dynamics of Polymeric Liquids, Vol.1 Fluid Mechanics, John Wiley and Sons Inc., New York (1987).
17. Hingmann, R., and Marczinke, B.L., *Journal of Rheology*, **38** (3), May / June 1994.
18. Ishibashi, T., Aoki, K., and Ishii, T., *Journal of Applied Polymer Science*, **14**, 1597, (1970).
19. Ziabicki, A., Fundamentals of Fiber Formation, , John Wiley and Sons Inc., New York (1976).
20. Ahmed, M., Polypropylene Fibers - Science and Technology, Elsevier Scientific Publishing Company, New York, 1982.
21. Ide, F., Hasegawa, A., *Journal of Applied Polymer Science*, **18**, 963,(1974).
22. Marco, C., Ellis, G., Gomez, M.A., Fatou, J.G., Arribas, J.M., Campoy, I., and Fontecha, A., *Journal of Applied Polymer Science*, **65**, 2665, (1997).
23. Duvall, J., Sellitti, C., Myers, C., Hiltner, A., and Baer, E., *Journal of Applied Polymer Science*, **52**, 195, (1994).
24. Gonzalez-Montiel, A., Keskkula, H., and Paul, D. R., *Journal of Polymer Science: Part B: Polymer Physics*, **33**, 1751, (1995).
25. Boucher, E., Folkers, J.P., Hervet, H., Leger, L. and Creton, C., *Macromolecules*, **29**, 774, (1996).
26. Boucher, E., Folkers, J.P., Creton, C., Hervet, H., and Leger, L., *Macromolecules*, **30**, 2102, (1997).
27. Bidaux, J., Smith, G.D., Bernet, N., and Manson, J.E., *Polymer*, **37**, 1129, (1996).
28. Al-Malaika, S., Reactive Modifiers for Polymers, Chapman and Hall, London, 1997.

29. De Roover, B., Sclavons, M., Carlier, V., Devaux, J., Legras, R., Momtaz, A., *Journal of Polymer Science: Part A: Polymer Chemistry*, **33**, 829, (1995).
30. De Roover, Devaux, J., Legras, R., *Journal of Polymer Science: Part A: Polymer Chemistry*, **34**, 1195, (1996).
31. Paul, D.R.,Oshinski, A.J., Keskkula, H., *Polymer*, **33** (2), 284, (1992).
32. Muller, M., *Macromolecules*, **30** (20), 6353, (1997).
33. Dumoulin, M.M., Carreau, P.J., *Polymer Engineering and Science*, **27** (20), 1627, (1987).
34. Park, C.D., Jo, W.H., Lee, M.S., *Polymer*, **37** (14), 3055, 1996.
35. D'Orazio, L., Guarino, R., Mancarella, E., Cecchin, G., Journal of Applied Polymer Science, **65**, 1539, (1997).
36. Garcia-Martinez, J.M., Laguna, O., Collar, E.P., *Journal of Applied Polymer Science*, **68**, 483, (1998).
37. DeRoover, B., Devaux, J.Legras, R, *Journal of Polymer Science: Part A: Polymer Chemistry*, **34**, 1195, (1996).
38. Gonzalez, E.A., Gonzalez, M.J.L., Gonzalez, M.C., *Journal of Applied Polymer Science*, **68**, 45, (1998).
39. Spruiell, J.E., Lu, F.M., Ding, Z., Richeson, G., *Journal of Applied Polymer Science*, **62**, 1965, (1996).
40. Zhang, X., Li, X.L., Wang, D., Yin, Z., Yin, J., *Journal of Applied Polymer Science*, **64**, 1489, (1997).
41. Li, H., Chiba, T., Higashida, N., Yang, Y., Inoue, T., *Polymer*, **28** (15), 3921, (1997).
42. Sanchez-Valdes, S., Yanez-Flores, I., Ramos De Valle, L.F., Rodriguez-Fernandez, O.S., Orona-Villarreal, F., Lopez-Quintanilla, M., *Polymer Engineering and Science*, **38** (1), 127, (1998).
43. Creton, C., Kramer, E.J., Huim, C., Brown, H.R., *Macromolecules*, **25**, 3075, (1992).
44. Kramer, J. Norton, L.J., Dai, C., Sha, Y., Hui, C., *Faraday Discussions*, **98**, 31, (1994).
45. Heino, M., Hietaoja, P., Seppala, J., Harima, T., Friedrich, K., *Journal of Applied Polymer Science*, **66**, 2209, (1997).
46. Carvalho, B., Bretas, R.E.S., *Journal of Applied Polymer Science*, **68**, 1159, (1998).
47. Starkweather, W.H., Moynihan, R.E., *Journal of Polymer Science*, **22**, 363, (1956).
48. Ramesh, C., Gupta, V.B., Radhakrishnan, J., *Journal of Macormolecular Science - Physics*, **B36** (2), 281, (1997).
49. Suping, H., Chengxun, W., Huifen, J., *Journal of China Textile University*, **8** (1), 39, (1991).
50. Ji, C., Yang, J.C., Lee, W., *Polymer Engineering and Science*, **36** (10), 1399, (1996).
51. Lee, W.S., Park, C.W., *Journal of Applied Mechanics*, **62**, 511, (1995).
52. Gonzalez-Nunez, R., Chan Man Fong, C.F., Favis, B.D., Kee, D.D., *Journal of Applied Polymer Science*, **62**, 1627, (1996).

53. Kikutani, T., Rahdakrishnan, J., Arikawa, S., Takaku, A., Okui, N., Jin, X., Niwa, F., Kudo, Y., *Journal of Applied Polymer Science*, **62**, 1913, (1996).
54. Schmack, G., Schreiber, R., Veeman, W.S., Hofmann, H., Beyreuther, R., *Journal of Applied Polymer Science*, **66**, 377, (1997).
55. Fouda, J.M., El-Tonsy, M.M., Hosny, H.M., Metawe, F.M., Easawi, K.H., *Journal of Applied Polymer Science*, **66**, 395, (1997).
56. Simal, A.,L, Martin, A.,R., *Journal of Applied Polymer Science*, **68**, 453, (1998).
57. Simal, A., L., Martin, A.R., *Journal of Applied Polymer Science*, **68**, 441, (1998).
58. Gupta, V.B., Mondal, S.A., Bhuvanesh, Y.C., *Journal of Applied Polymer Science*, **65**, 1773, (1997).
59. Aslan, S., Laurienzo, P., Malinconico, M., Martuscelli, E., Pota, F., Bianchi, R., Dino, G.D., Giannotta, G., *Journal of Applied Polymer Science*, **55**, 57, (1995).
60. Radhakrishnan, S., Tapale, M., Shah, N., Rairkar, E., Shirodkar, V., Natu, H.P., *Journal of Applied Polymer Science*, **64**, 1247, (1997).
61. Akrman, J., Prikryl, J., *Journal of Applied Polymer Science*, **66**, 543, (1997).
62. Rodriguez-Cabello, J.C., Alonso, M., Merino, J.C., Pastor, J.M., *Journal of Applied Polymer Science*, **60**, 1709, (1996).
63. Zhang, X., Yin, Z., Yin, J., *Journal of Applied Polymer Science*, **62**, 893, (1996).
64. Michielsen, S., *Journal of Applied Polymer Science*, **67**, 1541, (1998).
65. Tang, T., Li, H., Huang, B., *Macromolecular Chemistry and Physics*, **195**, 2931, (1994).
66. Huang, H., Liu, N.C., *Journal of Applied Polymer Science*, **67**, 1957, (1998).
67. Isayev, A.I., Catignani, B.F., *Polymer Engineering and Science*, **37** (9), 1526, (1997).
68. Southern, J.H., Martin, D.H., Baird, D.G., *Textile Research Journal*, 411, July 1980.
69. Lee, W.S., Park, C.W., *ANTEC 1992*, 2181.
70. Torres, A., Hrymak, A.N., Vlachopoulos, J., Dooley, J., Hilton, B.T., *Rheologica Acta*, 32, 513, (1993).
71. Macosko, C.W., Rheology - Principles, Measurements, and Applications, VCH Publishers Inc., New York, 1994.
72. Heimenz, P.C., Polymer Chemistry - The Basic Concepts, Marcel Dekker Inc., New York, 1984.
73. Jeffries, R., Bicomponent Fibers, Merrow Publishing Co. Ltd, England, 1971.
74. Grulke, E.A., Polymer Process Engineering, Prentice Hall, Englewood Cliffs, 1994.
75. Zang, Carreau, *Journal of Applied Polymer Science*, **42**, (1991).
76. Kohan, M.I., Nylon Plastics, Wiley-Interscience, New York, 1973.
77. Norton, D.R., Keller, A., *Polymer*, **26**, 704, 1985.
78. Brandrup, J., Immergut, E. H**.,** Polymer Handbook - 2nd ed., Wiley-Interscience, New York, 1975.
79. Tadmor, Z., and Gogos, C.G., Principles of Polymer Processing, Wiley-Interscience, New York, 1979.

80. Shucai Li, Jarvela, P.K., Jarvela, P.A., *Journal of Applied Polymer Science*, **71**, 1641, (1999).
81. Shucai Li, Jarvela, P.K., Jarvela, P.A., *Journal of Applied Polymer Science*, **71**, 1649, (1999).

VITA

David Leonard Godshall was born August 28, 1973 in Antioch, Illinois though the majority of his primary education was received in Naperville, Illinois. Upon graduation from high school in 1991, he attended Michigan State University and obtained his Bachelors degree in Chemical Engineering in 1995. He then spent four months dropping bottles filled with carbonated water in the name of science for Crown Cork and Seal Inc. at their corporate research headquarters in Alsip, Illinois. David then returned to MSU for eight months of lab work with Dr. Scranton before joining Virginia Polytechnic Institute & State University to obtain his M.S. under the guidance of Dr. Wilkes in the Chemical Engineering Department. He has decided to remain at Virginia Tech to pursue a Ph.D. With Dr. Wilkes.